FEDERAL UNIVERSITY OF SANTA CATARINA

GRADUATE PROGRAM IN MECHANICAL ENGINEERING

Development and Application of Detailed Chemical Kinetics Mechanisms for Ethanol and Ethanol Containing Hydrocarbon Fuels

Leonel Rincón Cancino

Thesis

Submitted in partial fulfillment of the requirements
For the degree of
Doctor in Mechanical Engineering

Prof. Amir Antônio Martins de Oliveira Junior, Ph.D.
Federal University of Santa Catarina - Brazil
Advisor

Prof. Christof Schulz, Ph.D
University of Duisburg-Essen - Germany
Co-advisor

FLORIANÓPOLIS, AUGUST 2009.

Development and Application of Detailed Chemical Kinetics Mechanisms for Ethanol and Ethanol Containing Hydrocarbon Fuels

by

Leonel Rincón Cancino

This doctoral thesis was judged adequate as partial requisite to the degree of

Doctor in Mechanical Engineering

and approved on its final version by the Graduate Program in Mechanical Engineering.

Prof. Amir Antônio Martins de Oliveira Junior, Ph.D.
Universidade Federal de Santa Catarina – UFSC - Brazil
Advisor

Prof. Christof Schulz, Dr. rer. nat. habil.
University of Duisburg - Essen - Germany
Co-advisor

Prof. Eduardo Alberto Fancello, D.Sc.
Coordinator of the Graduate Program in Mechanical Engineering – POSMEC - UFSC

Referee Committee

Prof. Luis Fernando Figueira da Silva, Dr.
Pontifícia Universidade Católica do Rio de Janeiro – PUC-Rio (Relator)

Edimilson Jesus de Oliveira, Dr.
Centro de Pesquisas e Desenvolvimento Leopoldo Américo Miguez de Mello - CENPES - PETROBRAS

Profa. Patrícia Regina Pereira Barreto, Dr.
Instituto Nacional de Pesquisas Espaciais – INPE

Prof. Guenther Carlos Krieger Filho, Dr. Eng.
Universidade de São Paulo - USP

Prof. Clovis Raimundo Maliska, Ph.D.
Universidade Federal de Santa Catarina – UFSC

Summary

List of Figures.

List of Tables

List of Symbols

ρ	[kg/m^3]	Density
u_i , u_j , u_k	[m/s]	Velocities
p	[bar]	Pressure
Y_k	[kg/kg]	Mass fraction of chemical species
μ	[N s/m^2]	Dynamic viscosity
D_k	[m^2/s]	Fick diffusion coefficient
h	[kJ/kg]	Enthalpy
V_k	[m/s]	Diffusion velocity
λ	[W/(m K)]	Thermal conductivity
T	[K]	Temperature
$\dot{Q}$	[W/m^3]	Volumetric energy generation
$\dot{\omega}$	[mol/(m^3 s)]	Reaction rate
t	[s]	Time
ν', ν''	---	Stoichiometric coefficient
W	[kg/mol]	Molar mass
k_f , k_b	mol, cm^3, s, K	Rate constants, *forward*, *backward*
E_a	[kJ/mol]	Activation Energy
T_a	[K]	Activation Temperature
A	---	Preexponential factor
$\Re$	[J/(mol K)]	Universal gas constant
p_r	---	Reduced pressure
l_0	[m]	Mean free path

c_p	[J/(kg K)]	Specific heat capacity
τ_{ing}	[μs]	Ignition delay time
ϕ	---	Stoichiometric ratio
Q_c , K_{eq}	---	Equilibrium constant
β	---	Temperature exponent (Arrhenius rate)
k	---	Rate coefficient vector
c	---	Chemical species concentration vector
Δt_{ms}	[μs]	Available time for measurements.

Dedication

This work is dedicated to:

- My Mother, Cecilia Cancino de Rincón, I am very grateful for the encouragement and support she has always give me.
- My Brothers, Cesar, Rosario and Costanza.
- My Nephews, Leonardo, Jhonatan Alberto and Amir Gabriel.
- My Uncles, Marina, Lucia and Ricardo.
- My Father, Alejando Rincón Osorio (in memoriam).

Acknowledgments

"…. Rejoice always, pray constantly, give thanks in all circumstances; for this is the will of God in Christ Jesus for you…."

I Thessalonians 5:16-18

I have benefited from the kindness, experience and technical expertise of numerous people during the development of this work. I would like to begin by thanking my excellent full supportive and encouraging thesis advisors Prof. Amir A.M. Oliveria Jr, and Prof. Christof Schulz. I always appreciated and benefited from the enthusiasm that you bring to research. Amir and Christof, I am very grateful for the guidance and timely advice you have always given me. I feel blessed to have had two brilliants advisors that I am happy to know as both colleagues and friends.

I would like to particularly express my sincere gratitude to Dr. Mustapha Fikri, who provided excellent tutoring in the development of this Doctoral thesis. Mustapha, thanks very much for assistance, timely information and friendship you have always given me.

Many thanks also go to my thesis committee member, Dr. Luis Fernando Figueira da Silva, Dr. Patrícia Regina Pereira Barreto, Dr. Guenther Carlos Krieger Filho, Dr. Clovis Raimundo Maliska and Dr. Edimilson Jesus de Oliveira. I have benefited from their enthusiastic involvement and contributions at thesis presentation and useful discussions at other times.

Many people have given me tremendous help on various parts of this thesis. I would like to thank Ms. Natascha Schlösser for teaching me the operation of the high pressure shock tube at IVG-UDE. Thank also to Mr. Marcos Longo for the help in the computer network at LABCET-UFSC. I also must deeply thank Dr. Alexander Konnov, Dr. John Simmie and Dr. Henry Curran for always begin available to answer my chemistry questions, timely information and discussions about ethanol and hydrocarbons fuel kinetics.

Financial support for this work was provided by *Conselho Nacional de Desenvolvimento Científico e Tecnológico* – CNPq – Brazil, *Deutscher Akademischer Austausch Dienst* – DAAD – Germany, *Institut für Verbrennung und Gasdynamik* – IVG at *Universität Duisburg-Essen – Germany*, and *Labotatório de Combustão e Engenharia de Sistemas Térmicos* – LABCET at *Universidade Federal de Santa Catarina* – Brazil.

I would like to thank the friends that have made my time at LABCET/Brasil and IVG/Germany fun. Thank you Alexandre Ryoiti Takahashi, Alvaro Hernán Restrepo Victoria,

Alvaro Nacif de Carvalho, Ana Paula Silva, Anne, Carla Souza and Gonçalo, Cindy Ibarra, Ciriam Lopez, Cirilo Seppi Bresolin, Cristina Stern, Dalton Bertoldi, Donato Gonçalves do Nascimento, Edevaldo Brandilio Reinaldo, Eduardo Choozo Arenas Kami (Kami, thanks very much for all moments and experiences shared and lived in Germany and Brasil, I always felt very close a big friend, like a brother here in Germany, thanks very much.!) , Eduardo Gonçalves Reimbrecht, Eduardo Morel Hartmann, Elaine Cardoso, Elthon Albanas, Eros Alfredo Jahn Filho, Fábio Kleveston, Fabyo Luis Pereira, Felipe Pereira Rodrigues, Fernando Lopez, Fernando Marcelo Pereira, Gilson Nunes Maia, Helena Nandi, Isaias Masiero, Jaime Lozano, Janaina Schmitt, Janilson da Rossa, Jesus Ortiz, José Alexandre Matelli, Juan Pablo Florez Mera, Kadu, Kamila Heffel Farias, Leonardo Lopez, Leticia Matelli, Lourival Mendes, Lucas Freitas Berti, Luis Clasen, Luis Evélio Garcia Acevedo, Luz Karime Hernandez Gegen, Manfred Molz, Marcelo (Xerox), Márcio Caldeira Pierobom, Marcio Demetrio, Marcos Francisco Longo, Marcos Picanço, Maria de Lourdes da Cunha, Maria Goreti Alves, Maria Luiza Bazzo, Omar Suescun, Patrícia Ortega, Paulo Henrique Dias dos Santos, Paulo Steidel, Prof. Antônio Carlos Ribeiro Nogueira, Prof. Edson Bazzo, Prof. Eduardo Fancello, Prof. Fernando Cabral, Prof. José A Bellini da Cunha Neto, Prof. Narciso Arroyo, Prof. Vicente de Paulo Nicolau, Rafael de Camargo Catapan, Rafael Hafemann Moser, Rafael Pugar, Raphael Guardini Miyake, Raquel Dotta Corrêa, Renan Manozzo Galante, Renato Oba, Renzo Fabrício Figueroa Piña, Ricardo Morel Hartmann, Rodrigo Pizarro, Rodrigo Velásquez, Rosinei e André Werle, Sara Dotta Corrêa, Sergio Pereira, Tales Jahn, Talita Sauter Possamai, Tatiana Pineda, Thiago Fabricius Konopka, Thiago Loss, Vanessa Michels, Veronica Moreno, Vicente de Paulo Nicolau, Vinicuis Ayello, William Carrillo Ibañez, Wilson Tafur and Yesid Ernesto Asaff Mendoza, Alana Byald, Ali Abdali, Anoop Gupta, Barbara Graf, Benjamin Tribalet, Birgit Nelius, Christian Hecht, Christopher Gessenhardt, Dennis Bensing, Dieter Hermanns, Dr. Ralf Starke. Dr. Thomas Dreier, Hans Orthner, Helmut Kronemayer, Huinan Yang, Irenäus Wlokas, Jörg Albrecht, Kemal Omerbegovic, Khadijeh Mohri, Ludger Jerig, Mark Colberg, Markus Röder, Martin Leschowski, Metehan Bozkurt, Michaela Hartmann, Miriam Primbs, Ms. Iris Steiner, My Yen Luong, Robin Devillers and Stephan Faust

Lastly, I would like to thank Tereza Aguiar, Nelton Velho, Moises, André, Beatriz, Helena and Gabriel, my dear Brazilian's parents, thank a lot for all moments during my stay in this big country, Brazil!!!!

Abstract

There are several reasons to the increased interest in ethanol as a fuel. In summary, there is a current global need of a) alternatives to conventional oil derived fuels, especially those obtained from renewable sources, b) reduction of pollutant and carbon emissions from energy and power systems, and c) additives to reduce engine knock. These needs are based on economic and environmental considerations. Part of the effort needed nowdays is centered on understanding the oxidation mechanisms of ethanol and ethanol containing fuels using a combination of simulation and fundamental experiments developed at conditions close to the applications. In order to contribute to this area, this work proposes several detailed kinetic models for pure ethanol and for multicomponent gasoline surrogate mixtures involving ethanol, iso-octane, n-heptane, toluene and di-iso-butylene. This work reports the first detailed kinetic model for ethanol and a five-component gasoline surrogate oxidation at high pressure and intermediate temperatures validated against shock tube ignition delay times.

Here, the thermal decomposition routes of ethanol are identified and discussed. A low temperature and high pressure oxidation route for ethanol is proposed for modeling pure ethanol and gasoline surrogates. The proposed detailed kinetics models were built by adding and tailoring kinetics submechanisms for each of the components of interest available in the literature. In order to validate the proposed detailed kinetic models, shock tube experiments of ignition delay times were performed at Institute for Combustion and Gasdynamic – IVG at the University of Duisburg-Essen, Germany. The experiments were performed for pure ethanol and for binary and ternary surrogate mixtures involving ethanol, covering a pressure range of 10 bar to 50 bar, temperature range of 690 K to 1220 K, for stoichiometric and lean mixtures of ethanol/air, and gasoline surrogate/air. These conditions approximate those reached in the operation of internal combustion engines in the automotive industry. To the author's knowledge, these are the highest pressures reported so far for ethanol oxidation. The tailored detailed kinetic models were then tuned to the experimental results of ignition delay time by using sensitivity analysis methods. Simulations using the SHOCK 1-D code from CHEMKIN package were performed in order to validate the proposed detailed kinetic models over the experimental conditions, and a good agreement was found.

Keywords: Ethanol, Gasoline surrogates, Detailed chemical kinetics models, Shock tube ignition delay.

Resumo

O crescente interesse em etanol como combustível é motivado por varias razões. Resumidamente, existe uma necessidade global de a) alternativas para combustíveis convencionais derivados do petróleo, especialmente aqueles obtidos de fontes renováveis, b) redução da emissão de dióxido de carbono e poluentes a partir da produção de energia em sistemas de potência, e c) aditivos para reduzir a batida de pino em motores a combustão interna. Estas necessidades são fundamentadas em considerações econômicas e ambientais. Parte do esforço requerido hoje em dia é centrado no entendimento dos mecanismos de oxidação de etanol e de misturas de combustíveis de contendo etanol, usando uma combinação de simulação numérica e experimentos fundamentais realizados em condições similares às aplicações.

Para contribuir nesta área, este trabalho propõe vários modelos cinéticos detalhados para etanol puro, e para misturas multicomponentes de substitutos de gasolina contendo etanol, iso-octano, n-heptano, tolueno e di-iso-butileno. Este trabalho apresenta o primeiro modelo cinético detalhado para a oxidação de etanol e para uma mistura quinária de substitutos de gasolina, a altas pressões e temperaturas intermediárias, validado com medições de atraso de ignição em tubo de choque. As rotas da decomposição térmica do etanol são identificadas e discutidas. Uma rota de oxidação de etanol a baixas temperaturas e altas pressões é proposta para a modelagem de etanol puro e substitutos de gasolina contendo etanol.

Os modelos cinéticos detalhados propostos foram construídos adicionando e juntando subestruturas cinéticas de cada espécie química de interesse disponíveis na literatura. Para validar os modelos cinéticos detalhados propostos, experimentos de atraso de ignição em tubos de choque foram realizados no Instituto de Combustão e Dinâmica de Gases – IVG na Universidade de Duisburg-Essen, Alemanha. Os experimentos foram realizados para etanol puro e para misturas binárias e ternárias de substitutos de gasolina contendo etanol, em uma faixa de pressão de 10 até 50 bar, temperaturas de 690 K até 1220 K, misturas pobres e estequiométricas de etanol/ar e substituto de gasolina/ar.

Estas condições aproximam as condições reais de operação de motores a combustão interna na indústria automotiva. No conhecimento do autor, as pressões nas quais as medições foram realizadas são as mais altas já reportadas na literatura para etanol. Os modelos cinéticos detalhados propostos neste trabalho foram ajustados para reproduzir os resultados experimentais de atraso de ignição, usando métodos de análise de sensibilidade. Foram

realizadas simulações usando o pacote SHOCK 1-D do programa CHEMKIN para validar os modelos cinéticos propostos nas condições experimentais de temperatura e pressão, boa concordância entre resultados numéricos e experimentais foi encontrada.

Palavras Chave: Etanol, Substitutos de gasolina, Modelos cinéticos detalhados, Atraso de ignição em tubo de choque.

Resumen

El creciente interés en etanol como combustible es motivado por varias razones. De forma resumida, existe una necesidad global de a) alternativas para combustibles convencionales derivados del petróleo, especialmente de aquellos obtenidos de fuentes renovables, b) reducción de la emisión de carbono e contaminantes a partir de la producción de energía y sistemas de potencia, y c) aditivos para reducir el cascabeleo (knock) en motores a combustión interna. Estas necesidades se fundamentan en consideraciones económicas y ambientales. Parte del esfuerzo requerido hoy en día es centrado en el entendimiento de los mecanismos de oxidación de etanol y de mezclas de combustibles conteniendo etanol, usando una combinación de simulación numérica y experimentos fundamentales realizados en condiciones similares a las de las aplicaciones. Para contribuir en esta área, este trabajo propone varios modelos cinéticos detallados para etanol puro y para mezclas multicomponentes de substitutos de gasolina conteniendo etanol, iso-octano, n-heptano, tolueno y di-iso-butileno. Este trabajo presenta el primer modelo cinético detallado para la oxidación de etanol e para una mezcla quinaria de substitutos de gasolina, a altas presiones y temperaturas intermediarias, validado con mediciones de atraso de ignición en tubo de choque. Las rutas de descomposición térmica de etanol son identificadas y discutidas. Una ruta de oxidación de etanol a bajas temperaturas y altas presiones es propuesta para la modelación de etanol puro y substitutos de gasolina conteniendo etanol. Los modelos cinéticos propuestos fueron construidos adicionando e uniendo subestructuras cinéticas de cada especie química de interés disponible en la literatura. Para validar los modelos cinéticos detallados propuestos, experimentos de atraso de ignición en tubos de choque fueron realizados en el Instituto de Combustión y Dinámica de Gases – IVG, en la Universidad de Duisburg-Essen, Alemania. Los experimentos fueron realizados para etanol puro y para mezclas binarias y cuaternarias de substitutos de gasolina conteniendo etanol, en una facha de presión de 10 hasta 50 bar, temperaturas de 690 K hasta 1220 K, mezclas pobres y de composición estequiométrica de etanol/aire e substituto de gasolina/aire. Estas condiciones de temperatura y presión se aproximan a las condiciones reales de operación de motores a combustión interna en la industria automotriz. En el conocimiento del autor, los resultados de oxidación térmica de etanol en los niveles de presión presentados en este trabajo son los más altos ya reportados en la literatura. Los modelos cinéticos detallados propuestos en este trabajo fueron ajustados para reproducir los resultados experimentales de atraso de ignición usando métodos de análisis de sensibilidad. Fueron realizadas simulaciones usando o código

SHOCK 1-D de el programa CHEMKIN para validar los modelos cinéticos propuestos, en las condiciones experimentales de temperatura y presión, buena concordancia entre los resultados numéricos y experimentales fue encontrada.

Palabras clave: Etanol, Substitutos de gasolina, Modelos cinéticos detallados, Atraso de ignición en tubo de choque.

Chapter 1: Introduction

Research institutions and industry have spent a considerable amount of resources in developing methods for the numerical simulation of practically relevant processes covering several areas. Usually, simulations aim at yielding information at lower cost compared to experimental approaches and frequently simulations provide details that are inaccessible in experiments. This is especially true in the simulation of combustion processes, in which more complete information can be acquired from simulations than from experiments with relatively low cost. This information can then be used to the design of combustion devices, for example, to predict the temperature and pressure distribution as well as chemical species formation/depletion during the energy release inside the combustion chamber of an internal combustion engine. Once this information is obtained, new parameters concerning the engine design and operation could be adopted. The same can be said of the development of fuel mixtures where minute variations of components may result in large variations of performance.

There are several critical points when simulating combustion processes. For example, sometimes it is only important to know approximately the maximum temperature and global reaction rate in a given process. Then, usually the modeling with a simple global kinetics model suffices to represent the kinetics process. Other times, however, the target is to determine the concentration of a specific chemical species, such as the hydroxyl radical, and in this case a somewhat more refined detailed kinetics model is needed to represent the kinetics process. In summary, the simulation of the dynamics of a combustion process frequently requires some kinetics modeling and the complexity of such modeling grows as more detailed information is pursued.

The automotive industry presents a particular environment in which experiment, modeling and computation of the behavior of combustion has the potential to aid in performing engine optimization, develop in-cylinder and after-burn pollutant control and to synthesize new formulations for practical fuels. However, as much as computational resources, numerical methods and chemical knowledge have increased over the last few years, the combustion of practical fuels is still basically investigated using experimental approaches. The reason for this limitation is the inherent complexity of the fuel mixtures.

1.1 Practical fuels and gasoline surrogates

As mentioned by Westbrook et al. (2005), computer modeling has grown rapidly to play a major role in virtually every field of science and engineering. Today it is common to find numerical models attempting to represent combustion process of single hydrocarbon fuels, and depending on the desired quality or target of the results, one may find global or detailed kinetics mechanisms. In this direction, many researchers have devoted considerable time studying and proposing global and detailed kinetics models (see, for example, references in Griffiths, 1995 and Simmie, 2003) for pure hydrocarbon oxidation. The number of chemical species that can be present in a real gasoline can be, however, in the order of hundreds, involving saturated and unsaturated hydrocarbons including alkanes, cycloalkanes, alkenes, cycloalkenes, aromatic, ethers and esters, components whose identity and amounts are often unknown (Metcalfe et al. 2007). The well-known kinetic model for pure iso-octane oxidation of Curran et al. (2002) is composed by 857 chemical species allowing 3606 elementary reactions. A detailed kinetics model for a practical fuel involving a hundred of chemical species in the fuel composition would demand a dramatically increase in the number of elementary reactions, making the problem intractable with current computational capabilities.

The development of gasoline surrogates is one of the ways to make the development of chemical kinetics mechanisms for practical fuels tractable. A surrogate fuel consists of a mixture of a small number of components that are used to represent the practical fuel and still predict characteristics of the real fuel. These desirable characteristics may include ignition behavior, burning velocity, viscosity, vaporization, and emission such as carbon monoxide, hydrocarbons, soot and nitrogen oxides (Metcalfe et al. 2007). The early kinetics modeling studies of n-heptane by Curran et al. (1998b) and iso-octane by Curran et al. (2002) covering the parameters used to qualified fuel ignition, the Research Octane Number – RON and the Motor Octane Number – MON, were first attempts to develop gasoline fuel surrogates. The RON and MON scales are both based on Primary Reference Fuels – PRF, n-heptane (RON = MON = 0) and iso-octane (RON = MON = 100), and are used to qualify the knocking behavior of real fuels. However, real gasoline fuels are not composed only by n-heptane and iso-octane. In fact, gasoline consists of many different classes of saturated and unsaturated hydrocarbons, including straight and branched alkanes (n-parafins, iso-parafins), cicloalkanes (naphthenes), alkenes (olefins), cicloalkenes (cycloolefins) and aromatics (Aryl compounds). Table 1 from Cataluña and Silva (2006) lists the chemical composition of a typical Brazilian base gasoline (without the addition of ethanol) as volume percent of the fuel total volume.

The chemical composition is listed according to the carbon atoms present in the hydrocarbon group.

Table 1. Chemical composition of one kind of Brazilian base gasoline (mol %) (Adapted from Cataluña and Silva, 2006).

	Saturated compounds		**Unsaturated compounds**		
	n-parafins	**iso-parafins**	**naphthenes**	**olefins**	**aromatics**
	[%]	**[%]**	**[%]**	**[%]**	**[%]**
C4	1.07	***	***	0.04	***
C5	5.07	5.10	0.65	0.06	***
C6	5.10	6.50	4.30	10.50	0.51
C7	4.40	5.20	7.20	***	16.60
C8	5.20	16.65	3.15	0.01	0.41
C9	0.12	0.60	0.30	0.07	***
C10	***	***	***	***	***
C11	***	***	***	***	***
Total	**21.0**	**34.2**	**14.6**	**10.7**	**17.5**

From Table 1 one can see that in the group of n-parafins, the pentanes, hexanes, heptanes and octanes (C_5, C_6, C_7 and C_8) compounds are predominant. In the iso-parafins group, the octane is predominant. The cycloalkanes with seven carbon atoms represent about 50% of the naphthenes group. The alkenes with six carbon atoms characterize the olefins group and finally, the toluene represents about 95% of the aromatic group.

One approach to surrogate fuels is to include one or more components from each group of hydrocarbons present in gasoline, so that the unique molecular structure of each group is represented. For example, one may suggest a gasoline surrogate for the Brazilian base gasoline from Table 1, as follows: n-octane (or n-heptane) 21%, iso-octane 34.2%, methyl-cyclohexane (or cycloheptane) 14.6%, 1-hexene (or diisobutylene) 10.7% and toluene 17.5%. The di-iso-butylene is intended to represent the hydrocarbon class of alkenes in practical fuels (Metcalfe et al. 2007).

This approach may lead to reliable predictions of many of the combustion properties of the practical fuel. In order to obtain a fuel surrogate mechanism, detailed kinetics mechanisms must be developed for each component in the mix compound (Metcalfe et al. 2007).

1.1.1 Molecular structure of gasoline surrogates considered in this work

The proposed gasoline surrogate is composed of ethanol (oxygenated hydrocarbon), iso-octane (saturated iso-parafin), n-heptane (saturated n-parafin), toluene (unsaturated

aromatic) and diisobutylene (unsaturated olefin). The selected chemical species cover the major hydrocarbon class constituents of the gasoline. Figure 1 shows the different molecular structures of the hydrocarbons selected in this work as components of gasoline surrogates.

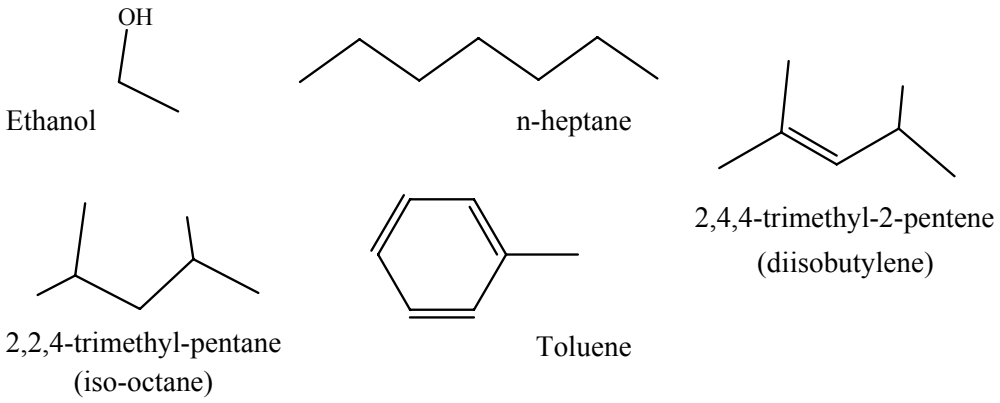

Figure 1. Structure of the components of the gasoline surrogates considered in this work.

Table 2 list some properties of the components of the gasoline surrogates considered in this work.

Table 2. Properties of the components of thegasoline surrogates considered in this work

Name	**Ethanol**	**Pentane, 2,2,4-trimethyl-**	**Heptane**	**Toluene**	**2-Pentene, 2,4,4-trimethyl-**
Other names	Ethyl alcohol; Alcohol; Alcohol anhydrous	iso-octane	n-Heptane; Dipropylmethane	Toluol; Methane, phenyl-	di-iso-butylene, DIB
Formula	C_2H_5OH	C_8H_{18}	C_7H_{16}	C_7H_8	C_8H_{16}
Molecular weight	46.06	114.228	100.2	92.13	112.21
Enthalpy of vaporization [kJ/mol]	38.56 (@ 351.5 K)	30.79 (@ 372.4 K)	31.77 (@ 371.6 K)	33.18 (@ 383.8 K)	35.2 (@ 374.6 K)
Enthalpy of fusion [kJ/mol]	3.14 (@ 111.4 K)	9.2115 (@ 165.79 K)	13.99 (@ 182.57 K)	6.636 (@ 178.15 K)	6.8 (@ 166 K)
Constant pressure heat capacity of liquid [J/mol K]	112.4 (@ 298.15 K)	242.49 (@ 298.15 K)	224.64 (@ 298.15 K)	157.09 (@ 298.15 K)	233.5 (@ 296 K)

Font: National Institute of Standards and Technology - http://webbook.nist.gov/

1.2 Thesis objectives

This work attempts to supply a detailed kinetics model for simulation purposes and experimental data for the validation process. The objectives can be listed as:

General objective

Development and application of detailed chemical kinetics mechanisms for pure ethanol and ethanol containing multi-component gasoline surrogates.

Specific objectives

In order to reach the general objective, several targets were pursued in both, the numerical and experimental approaches:

- The development of a detailed kinetics model for ethanol oxidation for the conditions found in internal combustion engines, both in high pressures and intermediate temperatures,
- The use of a tailoring process to the development of detailed kinetics models for oxidation of multi-component gasoline surrogates including ethanol, iso-octane, n-heptane and toluene,
- The measurement of ignition delay times in shock tube as an experimental technique to provide temperature and pressure dependent data to develop and test detailed chemical kinetics models,
- The use of computational tools as sensitivity analysis for improvement of detailed kinetics models.

1.3 Thesis organization

This manuscript is structured in five chapters, beginning in chapter 1 with the objectives and contributions.

In chapter 2, the basic theories about the different areas involved in this work are reviewed. The chapter starts with a review of the numerical modeling of combustion process and the set of equations for laminar and RANS turbulent models are reviewed. Then, the structure of macroscopic chemical kinetics models are presented with emphasis to the submechanisms for small hydrocarbons, ethanol and primary reference fuels. The fundamentals of chemical kinetics mechanism applied to hydrocarbon oxidation are discussed. The sensitivity analysis of chemical kinetics models is presented as a computational tool for optimization process of large chemical schemes and an extension of this methodology developed in this work is explained. The fundamentals of shock tubes are reviewed in two sections, one describing the shock tube experiments and the other presenting the shock wave theory involving only two topics; the physics of shock waves and the modeling of the CHEMKIN SHOCK package of the flow behind a shock wave. The simulation of compressible flow in shock tubes is commented in two sections; one on

interaction of propagating shock wave and turbulence and the other on shock wave and boundary layer interaction in shock tubes.

In chapter 3, the experimental approach used in this work is described. The chapter starts with the description of the High Pressure Shock Tube at University of Duisburg-Essen and then follows describing the mixture preparation and measurement procedures. Then the results of ignition delay times from all experiments performed in this study; Ethanol pure, Gasoline Surrogate A (ethanol / iso-octane – 25% / 75% by liquid volume), and Gasoline Surrogate B (ethanol / iso-octane / n-heptane / toluene – 40% / 38.7% / 10.2% / 12% by liquid volume) are presented and discussed.

In chapter 4, the simulation models adopted in this work are presented. The chapter starts with the description of the tailoring process of the kinetics models adopted. The proposed detailed kinetics model for ethanol oxidation is explained and the results of the validation against the measurements are presented. The numerical results for the multi-component gasoline surrogate models; GS-A (ethanol / iso-octane / n-heptane), GS-B (ethanol / iso-octane / n-heptane / toluene), GS-C (ethanol / iso-octane / n-heptane), GS-D (iso-octane / n-heptane / toluene) and GS-E (ethanol / iso-octane / n-heptane / di-isobutylene) are also presented.

Finally, in chaper 5, conclusions and recommendations for future work involving ethanol kinetics and gasoline surrogates are presented, followed by references and appendices.

Chapter 2: Background

2.1 Numerical modeling of combustion processes

The modeling of chemically reacting flow and heat transfer demand the solution of conservation equations for mass, momentum, energy and mass of chemical species. This set of conservation equations has to be solved with a chemical kinetics mechanism which describes the transformation of reactants to products. The development of this set of conservation equations is available elsewhere (Kuo, 1986; Peters, 2000; Poinsot e Veynante, 2001).

2.1.1 Transport equations for laminar chemically reacting fluid flow

The modeling of reacting fluid flow in the continuum regime is based on the conservation equations that can be written as (Poisont and Veynante, 2001):

Mass:

$$\frac{\partial \rho}{\partial t} + \frac{\partial \rho u_i}{\partial x_i} = 0 \ , \qquad [1]$$

Momentum:

$$\begin{aligned} &\frac{\partial}{\partial t}\rho u_j + \frac{\partial}{\partial x_i}\rho u_i u_j = -\frac{\partial p}{\partial x_j} + \frac{\partial \tau_{ij}}{\partial x_i} + \rho \sum_{k=1}^{N} Y_k f_{k,j} \quad , \\ &\tau_{ij} = -\frac{2}{3}\mu \frac{\partial u_k}{\partial x_k}\delta_{ij} + \mu\left(\frac{\partial u_i}{\partial x_j} + \frac{\partial u_j}{\partial x_i}\right) \quad , \end{aligned} \qquad [2]$$

Energy:

$$\begin{aligned} &\frac{\partial \rho h}{\partial t} + \frac{\partial}{\partial x_i}\left(\rho u_i h\right) = \frac{Dp}{Dt} - \frac{\partial q_i}{\partial x_i} + \tau_{ij}\frac{\partial u_i}{\partial x_j} + \dot{Q} + \rho \sum_{k=1}^{N} Y_k f_{k,i} V_{k,i} \quad , \\ &q_i = -\lambda \frac{\partial T}{\partial x_i} + \rho \sum_{k=1}^{N} h_k Y_k V_{k,i} \quad , \end{aligned} \qquad [3]$$

Mass of chemical species *k*:

$$\begin{aligned} &\frac{\partial \rho Y_k}{\partial t} + \frac{\partial \rho u_i Y_k}{\partial x_i} = \frac{\partial}{\partial x_i}\left(\rho D_k \frac{\partial Y_k}{\partial x_i}\right) + \dot{\omega}_k, \quad k = 1,...,N. \\ &\rho Y_k V_{k,i} = -\rho D_k \frac{\partial Y_k}{\partial x_i} \end{aligned} \qquad [4]$$

In equations [1], [2], [3] and [4] $V_{k,i}$ represents the diffusion velocity, assumed to be proportional only to the gradient of the mass fraction, i.e., modeled by Fick's Law for a multi-component mixture, $f_{k,i}$ represents the body force f acting over the chemical species k in the direction i, $\dot{Q}$ is the source term of volumetric energy generation by other mechanisms not related to combustion and phase change, q_i represents the conduction heat transfer flux, modeled by Fourier's Law with an additional contribution from the mass diffusion, τ_{ij} represents the viscous stress tensor, modeled assuming a Newtonian fluid, Dp/Dt is the material derivate of the pressure p, λ represents the molecular thermal conductivity of the mixture, Y_k represents the mass fraction of chemical species k, D_k represents the Fick diffusion coefficient of species k in the mixture, ρ represents the density, u_i represents the component i of the velocity u, h represents the enthalpy, μ represents the dynamic viscosity and $\dot{\omega}_k$ represents the reaction rate of species k calculated using a chemical kinetics mechanism.

The multi-component mass diffusion modeling by Fick's Law may result in problems of global mass balance. Some techniques are used to guarantee the mass balance, and these are reviewed by Poinsot and Veynante (2001). Bird et al. (1954) and Kuo (1986) reviewed the fundamental models for transport properties in mixtures.

In order to obtain the reaction rate of species k, the reactions of the kinetics model can be represented as:

$$\sum_{k=1}^{N} \nu'_{k,j} \mathrm{M}_k = \sum_{k=1}^{N} \nu''_{k,j} \mathrm{M}_k \quad for \;\; j = 1,...,M \,, \qquad [5]$$

where N is the number of chemical species, M is the number of chemical reactions, $\nu'_{k,j}$ and $\nu''_{k,j}$, are the stoichiometric coefficients of species k, in the reaction j, in the reactants side and in the products side, respectively.

Naming W_k the molar mass of species k, the mass conservation requires

$$\sum_{k=1}^{N} \nu'_{k,j} W_k = \sum_{k=1}^{N} \nu''_{k,j} W_k \quad or \quad \sum_{k=1}^{N} \nu_{k,j} W_k = 0 \quad for \;\; j = 1,..,M \,, \qquad [6]$$

where

$$\nu_{k,j} = \nu''_{k,j} - \nu'_{k,j} \,. \qquad [7]$$

The reaction rate for species *k* is given by the sum of its production or depletion rates in each chemical reaction forming the kinetics model,

$$\dot{\omega}_k = \sum_{j=1}^{M} \dot{\omega}_{k,j} = W_k \sum_{j=1}^{M} v_{k,j} Q_j \quad with \quad \frac{\dot{\omega}_{k,j}}{W_k v_{k,j}} = Q_j , \qquad [8]$$

where Q_j is the progress rate of the chemical reaction *j*.

Mass conservation requires that the sum of the reaction rates of all chemical species is zero, i.e.,

$$\sum_{k=1}^{N} \dot{\omega}_k = \sum_{j=1}^{M} \left(Q_j \sum_{k=1}^{N} W_k v_{k,j} \right) = 0 . \qquad [9]$$

Using the Law of Mass Action, the progress rate of reaction *j* is a function of both forward and reverse rates of reactions with chemical kinetics constants $k_{f,j}$ and $k_{b,j}$ respectively;

$$Q_j = k_{f,j} \prod_{k=1}^{N} \left(\frac{\rho Y_k}{W_k} \right)^{v'_{k,j}} - k_{b,j} \prod_{k=1}^{N} \left(\frac{\rho Y_k}{W_k} \right)^{v''_{k,j}} , \qquad [10]$$

where the ratio $\rho Y_k / W_k$ is the molar concentration of species *k*.

Determining these rate constants, $k_{f,j}$ and $k_{b,j}$, constitutes a central problem in combustion modeling. For elementary reactions, they are modeled by using an extended form of Arrhenius law,

$$k_{f,j} = A_{f,j} T^{\beta_j} \exp\left(-\frac{E_{a,j}}{\Re T} \right) = A_{f,j} T^{\beta_j} \exp\left(-\frac{T_{a,j}}{T} \right), \qquad [11]$$

where $A_{f,j}$ is the pre-exponential factor, $E_{a,j}$ is the activation energy, β_j is the temperature exponent for reaction *j* and $\Re$ is the universal gas constant. The ratio of activation energy to universal gas constant also can be represented as an activation temperature, $T_{a,j}$. The description of kinetics models will be explored in section 2.2.

The system of conservation equations is closed with the fluid equation of state $\rho = \rho(T, p)$ and caloric equations of state for the calculation of specific enthalpy and entropy. For ideal gases, these can be obtained from the integration of specific heat functions expressed in polynomial form (NASA Glenn thermodynamic database). This set of equations is used to solve reacting fluid flow in laminar regime and is the same used in the Direct

Numerical Simulation – DNS for turbulent flow, using mesh resolution and time steps according to the DNS technique.

Alternative methodologies not involving DNS are the Large Eddy Simulation – LES and Reynolds Averaged Navier Stokes – RANS approaches. In the next section, the equations used in the RANS models are reviewed.

2.1.2 Transport equations for turbulent combustion by using RANS

Introducing the concept of Favre averaging (Favre, 1969) of the conservation equations, the averaged conservation equations become:

Mass:

$$\frac{\partial \overline{\rho}}{\partial t} + \frac{\partial}{\partial x_i}\left(\overline{\rho}\tilde{u}_i\right) = 0\,, \qquad [12]$$

Momentum:

$$\frac{\partial \overline{\rho}\tilde{u}_j}{\partial t} + \frac{\partial}{\partial x_i}\left(\overline{\rho}\tilde{u}_i\tilde{u}_j\right) + \frac{\partial \overline{p}}{\partial x_j} = \frac{\partial}{\partial x_i}\left(\overline{\tau}_{ij} - \overline{\rho}\widetilde{u_i''u_j''}\right), \qquad [13]$$

Energy:

$$\frac{\partial \overline{\rho}\tilde{h}_s}{\partial t} + \frac{\partial}{\partial x_i}\left(\overline{\rho}\tilde{u}_i\tilde{h}_s\right) = \overline{\dot{\omega}_T} + \frac{\overline{Dp}}{Dt} + \frac{\partial}{\partial x_i}\left(\overline{\lambda\frac{\partial T}{\partial x_i}} - \overline{\rho}\widetilde{u_i''h_s''}\right) + \overline{\tau_{ij}\frac{\partial u_i}{\partial x_j}} - \frac{\partial}{\partial x_i}\left(\overline{\rho\sum_{k=1}^{N}V_{k,i}Y_k h_{s,k}}\right)\,,$$
$$\frac{\overline{Dp}}{Dt} = \frac{\partial \overline{p}}{\partial t} + \overline{u_i\frac{\partial p}{\partial x_i}} = \frac{\partial \overline{p}}{\partial t} + \tilde{u}_i\frac{\partial \overline{p}}{\partial x_i} + \overline{u_i''\frac{\partial p}{\partial x_i}}\,, \qquad [14]$$

Mass of chemical species:

$$\frac{\partial \overline{\rho}\tilde{Y}_k}{\partial t} + \frac{\partial}{\partial x_i}\left(\overline{\rho}\tilde{u}_i\tilde{Y}_k\right) = -\frac{\partial}{\partial x_i}\left(\overline{V_{k,i}Y_k} - \overline{\rho}\widetilde{u_i''Y_j''}\right) + \overline{\dot{\omega}_k}\,, \qquad [15]$$

In equations [13], [14] and [15], terms involving means of fluctuation appear as a result of the averaging process. These terms, $\overline{\rho}\widetilde{u_i''u_j''}$, $\overline{\rho}\widetilde{u_i''h_s''}$ e $\overline{\rho}\widetilde{u_i''Y_j''}$, were grouped with the diffusive terms and require a treatment for the closure of the system of equations. The terms $-\overline{\rho}\widetilde{u_i''u_j''}$ are called Reynolds stresses. Wilcox (1994) presents the derivation of an equation for the Reynolds stresses, starting with the six stress components and showing the difficulties related to a rigorous treatment of these terms.

The last term in equation [15], demands special attention. This term represents the time-average of the reaction rate of chemical species *k*. It must be observed that, in general,

the average value of the reaction rate is not equal to the reaction rate calculated using the mean values of temperature and mass fraction, because the fluctuations can be expressive, when compared to the mean values.

The numerical solution of the last set of equations gives the numerical response a combustion process. Depending on the level of the phenomenological complexity allowed in the numerical simulation the numerical solution using current computational resources may not be possible or tractable. Figure 2 presents a diagram of the computational viability as related to the phenomenological complexity in the numerical simulation of a combustion process.

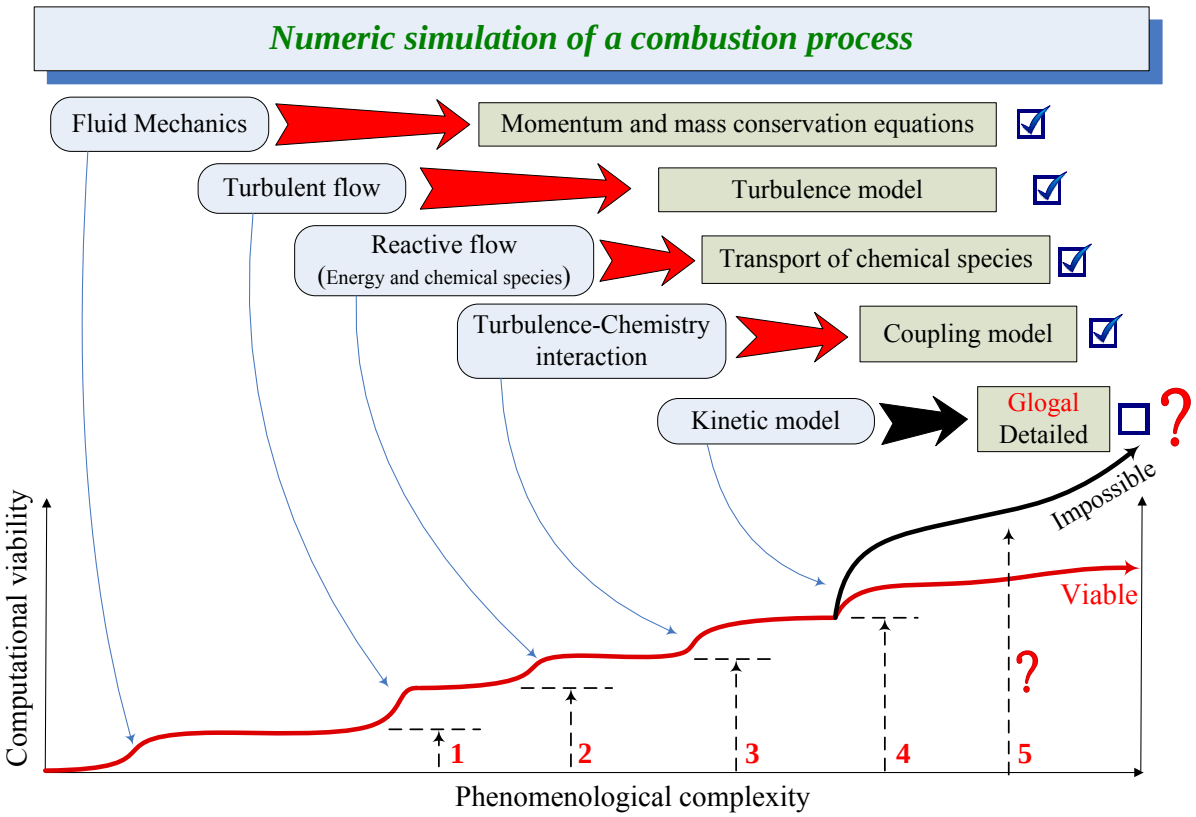

Figure 2. Computational viability related to the phenomenological complexity in the numerical simulation of a combustion process

The first stage of the computational difficulty in Figure 2 is related to the solution of the momentum equations and global mass conservation; interpolation functions, pressure-velocity coupling, and other numerical factors. The second stage is associated to the flow regime. A great part of the combustion applications are in turbulent regime, this aspect demanding the choice of a turbulence model.

The third level of computational difficulty is related to the reactive flow regime. This involves the solution of the energy conservation equation and the solution of a set of (N – 1) conservation equations of the N chemical species present in the combustion process. The interaction of turbulence and chemistry gives the fourth increase in the computational complexity. Different approaches have been used in order to represent this interaction such as Laminar finite-rate, Eddy dissipation, Laminar finite-rate/Eddy dissipation and EDC Eddy Dissipation Concept, to cite only the commonly available in commercial CFD packages. They are not, by far, general and much development is needed. The fifth increment in the computational complexity is related to the kinetics model used to represent the formation/depletion of chemical species. The chemical kinetics model employed plays an important role in the computational viability of a numerical simulation. Figure 3 presents schematically the influence of the kinetics model (global or detailed), on the computational viability for a numerical simulation of a combustion process.

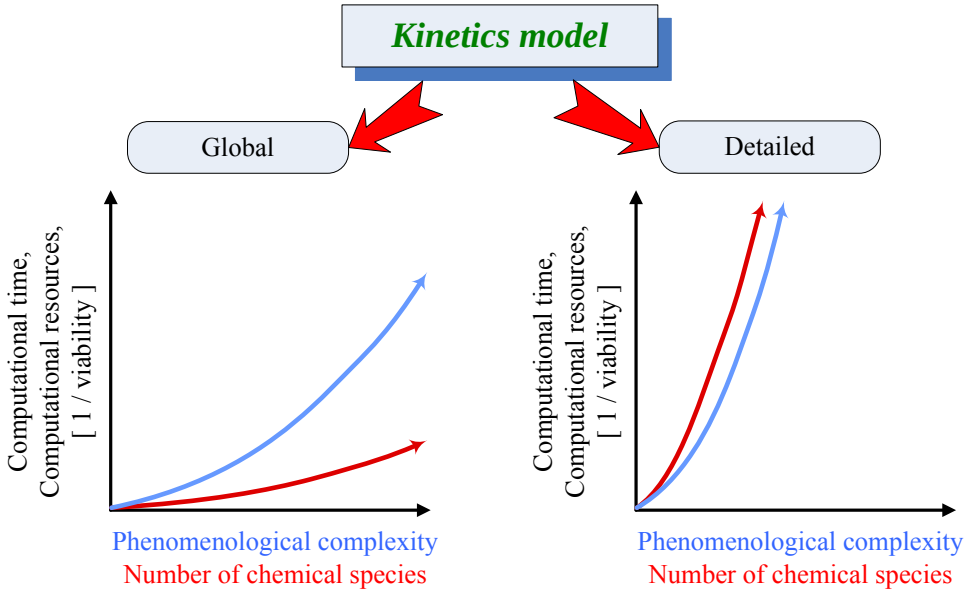

Figure 3. Influence of the kinetics model on the computational time, computational resources and viability of a numerical simulation of a combustion process.

When a global kinetics model (reduced model, small number of chemical species) is chosen the simulation becomes viable using current computational resources including many phenomenological complexities of the real process. When a detailed kinetics model is selected, the numerical simulation viability is limited to a discrete number of chemical species and a limited description of the phenomenological complexities.

2.2 Chemical kinetics models

The chemical kinetics models feed the reaction rate term in equation [10]. The description of chemical kinetics, depending on the level of complexity, can be classified as global, reduced or detailed. The difference between detailed or semi-detailed mechanisms consists in the number of simplifications, such as quasi steady-state and equilibrium concentrations of intermediate species, assumed when arriving at the final set of reactions. This results in a smaller number of chemical species and chemical reactions in reduced schemes, when compared to detailed mechanisms for the same set of reactants. Therefore, the number of equations of conservation of mass of chemical species required to describe the combustion problem can be significantly smaller when using global or reduced chemical kinetics models.

2.2.1 Global kinetics models

Frequently, the target of the numerical solution of a given industrial application is only a reduced set of characteristic parameters of the combustion process, for example, the temperature, the pressure, the concentration of one or two chemical species, or a global fuel burning rate. Depending on the accuracy required, this small set of parameters can be predicted using global kinetics models. Since this result in a small number of chemical species involved in the problem, the solution of the set of conservation equations is relatively fast and the computational time in the numerical simulations is then reduced.

Global kinetics models are limited to a small number of chemical reactions (steps) and species. It is very common to find global models of one or two steps involving three or four chemical species for the most common hydrocarbons used in the industry. Westbrook and Dryer (1981) presented a database of reduced kinetics models for the combustion of CH_4, C_2H_6, C_3H_8, C_4H_{10}, C_5H_{12}, C_6H_{14}, C_7H_{16}, C_8H_{18}, C_9H_{20}, $C_{10}H_{22}$, CH_3OH, C_2H_5OH, C_6H_6, C_7H_8, C_2H_4, C_3H_6 and C_2H_2 with air. They present the global reaction rate in the form:

$$k_{ov} = AT^{\beta} \exp(-E_a / \Re T)[Fuel]^a [Oxidizer]^b . \qquad [16]$$

In equation [16], A is the pre-exponential factor, β is the temperature exponent, E_a is the activation energy, $\Re$ is the universal gas constant, [*Fuel*] and [*Oxidizer*] represent the concentrations of fuel and oxidizer with its concentration exponents a and b respectively.

Westbrook and Dryer (1981) provide a table with parameters A, β, E_a, a, b for single-step and two-steps mechanisms. Commercial CFD codes, such as FLUENT and ANSYS-CFX have implemented global kinetics models for several practical fuels of common use in the industry. Global kinetics models make it possible the numerical simulation of reacting flows in complex geometries with the present widely available computational resources.

2.2.2 Detailed kinetics models

Detailed kinetics models provide more in-depth information into the time and spatial evolution of the concentration of chemical species in a combustion system. A well structured detailed kinetics model must be able to describe all the stages of the kinetics process, beginning with the pyrolysis/thermal decomposition of the fuel, followed by the total or partial depletion of the fuel, formation and consumption of intermediate species and finally describing the formation of saturated combustion products.

2.2.2.1 Fundamentals of the chemical kinetics mechanisms of oxidation of hydrocarbons

The oxidation of hydrocarbons proceeds either by hydrogen atom abstraction or by cleavage of C–C bonds at primary or secondary carbon atoms. In the case of aliphatic alcohol hydrocarbons, the hydroxyl group plays a very important role for the oxidation and as a third pathway the cleavage of the C–O bond can occur. Any of the three paths proceeds after a temperature activated perturbation of the energy field of the molecule and can proceed either intramolecular (isomerization) giving several sub-structures or as a result of collision with active radical species. Independently of the case, reaction mechanisms show several characteristic properties. Usually, reaction mechanisms in combustion follow a chain process composed by initiation, propagation, branching and termination reactions. As an example, we can take the mechanism for the ignition process of the hydrogen-oxygen system.

Table 3 shows the set of the most important reactions with respect to the low pressure high temperature ignition in the hydrogen-oxygen system. The initiation reaction produces active radical species. The propagation reactions produce the same number of radicals as are consumed. The chain branching reactions produce more active radical species than are consumed. Finally, the chain termination reactions lead active to stable species, at the vessel surface (R5) or in the gas phase (R6).

Table 3. Most important reactions with respect to ignition in the hydrogen-oxygen system (adapted from Warnatz et al., 1999).

rxr #	Reaction							Kind
(1)	H2	+	O2	=	2 OH•			chain initiation
(2)	OH•	+	H2	=	H2O	+	H•	chain propagation
(3)	H•	+	O2	=	OH•	+	O•	chain branching
(4)	O•	+	H2	=	OH•	+	H•	chain branching
(5)	H•			=	1/2 H2			chain termination (heterogeneous)
(6)	H•	+	O2 + M	=	HO2	+	M	chain termination (homogeneous)

The oxidation of hydrocarbons also follows a chain process. Methane was the first hydrocarbon analyzed because of its simplicity. The first detailed kinetics model for high temperature oxidation of methane dealt with the methane reaction as an H-atom abstraction sequence from methane, forming methyl radical (CH_3), with posterior conversion to formaldehyde (CH_2O), and then to formyl radical (HCO) and carbon monoxide (CO) and finally oxidation to carbon dioxide (CO_2). This kinetics scheme for methane was discarded, because it was soon verified that CH_3 can recombine to ethane C_2H_6 and finally form H_2O and CO_2 (Westbrook et al., 2005). Afterward, a very important conclusion was obtained: A detailed kinetics model can be structured in a hierarchical form, taking as base the kinetics of small hydrocarbons and completing the kinetics model with additional reactions for the bigger chemical species. Figure 4 shows a schematic representation of the hierarchy of the kinetics model for hydrocarbons oxidation.

As an example of a detailed kinetics model, in the following, the detailed kinetics model for the H_2/O_2 system is presented. The model presented is a simplification of the first version of the GRIMech 3.0 mechanism and allows 28 elementary reactions among 9 chemical species.

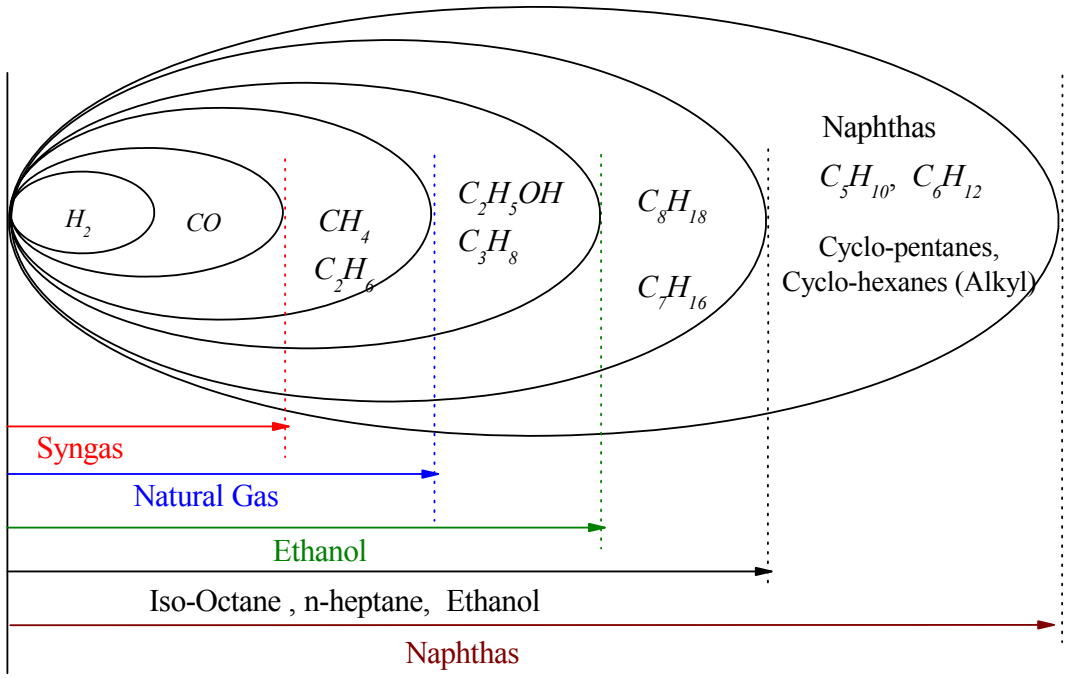

Figure 4. Hierarchy of kinetics models for hydrocarbons oxidation (adapted from Warnatz et al., 1999).

The kinetics data are presented in the Arrhenius form:

$$k_f = AT^{\beta} \exp\left(-\frac{E_a}{\Re T}\right), \qquad [17]$$

as described in equation [11]. In the detailed model, the reaction rate in the forward direction is calculated using equation [17] above, while the reaction rate in the backward direction is calculated from chemical equilibrium using the relation:

$$Q_c = \frac{[C]^c [D]^d}{[A]^a [B]^b} = K_{eq} = \frac{k_f}{k_b} \; . \qquad [18]$$

In equation [18], [I] represent the molar concentration of chemical species ***i*** in (kmol/m^3) and K_{eq} is the thermodynamic equilibrium constant of the reaction expressed in molar concentration units.

The Arrhenius parameters of the backward reaction can be specified in the mechanism, and this could be used to calculate the reverse reaction rate instead of the chemical equilibrium relation.

Table 4 shows the adequate form to write detailed kinetics models in order to be correctly interpreted by the pre-processor of CHEMKIN or CANTERA codes.

The representation of elementary reactions involving a third body "M", as reaction 1 in Table 4, is:

O+O+M<=>O2+M
H2/ 2.40/ H2O/15.40/ AR/ 0.83/

This notation indicates different efficiencies of chemical species during collision as a third body. Using this notation, the values for the pré-exponential coefficient in the Arrhenius equation is multiplied by the constant provided, depending of the third body "M". In the example above, if the third body "M" is H2 (hydrogen) the pre-exponential coefficient would be 2.4 times the specified value in the table for this reaction. If the third body "M" is AR (argon) its value would be 0.83 times the specified value in the table. Usually, molecules with a larger number of internal degrees of freedom are able to exchange a larger spectrum of energy levels (quantized) and therefore present higher efficiencies.

Table 4. Detailed kinetics model for the H_2/O_2 system (GRI-Mech Version 3.0 Thermodynamics released 3/12/99 with only the H/O/AR reactions).

	Elementary reaction	A mole-cm-sec-K	n	E_a cal/mole
1	O+O+M<=>O2+M H2/ 2.40/ H2O/15.40/ AR/ 0.83/	1.200E+17	-1.000	0.00
2	O+H+M<=>OH+M H2/ 2.00/ H2O/ 6.00/ AR/ 0.70/	5.000E+17	-1.000	0.00
3	H+H+M<=>H2+M H2/ 0.00/ H2O/ 0.00/ AR/ 0.63/	1.000E+18	-1.000	0.00
4	H+H+H2<=>2H2	9.000E+16	-0.600	0.00
5	H+H+H2O<=>H2+H2O	6.000E+19	-1.250	0.00
6	H+O2+M<=>HO2+M O2/ 0.00/ H2O/ 0.00/ AR/ 0.00/	2.800E+18	-0.860	0.00
7	H+O2+O2<=>HO2+O2	2.080E+19	-1.240	0.00
8	H+O2+H2O<=>HO2+H2O	11.26E+18	-0.76	0.00
9	H+O2+AR<=>HO2+AR	7.000E+17	-0.800	0.00
10	H+OH+M<=>H2O+M H2/ 0.73/ H2O/ 3.65/ AR/ 0.38/	2.200E+22	-2.000	0.00
11	OH+OH(+M)<=>H2O2(+M) LOW / 2.300E+18 -0.900 -1700.00/ TROE/ 0.7346 94.00 1756.00 5182.00/ H2/ 2.00/ H2O/ 6.00/ AR/ 0.70/	7.400E+13	-0.370	0.00
12	O+H2<=>H+OH	3.870E+04	2.700	6260.00
13	O+HO2<=>OH+O2	2.000E+13	0.00	0.00
14	O+H2O2<=>OH+HO2	9.630E+06	2.000	4000.00
15	H+O2<=>O+OH	2.650E+16	-0.6707	17041.00
16	H+HO2<=>O+H2O	3.970E+12	0.00	671.00
17	H+HO2<=>O2+H2	4.480E+13	0.00	1068.00
18	H+HO2<=>2OH	0.840E+14	0.00	635.00
19	H+H2O2<=>HO2+H2	1.210E+07	2.000	5200.00
20	H+H2O2<=>OH+H2O	1.000E+13	0.00	3600.00
21	OH+HO2<=>O2+H2O	2.160E+08	1.510	3430.00
22	OH+OH<=>O+H2O	3.570E+04	2.400	-2110.00

23	OH+HO2<=>O2+H2O DUPLICATE	1.450E+13	0.00	-500.00
24	OH+HO2<=>O2+H2O DUPLICATE	1.450E+13	0.00	17330.00
25	OH+H2O2<=>HO2+H2O DUPLICATE	2.000E+12	0.00	427.00
26	OH+H2O2<=>HO2+H2O DUPLICATE	1.700E+18	0.00	29410.00
27	HO2+HO2<=>O2+H2O2 DUPLICATE	1.300E+11	0.00	-1630.00
28	HO2+HO2<=>O2+H2O2 DUPLICATE	4.200E+14	0.00	12000.00

The reaction rate of uni-molecular and association reactions is pressure dependent. Figure 5 shows the behavior of the reaction rate for unimolecular reactions as a function of the reduced pressure, p_r, by using the Lindemann mechanism and RRKM theory. It shows also the empiric approximation developed by Troe et al. (1982).

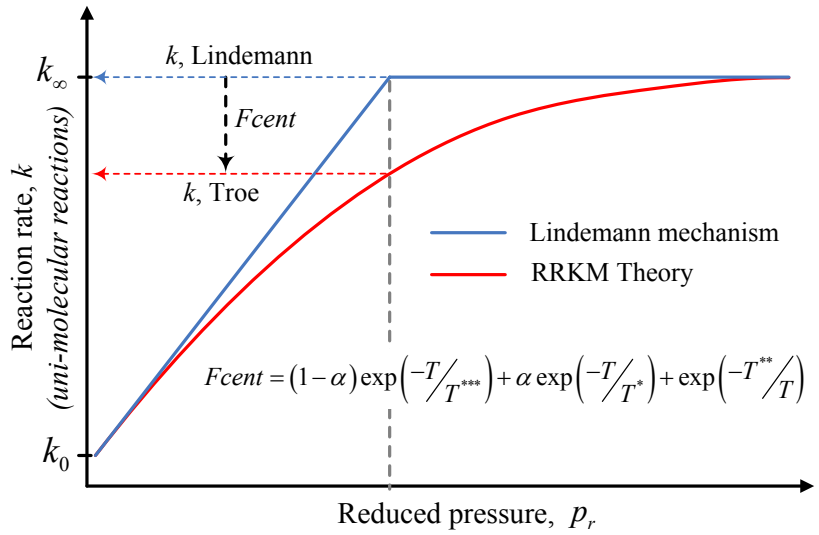

Figure 5. Reaction rate for unimolecular reactions, Lindemann mechanism, RRKM theory and empiric F_{cent} factor developed by Troe et al. 1982.

The behavior of the reaction rate of uni-molecular reactions can be modeled using the form proposed by Troe (CHEMKIN GAS PHASE KINETICS core manual *apude* Troe et al., 1982). An example is given by reaction 11 (from Table 4):

OH+OH(+M)<=>H2O2(+M)

LOW / 2.300E+18 -0.900 -1700.00/

TROE/ 0.7346 94.00 1756.00 5182.00/

H2/ 2.00/ H2O/ 6.00/ AR/ 0.70/

The word "LOW" indicates the low pressure limit, followed by the three numbers corresponding to A_0, n_0 and E_0, in the Arrhenius equation:

$$k_0 = A_0 T^{n_0} \exp\left(-\frac{E_0}{\Re T}\right) . \qquad [19]$$

Equation [19] is used by the program (CHEMKIN or CANTERA) in order to calculate the reaction rate for the low pressure range. Analogously, the Arrhenius parameters for the "HIGH" pressure limit A_∞, n_∞ e E_∞ are provided and used in the expression

$$k_\infty = A_\infty T^{n_\infty} \exp\left(-\frac{E_\infty}{\Re T}\right), \qquad [20]$$

for the high pressure limit. Once both the low and high pressure limits are provided the program calculates the reaction rate for the required pressure using the equation

$$k = k_\infty \left(\frac{p_r}{1+p_r}\right) F \ , \qquad [21]$$

where the reduced pressure, p_r, is calculated as:

$$p_r = \frac{k_0 [M]}{k_\infty} \qquad [22]$$

with [M] as the mixture concentration.

In equation [21], the function F can be defined by using two forms: Troe (CHEMKIN GAS PHASE KINETICS Core Manual *apude* Troe et al., 1982), or SRI approximation (CHEMKIN GAS PHASE KINETICS Core Manual *apude* Stewart et al., 1989).

The Troe form is

$$\log(F) = \left[1 + \left[\frac{\log(P_r) + c}{n - d\left[\log(P_r) + c\right]}\right]^2\right]^{-1} \log(F_{cent}) \ , \qquad [23]$$

where

$$c = -0.4 - 0.67 \log(F_{cent}) \ ,$$
$$n = 0.75 - 1.27 \log(F_{cent}) \ ,$$
$$d = 0.14 \ ,$$

and

$$F_{cent} = (1-\alpha)\exp\left(-T/T^{***}\right) + \alpha\exp\left(-T/T^{*}\right) + \exp\left(-T^{**}/T\right) . \quad [24]$$

When using this form, the four numbers listed after the word "TROE" below the reaction in the detailed kinetics model, are the four parameters α, T^{***}, T^{*} e T^{**} of equation [24]

The second form to define the function F is by using the SRI approximation, defined by the expression

$$F = d\left[a\exp\left(-b/T\right) + \exp\left(-T/c\right)\right]^{X} T^{e} , \quad [25]$$

where

$$X = \frac{1}{1+\log^{2}\left(P_r\right)} . \quad [26]$$

In the detailed kinetics model used in this work, only two reactions in the Konnov model use the SRI approximation for the calculation of the pressure dependent unimolecular reaction rates. The others reactions in the Konnov model are assumed to be non-pressure dependent.

Frequently, reactions taken as elementary are not in fact elementary in a collision sense. This is the case of the pressure sensitive unimolecular reactions discussed above. There are reactions that follow different reaction rates in low and high temperatures (Konnov, 2005). The word "DUPLICATE" in the Chemkin format allows the possibility of modeling these reactions in detailed kinetics models. When this word is found, the chemical reaction rate calculated by two or more sets of Arrhenius parameters for the same reaction are added.

The nitrogen chemistry is added when air is used as oxidizer. In this case, the $H_2/CO/N_2$ kinetics sub-structure is the starting point for building the desired detailed kinetics model (Simmie, 2003). For the combustion of hydrocarbons, the size of the kinetics structure grows as the number of carbon atoms in the molecule increase. For example, the well known detailed kinetics model for methane, the GRIMech 3.0, is composed by 325 elementary reactions among 53 chemical species. In the case of the iso-octane oxidation, the detailed kinetics model developed by Curran et al. (2002) at Lawrence Livermore National Laboratory is composed by 3606 elementary reactions among near 857 chemical species.

Figure 6 shows an estimate of the evolution in the number of chemical species and elementary reactions for the appropriate description of the detailed kinetics model as a function of the number of carbon atoms in the fuel molecule, for combustion of alkanes with

air. In the range of number of carbon atoms analyzed, a linear growth of the number of elementary reactions and chemical species is observed, reaching an estimated value of 1250 chemical species and 4600 elementary reactions for a hydrocarbon containing 16 carbon atoms in the molecule.

For iso-octane, Warnatz's predictions in Figure 6 indicate that a detailed kinetics model containing 500 chemical species forming 1500 elementary reactions should be sufficient to the correct description of the iso-octane oxidation. Note that the kinetics model developed by Curran et al. (2002) for iso-octane contains about twice this number of chemical species and elementary reactions. Table 5 presents a list (not intended to be exhaustive) of detailed kinetics models compiled from the open literature and some of their characteristics.

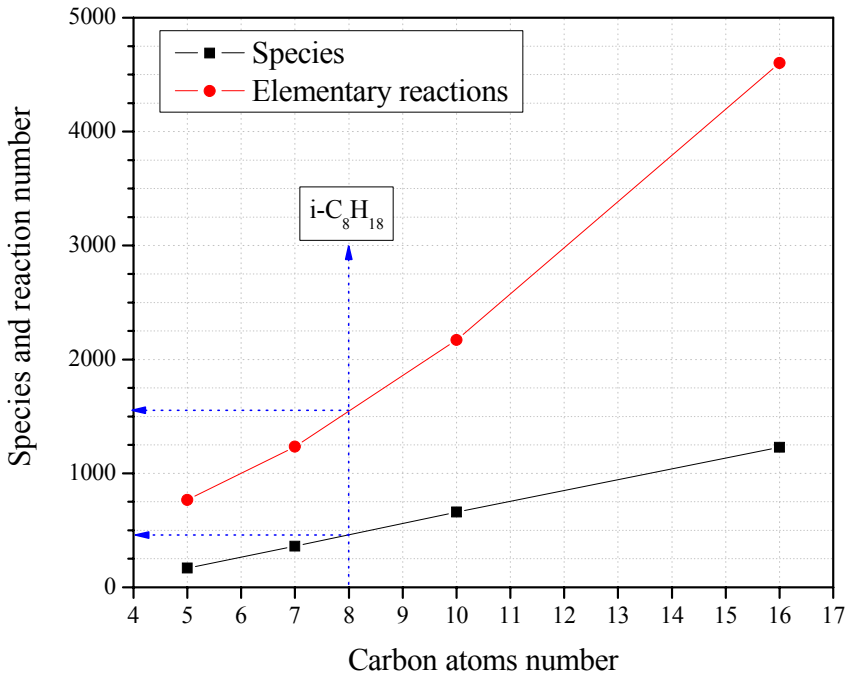

Figure 6. Number of species and reactions involved in the oxidation process of alkanes at low temperatures (adapted from Warnatz et al., 1999).

In this work several detailed kinetics models were used in order to build the proposed kinetics models for ethanol and gasoline surrogates.

2.2.3 Detailed kinetics models for small hydrocarbon oxidation

Several detailed kinetics model have been reported for the thermal oxidation and combustion of small hydrocarbons. In this work, the detailed kinetics model from Konnov

(2000) was used as a kernel for the sub-kinetics database for combustion of hydrocarbons containing up to three carbon atoms in the molecular structure. The Konnov's detailed kinetics model has been validated and tested numerically for several experimental conditions covering a wide range of pressures, temperatures and stoichiometric compositions, for several saturated and unsaturated hydrocarbons. Cancino (2004), Cancino and Oliveira (2005a, 2006) and Cancino et al. (2007, 2008a, 2008b, 2009a, 2009b, 2009c) presents the performance of the Konnov's detailed kinetics model in predicting reaction properties in perfectly stirred reactors and shock tubes for methane, acetylene, propane and ethanol.

Table 5. Available detailed kinetics models for combustion of hydrocarbons.

Author	Mechanism	Fuel	Elementary reactions	Chemical species	Numerically tested in	Year
O'Connaire et al.	Detailed	H2	20	10	Shock tube, Laminar flame, Flux reactor	2004
Marinov N.	Detailed	C2H5OH	372	54	Shock tube, Turbulent flux reactor, Laminar flame, Jet stirred reactor, Flux reactor	1999
Fischer et. al.	Detailed	Dimethyl Ether	351	79	Flux reactor, Shock tube, Jet stirred reactor	2000
Marinov et. al.	Detailed	CH4, C2H4, C2H6, C3H8, e nC4H10	689	155	PAH formation in flames	1998
Westbrook et al	Detailed	n-Octane to n-Hexadecane	8157	2115	Pyrolysis, Shock tube, Flux reactor, Jet stirred reactor	2008
Marinov et. al.	Detailed	CH4, C2H4, C2H6, C3H6, C3H8, Nox	638	126	NOX chemistry in flux reactor	1998
Silke et. al.	Detailed	Cyclohexane	4269	1081	Rapid compression machine, Jet stirred reactor	2006
Pitz et. al.	Detailed	Methylcyclohexane	4436	1001	Rapid compression machine	2007
Fischer et. al.	Detailed	Methyl-Butanoate e Methyl-Formate	1219	264	Static reactor	2000
Herbinet et. al.	Detailed	Methyl Decanoate	8555	2878	Jet stirred reactor, Rapid compression machine	2008
Laude et. al.	Detailed	Dimethyl Carbonate	443	102	Counter flow diffusion flame	2004
Curran et. al.	Detailed	n-heptane	2539	561	Flux reactor, Shock tube, Rapid compression machine	1998, 2002
Seiser et. al.	Semi-detailed	n-heptane	1540	160	Counter flow diffusion flame	2000
Curran et. al.	Detailed	n-heptane and iso-octane	4236	1034	High pressure flow reactor	1998
Konnov. A	Detailed	C1 - C3	1200	127	Shock tube, Laminar flame, Flux reactor	2002
Smith et. al. (GRIMech 3.0)	Detailed	CH4	325	53	Shock tube, Laminar flame, Flux reactor	***
Cancino et. al.	Detailed	C2H5OH, C1 - C3, NOx	1136	136	Shock tube	2009
Cancino et. al.	Detailed	Gasoline surrogates: iso-octane, n-heptane, toluene, ethanol	4448	1062	Shock tube	2008
Cancino et. al.	Detailed	Gasoline surrogates: iso-octane, n-heptane, toluene, ethanol, di-iso-butylene	4959	1126	Shock tube	2008
Cancino et. al.	Detailed	Gasoline surrogates: iso-octane, ethanol	4743	1056	Shock tube	2009
Metcalfe et. al.	Detailed	Di-iso-butylene	3783	897	Shock tube	2007
Petersen et. al.	Detailed	Natural gas	665	118	Shock tube	2007
Bourque et. al.	Detailed	Natural gas	821	132	Shock tube, Laminar flame speed	2008
Curran et. al.	Detailed	Iso-octane	3606	857	Shock tube, Rapid compression machine, Jet stirred reactor	2002

2.2.4 Detailed kinetics models for ethanol oxidation

Several authors have devoted considerable time studying thermal oxidation of ethanol. Natarajan and Bhaskaran (1981) reported the first detailed kinetics model for the high-temperature oxidation of ethanol containing 56 elementary reactions, including the bimolecular decomposition reaction $C_2H_5OH + M \rightarrow CH_2OH + CH_3 + M$, in other words, proposing the C–C cleavage of ethanol. Validation against experimental data of ignition delay time in a shock tube at pressures of 1.0 and 2.0 bar and temperatures between 1300 K to 1700 K resulted in good agreement with respect to the pressure dependence. The numerical model at pressure of 1.0 bar overestimates the IDT in about 13%, while for pressure of 2.0 bar the model underestimates the IDT in about 13%. Borisov et al. (1989, 1992) reported a second detailed kinetics model for the high-temperature ignition of ethanol involving 94 elementary reactions. This kinetics mechanism was built starting from the Natarajan and Bhaskaran model, adding reactions that describe the pyrolysis of ethanol and some reactions representing the thermal oxidation by active radicals, not considered in Natarajan's model. The model was validated against experimental results of ignition delay time in shock tubes for stoichiometric, lean and rich compositions at pressure of 1.0 bar.

In the nineties, Marinov (1999) developed a comprehensive model for the high-temperature ethanol oxidation. The detailed kinetics model of Marinov is composed by 383 elementary reactions among 57 chemical species. It included an accurate kinetics data-set for ethanol oxidation, reaction routes involving H abstraction, C–C and C–O cleavage were proposed and computational chemistry methods were used in order to determine the Arrhenius parameters. This mechanism was validated against experimental results of ignition delay time in shock tube, laminar flame speed in counterflow twin flame and chemical species concentrations in jet-stirred reactor. In the case of ignition delay time in shock tube, for mixtures with 1.25% C_2H_5OH, 3.75% O_2, and 95.0% Argon, (equivalence ratio ϕ=1.0), at 3.5 bar, the Marinov detailed kinetics model overestimates the global activation energy in about ~31 kJ/mol, when compared to the measurements from Dunphy and Simmie (1991) (E_a ~ 130 kJ/mol). In general, good agreement was found with all measurements. The Marinov model was tested for the temperature range of 1300 K to 1700 K, pressures of 1.0 bar to 4.6 bar and stoichiometries of 0.25, 0.5, 1.0 and 2.0.

More recently, Saxena and Williams (2007) reported a kinetics model with 288 elementary reactions among 57 chemical species. This model is about 100 elementary reactions smaller than Marinov's and also involves the nitrogen oxidation chemistry. It was

validated against experimental results of ignition delay time in a shock tube at high temperatures (1300–1700 K) and pressures of 1.0 and 2.0 bar for stoichiometric, lean and rich ethanol/O_2/Ar mixtures. The Saxena model was also validated with laminar burning velocity data from Egolfopulos et al. (1992).

Numerical studies on ethanol decomposition using computational chemistry have also been reported, which have been useful in completing the gaps on thermodynamic and chemical kinetics parameters as well as in pointing out important reactions and reactions with a very high reaction barrier. Marinov (1999) used Rice-Ramsperger-Kassel-Marcus (RRKM) theory to analyze the multichannel decomposition of ethanol. In this study, the reaction rate parameters of the thermal decomposition of ethanol at high temperatures, involving new degradation routes, such as H abstraction, were determined, this new data allowed to increase the accuracy of the kinetics modeling, the numerical model of Marinov, when compared to the experimental data of Natarajan and Bhaskaran (1981) at pressure of 1.0 bar, underestimates the IDT in about ~3.3 %, For pressure of 2.0 bar, the model also underestimates the IDT in about ~9.4%, which can be considered a good comparison.

Recently, Li et al. (2004) found, by using computational chemistry and taking into account all the routes (channels) of decomposition of ethanol, that Marinov's model underestimates the production rate of H_2O and C_2H_4 as well as the overall ethanol consumption. This led to the proposal of a new set of Arrhenius parameters for the decomposition reactions; $C_2H_5OH = C_2H_4 + H_2O$ and $C_2H_5OH = CH_3 + CH_2OH$. Finally, Lin et al. (2002, 2003 and 2004) published the most recent kinetics data obtained from computational chemistry for the thermal oxidation of ethanol. A new kinetics database was provided, thus allowing for the prediction of the thermal decomposition of ethanol and ethanol-radical reactions. High barrier reactions are detected and critical reactions are identified. Table 6 summarizes this overview of the experimental and numerical results of ethanol oxidation available in the literature.

2.2.5 Detailed kinetics model for Primary Reference Fuels.

Primary reference fuels (PRF) n-heptane and iso-octane are used to define the octane reference scale for fully blended gasolines. n-Heptane is a reactive straight-chain paraffin while iso-octane is a less reactive branched paraffin (Curran et al., 1998). Each fuel exhibits richly complex chemistry. At high temperatures, fuel decomposition reactions tend to dominate the combustion process, whereas at low temperatures, the chemistry is dominated

by addition of alkyl radicals to O_2 and subsequent isomerization reactions. The Curran's PRF model was based on previous detailed kinetics models developed at LLNL for n-heptane, iso-octane, n-butane and other pure hydrocarbon fuels. It was then tailored in a hierarchical form for hydrocarbon reactive systems, and starting with a core mechanism describing the H_2/O_2 and CO oxidation kinetics, as it will be reviewed in the next section.

Table 6. Summary of published work involving ethanol oxidation

Author	Study	Fuel	Oxidizer	Parameters analyzed	Φ	*T* [K]	*p* [bar]	Experimental Setup	Numerical model	Year
Barnard and Hughes	Experimental	Ethanol	***	Ethanol Pyrolysis	***	850 - 900	0.066 - 0.46	Reaction vessel	***	1959
Natarajan and Bhaskaran	Experimental and Numerical	Ethanol	O2	I. D. T	0.5 - 1.0 - 2.0	1300 - 1700	1.0 - 2.0	Shock tube	***	1981
Gülder	Experimental	Methanol Ethanol Isooctane	Air	L. B. V	0.7 - 1.4	300	1	Constant pressure bomb	***	1982
Borisov et al	Experimental	Ethanol Acetaldehyde	O2	I. D. T	***	700 - 1550	0.5 - 6	Shock tube	***	1985
Borisov et al	Experimental and Numerical	Ethanol	***	Ethanol Pyrolysis	***	700 - 1700	1	Reaction vessel	***	1987
Borisov et al	Numerical	Ethanol	O2	Chem Spec	***	900 - 1500	1	***	***	1988
Dunphy and Simmie	Experimental	Ethanol	O2	I. D. T	0.25 - 2.0	1080 - 1660	1.8 - 4.6	Shock tube	***	1991
Dunphy et al	Numerical	Ethanol	O2	I. D. T	0.25 - 2.0	1080 - 1660	1.8 - 4.6	***	RXR	1991
Egolfopulos et al	Experimental and Numerical	Ethanol	Air / O2	L. B. V Chem Spec IDT	0.6 -- 1.8 0.81 1.0	298 - 453 1090 1300 - 1600	1	C. F .Tw-F Flow Reactor Shock tube	CHEMKIN	1992
Curran et al	Experimental and Numerical	Ethanol isobutilene MTBE	O2	I. D. T	0.25 - 1.5 0.1 - 4.0 0.15 - 2.4	1100 - 1900	2.3 3.5 4.5	Shock tube	HCT	1992
Marinov	Experimental and Numerical	Ethanol	Air / O2	L. F. S I. D. T Chem Spec	0.6 - 1.4 0.5 - 2.0 0.2 - 2.0	298 - 453 1300 - 1700 1000 - 1200	1 - 2 1 - 3.4 1	C. F .Tw-F Shock tube Jet-stirred R	CHEMKIN	1998
Cancino and Oliveira	Numerical	Ethanol	Air	I. D. T	0.55 - 3.3	1200	1.0 - 5.0	***	CHEMKIN CANTERA	2005
Cancino and Oliveira	Numerical	Ethanol	Air	Ethanol Kinetics	1.0	1400	1	***	CHEMKIN CANTERA	2006
Li et al	Experimental and Numerical	Ethanol	Air	Chem Spec	0.3 - 1.4	800 - 950	3.0 - 12	Flow Reactor	***	2007
Kohse-Höinghaus	Experimental	Ethanol	O2	Flame structure	1.0 - 2.57	298	0.05	Flat flame	***	2007
Saxena and Williams	Experimental and Numerical	Ethanol	Air / O2	I. D. T L. B. V	0.5 - 2.0 0.6 - 1.7	1300 - 1700 298 - 453	1.0 - 4.6 1	Shock tube C. F .Tw-F	CHEMKIN FlameMaster	2007
Cancino et al	Experimental and Numerical	Ethanol	Air	I. D. T	1.0	690 - 1200	30	Shock tube	CHEMKIN	2007

I. D. T. = Ignition delay time
C. F. Tw-F = Counterflow Twin flame
L. F. S = Laminar Flame Speed
L. B. S = Laminar Burning Speed

The major classes of elementary reactions considered in the Curran et al. (1998) model include the following:

- Unimolecular fuel decomposition,
- H atom abstraction from the fuel,
- Alkyl radical decomposition,
- Alkyl radical + O_2 to produce olefin + $H\dot{O}_2$ directly,
- Alkyl radical isomerization,
- Abstraction reactions from olefin by $\dot{O}H$, $\dot{H}$, $\dot{O}$ and $\dot{C}H_3$,
- Addition of radical species to olefin,
- Alkenyl radical decomposition,
- Olefin decomposition,
- Addition of alkyl radicals to O_2,
- $\dot{R} + R'\dot{O}_2 = R'\dot{O} + R\dot{O}$,
- Alkyl peroxy radical isomerization ($R\dot{O}_2 = \dot{Q}OOH$),
- $R\dot{O}_2 + H\dot{O}_2 = RO_2H + O_2$,
- $R\dot{O}_2 + H_2O_2 = RO_2H + H\dot{O}_2$,
- $R\dot{O}_2 + CH_3O_2 = R\dot{O} + CH_3\dot{O} + O_2$,
- $R\dot{O}_2 + R'O_2 = R\dot{O} + R'\dot{O} + O_2$,
- $RO_2H = R\dot{O} + \dot{O}H$,
- $\dot{Q}OOH =$ cyclic ether + $\dot{O}H$ (cyclic ether formation via cyclisation of diradical),
- $\dot{Q}OOH =$ olefin + $H\dot{O}_2$ (radical site β to OOH group),
- Addition of $\dot{Q}OOH$ to O_2,
- Isomerization of $\dot{O}_2QOOH$ and formation of carbonylhydroperoxide and $\dot{O}H$,
- Decomposition of carbonylhydroperoxide to form oxygenated radical species and $\dot{O}H$,
- Cyclic ether reactions with $\dot{O}H$ and $H\dot{O}_2$,

where $\dot{R}$ and R' are alkyl radicals or structures and Q are C_nH_{2n} are species or structures. All of these reaction groups are described with details in Curran et al. (2002).

From the description above, the treatment of binary mixtures of pure components is already fairly complex and the complexity increases largely as the number of components increases. In this work, the detailed kinetics model for PRF of Curran et al. (1998) was adopted as kernel for the tailoring process of the multi-component gasoline surrogates models proposed in chapter 4.

2.3 Sensitivity analysis as a method for analysis and optimization of kinetics models

Sensitivity analysis is a computational tool widely used for optimization of detailed kinetics models (Cancino et al., 2009b; Metcalfe et al., 2007, Andrae et al., 2005; Brezinsky et. al., 2005; Dagaut et al., 2002; Glarborg et al., 2001; Dunphy et al., 1991; Egolfopoulos et al., 1992; Andrae, 2008; Andrae et al., 2008; Griffiths, 1995) since it gives information about the more important (sensitive) reactions of a kinetics scheme. The methodology can be applied to the time-evolution of the chemical species of a reactive system as found, for example, in the autoignition of reactive mixtures in perfectly stirred reactors. The target in the sensitivity analysis has to be at least one of the dependent variables involved in the problem, for example, sensitivity on temperature, concentration or reaction rate of a chemical species. Independent variables can not be defined as target for sensitivity analysis. For example, it is not possible to perform a sensitivity analysis on ignition delay time of thermal oxidation of hydrocarbons.

When the target is an independent variable of the system, the methodology is based on an indirect approach. For thermal ignition, for example, it is known that the hydroxyl radical is a very important chemical species affecting both the fuel depletion and the temperature increase. Then, to study the prediction of ignition delay time, the target can be fixed as the sensitivity on the concentration of the hydroxyl radical. In the next sections, the fundamentals of the sensitivity analysis are reviewed. Additionally, an extension of this method, developed and applied in this work, is presented.

2.3.1 Sensitivity Analysis.

The major purpose of the sensitivity analysis is to determine the local performance of a system of equations when there is a perturbation in a selected parameter. In a kinetics context, the response of the system is examined when the Arrhenius parameters of the kinetics mechanism are changed, for a set of boundary conditions. The response is usually measured

relative to the magnitude of the changes that are introduced. The magnitude of the sensitivity coefficient for a particular rate constant is related to the influence on the behavior of that particular reaction, i.e., the sensitivity analysis represents a local analysis in a reactive system. The mathematical approach of sensitivity analysis is presented following Griffiths (1994).

Consider the non-linear mass conservation equation

$$\frac{dc_i}{dt} = f_i(\mathbf{k},\mathbf{c}) \quad , \quad i = 1,...,N \qquad [27]$$

in which **k** and **c** are the rate coefficient and species concentration vectors, respectively and N is the number of chemical species. In order to generate a solution for equation [27], it is necessary to specify the component values for the vector **k**. The concentration vector **c** is a function of the parameter vector as well as time **c**(**k**,t). A first order sensitivity coefficient with respect to species $\mathbf{c_i}$ may be defined as

$$\frac{\delta c_i}{\delta k_j}(\mathbf{k},t) = \frac{\mathbf{c}_i(k_j + \Delta k_j, t) - \mathbf{c}_i(k_j, t)}{\Delta k_j} \ , \qquad [28]$$

and represents the change in a species concentration $\mathbf{c_i}$ at time t owing to a change in the j^{th} rate parameter k_j (or the j^{th} component of any parameter vector, in general). The gradient and its second order counterpart,

$$\frac{(\delta^2 c_i)}{(\delta k_j)^2} \ , \qquad [29]$$

convey quantitative information about the solution in the vicinity of the operating point. The linearized response of the sensitivity with respect to time throughout the reaction data set is given by

$$\frac{d}{dt}\left[\frac{\delta c_i}{\delta k_j}\right] = \sum_l J_{il}\frac{\delta c_i}{\delta k_j} + \frac{\delta f_i}{\delta k_j}, \qquad [30]$$

in which $\boldsymbol{J_{il}}$ is the Jacobian matrix defined as

$$J_{il} = \frac{\delta f_i}{\delta c_l} \qquad [31]$$

Equation [30] must be solved by numerical integration in order to obtain deviations in $\mathbf{c_i}(t)$ as a result of the changes in k. If the ordinary differential equations describing the species concentration of time are stiff, as is normally the case in combustion reactions, then the

sensitivity equations are likely to be difficult and computationally expensive to solve. Once the sensitivity coefficients have been obtained, they are usually normalized using the expression

$$\omega_{ij} = \frac{\delta\left[\ln c_i(t)\right]}{\delta\left[\ln k_j\right]} \quad . \qquad [32]$$

The order of magnitude of ω_{ij} gives the relative importance of the j^{th} reaction in influencing the concentration of species i at time t. Setting each k_i to zero and calculating the corresponding sensitivities, ω_{ij} indicates the significance of the j^{th} reaction. If all coefficients ω_{ij} for the j^{th} reaction are very small, in relation to the higher value, then the j^{th} reaction may be regarded to be unimportant. Conversely, if one or more of the normalized sensitivities ω_{ij} are large, then the j^{th} reaction is said to be determining for the i^{th} species.

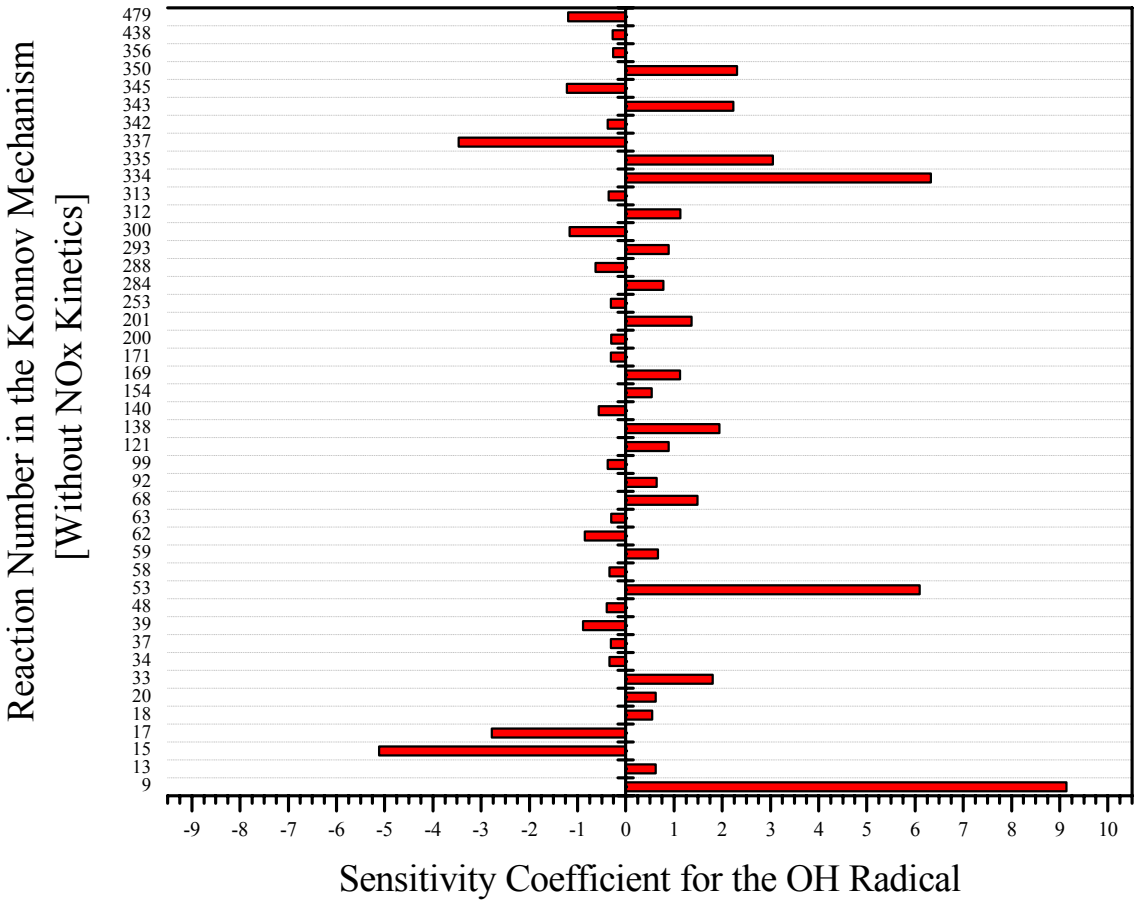

Figure 7. Typical bar diagram for sensitivity analysis at a specific elapsed time.

Figure 7 shows a typical bar diagram of sensitivity analysis applied on the Konnov (2000) detailed kinetics model. In the diagram, it is possible to determine the more important reactions for the production and consumption of radical hydroxyl, just at ignition time.

2.3.2 Integral form of the sensitivity analysis

The sensitivity coefficients in a sensitivity analysis, as described above, may be obtained for each time-step of a transient solution. For example, in a simulation of thermal oxidation the output file from CHEMKIN contains the sensitivity coefficients of all reactions for all time-steps, and thus can be analyzed as a function of time-step, as shown in Figure 8.

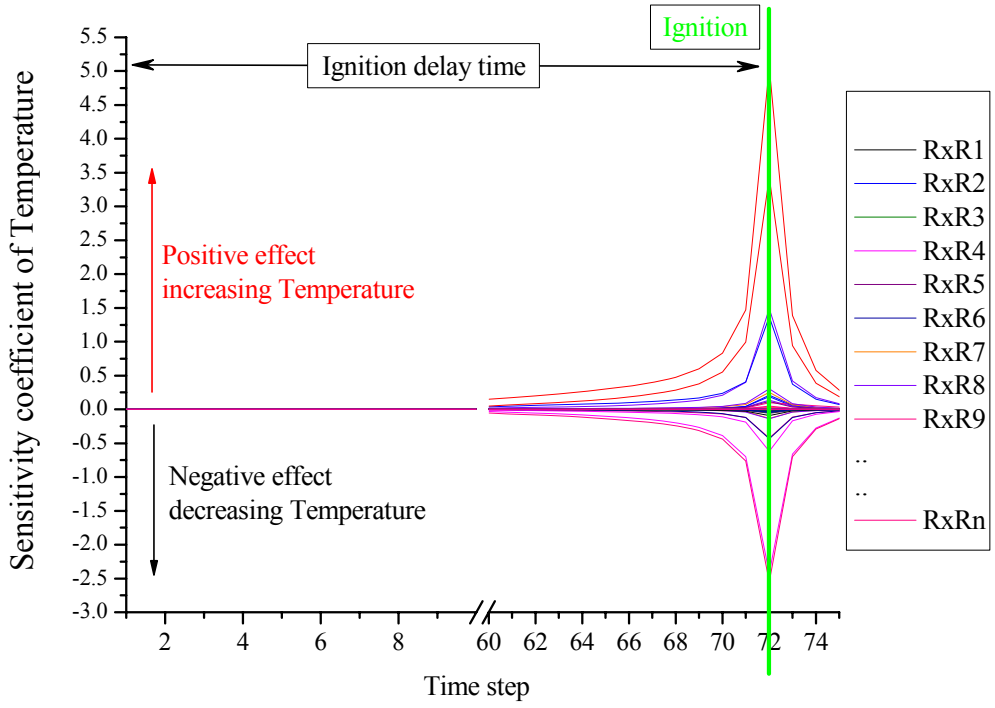

Figure 8. Example of sensitivity output file for a reactive system showing the sensitivities of reactions R_i on the temperature at each elapsed time.

The analysis of graphics as Figure 8 is relatively easy when the number of reactions forming the system is relatively small. However, when the kinetics scheme is large and the number of important reactions is substantial it is very difficult to extract useful information from such diagrams. In these cases, it is necessary the use of computational tools for automatic data post-processing.

It is common to find in the literature results of sensitivity analysis on temperature or chemical species in the form of Figure 7, showing the results at a specific elapsed time of a thermal oxidation process, for example, just at the ignition time (see ref. Cancino and Oliveira

2006; Metcalfe et al., 2007, Andrae et al., 2005; Brezinsky et. al., 2005; Dagaut et al., 2002; Glarborg et al., 2001; Dunphy et al., 1991; Egolfopoulos et al., 1992; Andrae, 2008; Andrae et al., 2008). The reactions are indentified at the ignition time and their Arrhenius parameters are altered or optimized in order to better reproduce the experimental data. However, when the analysis at a single elapsed time is used, although some reasonable results may emerge, a large amount of information is lost. The reason is that the ignition event does not depend only on the set of reactions with higher sensitivity at the ignition point, but rather on all the kinetics events that occurred previously to that point, from the "start" of the kinetics process up to the "ignition point". In other words, the ignition is a consequence of the kinetics events in the system that occurred during the entire ignition delay period.

Therefore a computational tool for the data post-processing of output files from CHEMKIN sensitivity analysis was developed in this work to account for the response of the sensitivity analysis of all reactions at all time-steps during the ignition delay period. This procedure will be called the overall analysis. In this overall analysis, reactions are classified in three levels of "importance" depending on the value of the sensitivity coefficient calculated by CHEMKIN. This classification is applied independently for positively and negatively affecting reactions at each time step. Figure 9 presents an example of this classification for a given elapsed time.

Reactions identified with (+ + +), (+ +) and (+) represent the three levels of importance: (+ + +) to the reaction with the largest sensitivity coefficient, (+ +) to the reaction with the second largest sensitivity coefficient, and (+) to the reaction with the third largest sensitivity coefficient. The same procedure is applied for the reactions with negative effect. Figure 10 and Figure 11 present an application of this classification procedure at three different time steps, two before ignition (time steps 1 and 17) and the last at the ignition time (time step 89). In Figure 11 one can see that at the beginning of the kinetics process (time-steps 1 and 2), reactions RxR-332, RxR-56 and RxR-389 have the largest positive sensitivity coefficients, and reactions RxR-336, RxR-918 and RxR-787 have the largest negative sensitivity coefficients.

Afterwards, at time-step 17, a new set of reactions hold the largest values (positives and negatives) of sensitivity coefficients. Finally, at the ignition point, time-step 89, a new set of reactions are found the most important: Reactions RxR-332, RxR-21 and RxR-389 with positive effects; and RxR-19, RxR-761 and RxR-321 with negative effects. Once this classification is completed, the method calculates the amount of the ignition delay period in which each reaction remains important, generating an output file as exemplified in Figure 12.

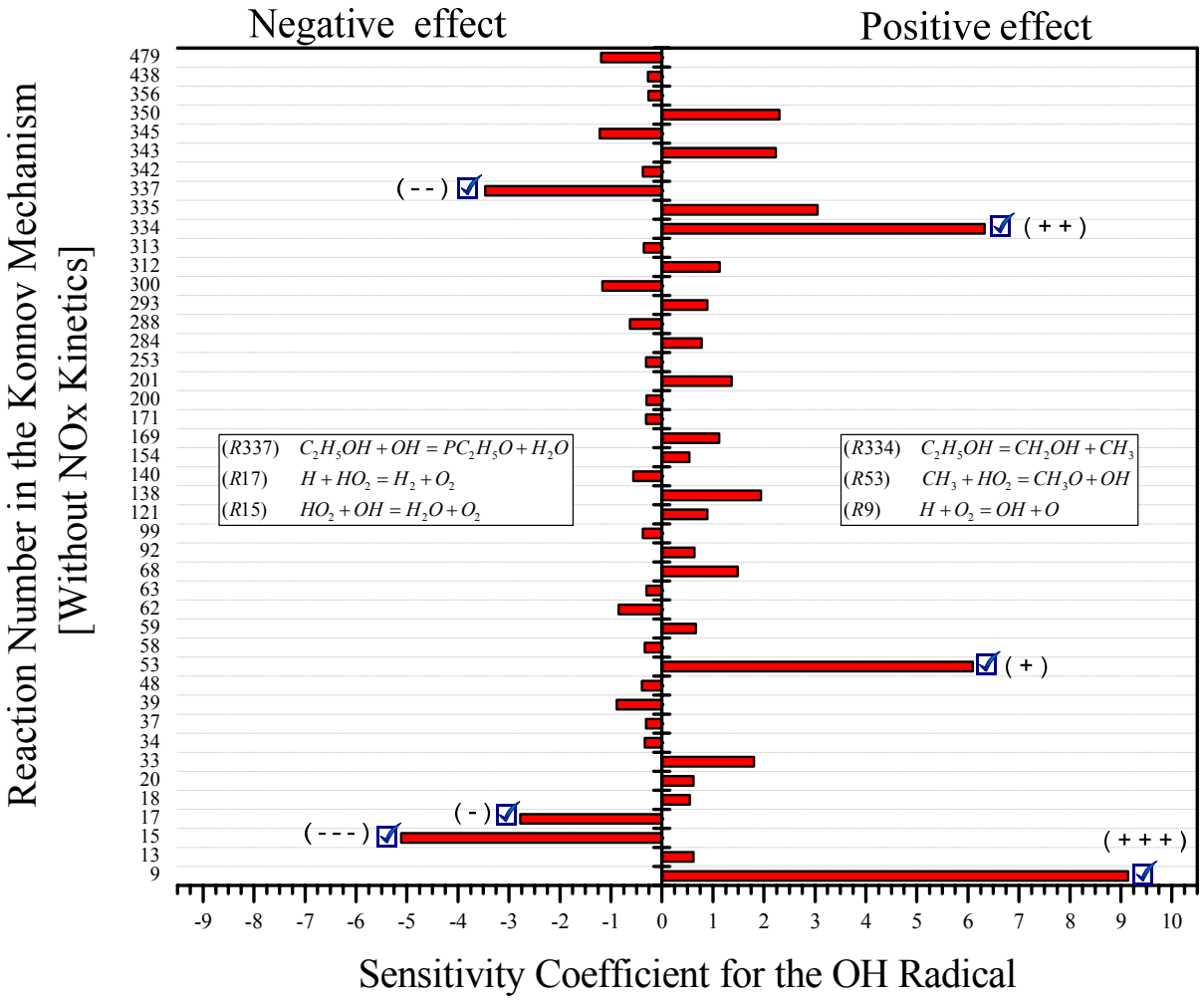

Figure 9. Example of importance levels for sensitivity coefficients adopted in this work.

This output presents the percentage of the total ignition delay period that a given reaction remains as the reaction with the first, second or third largest sensitivity coefficient, ranked separately for positive and negative effects. Note that this technique does not yield any time-integral (absolute) sensitivity coefficient. Rather, it gives information about what reactions are more important during the ignition delay time based on the values of sensitivity coefficients calculated for each time step.

Figure 13 presents the information obtained by using this overall method of sensitivity analysis when compared to the information generated by the sensitivity analysis only at the ignition point. At the ignition point, only six reactions are pointed out as most sensitive, while the overall analysis provides more complete information. From the reactions with the largest

negative coefficients, at ignition point, reaction RxR-19 is the most important reaction responsible for the decrease of temperature.

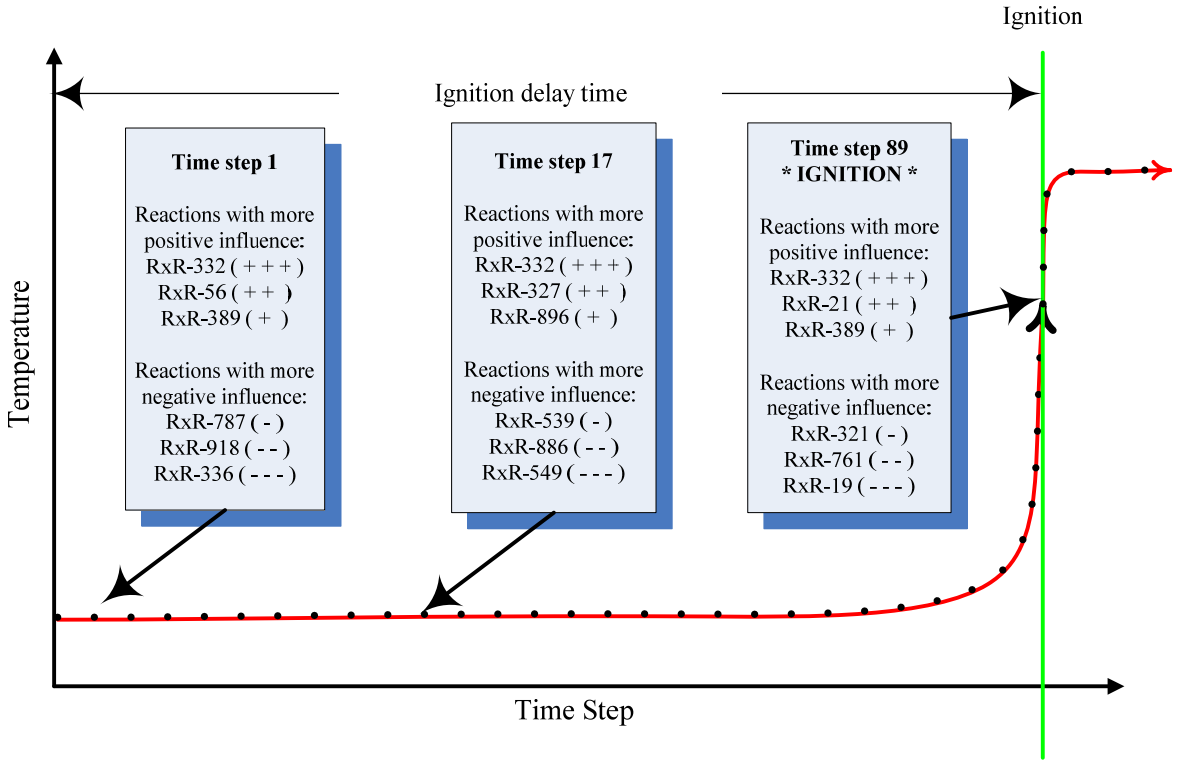

Figure 10. Classification of reactions in three different time steps (time steps 1, 17 and 89) during the ignition delay period.

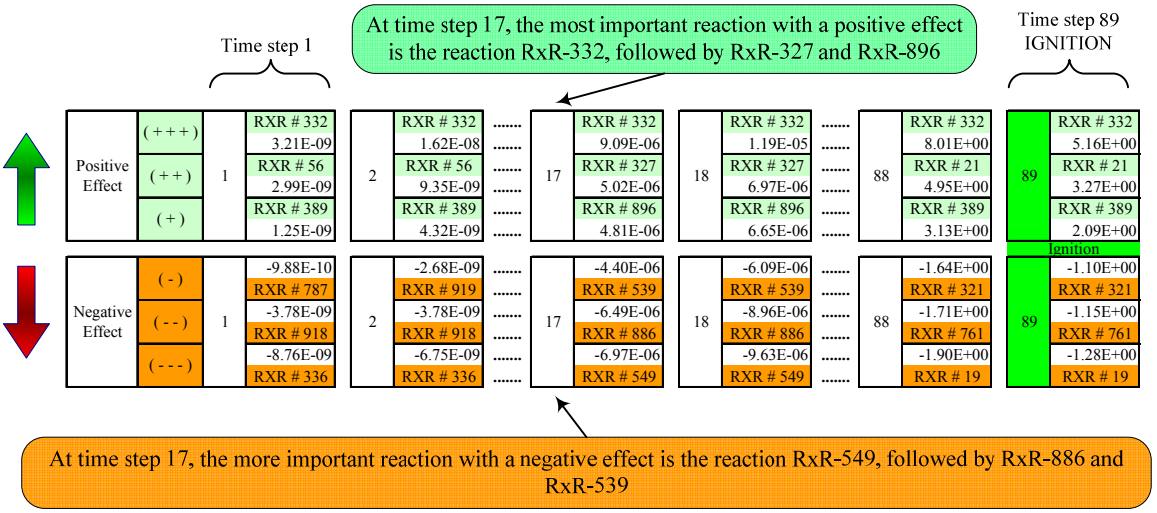

Figure 11. Reactions selected as the most important with positive and negative effects.

From the overall analysis, it is verified that reaction RxR-19 is at first place/level as most important reaction during only ~6% of the ignition delay period, while reaction RxR-

321 is at first place/level during ~82% of the ignition delay period. Therefore, RxR-321 has a higher or at least equivalent importance as reaction RxR-19.

```
*********************************************
***** Third (-) Temp  ********************
Reaction       Ranking (% of IDT)
  19.00000       2.247191
  56.00000       23.59550
  321.0000       3.370786
  327.0000       23.59550
  336.0000       1.123595
  539.0000       7.865169
  549.0000       6.741573
  761.0000       16.85393
  787.0000       1.123595
  886.0000       4.494382
  909.0000       1.123595
  919.0000       7.865169
*********************************************
***** Second (- -) Temp  *****************
Reaction       Ranking (% of IDT)
  19.00000       22.47191
  56.00000       21.34831
  321.0000       3.370786
  327.0000       30.33708
  549.0000       4.494382
  761.0000       3.370786
  886.0000       8.988764
  918.0000       2.247191
  919.0000       3.370786
*********************************************
***** First (- - -) Temp  ****************
Reaction       Ranking (% of IDT)
  19.00000       6.741573
  321.0000       82.02247
  336.0000       2.247191
  549.0000       8.988764
*********************************************
```

Figure 12. Example of an output file of the ranking process of reactions with negative effect on temperature over the ignition delay period.

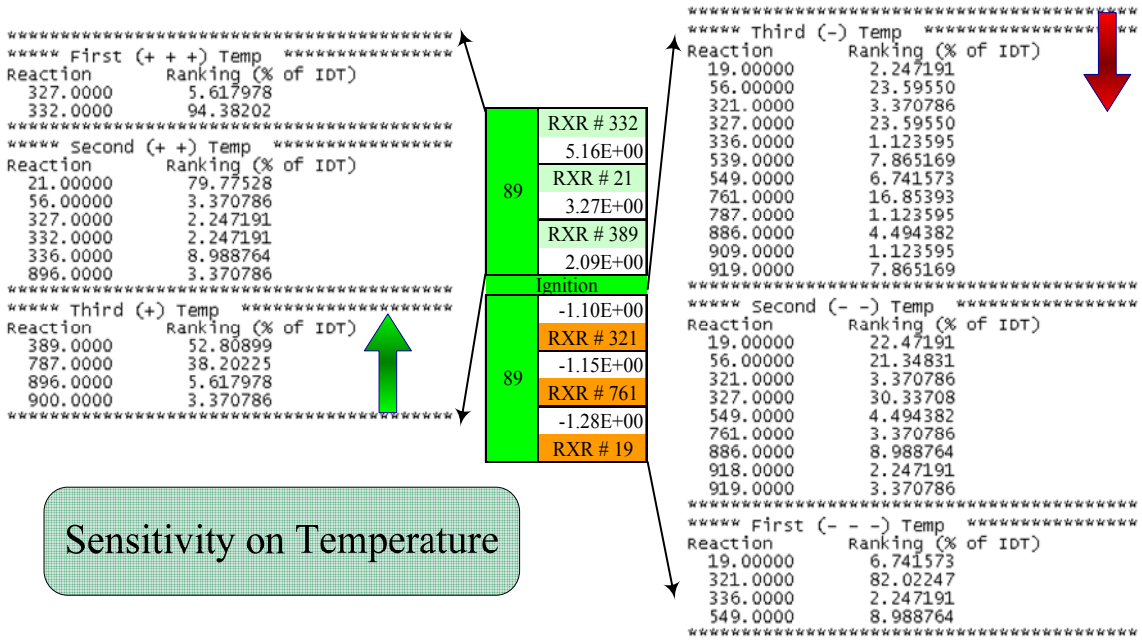

Figure 13. Additional information obtained by using the overall analysis developed in this work.

In the second level of importance, at the ignition point, reaction RxR-761 is the second most important reaction to be optimized. However, from the overall analysis, reaction RxR-761 is the second most important reaction at about ~4% of the ignition delay period, while reactions RxR-327, RxR-19 and RxR-56 are in the second place of the ranking during about ~30%, 21% and 20% of the ignition delay period. In the third level of importance, at the ignition point, reaction RxR-321 appear as the third most important reaction while from the overall analysis, reaction RxR-321 is the third most important reaction at only about ~3% of the ignition delay period while reactions RxR-327, RxR-56 and RxR-761 appear in the third level during ~23%, ~23% and ~16% of the ignition delay period. Therefore, the overall analysis points out those reactions RxR-327, RxR-56, RxR-336, RxR-549, RxR-886 are important reactions to be optimized in order to improve the kinetics model with respect to the ignition delay time.

This overall method developed in this work was applied to the optimization process of the ethanol detailed kinetics model described in section 4.1.

2.4 Fundamentals of shock tube

2.4.1 Shock tube experiments

The shock tube is a laboratory device which is extensively used in studying unsteady short-duration phenomena in the fields of aerodynamics, physics and chemistry (Saad, 1993). Transient wave phenomena occurring when a shock wave propagates at high speed, as well as the wave structure and wave interactions, can be studied in shock tubes.

Because of the high stagnation enthalpies (and temperatures) that are obtained, the shock tube provides means to study phenomena, such as the thermodynamic properties of gases at high temperatures, dissociation, ionization and chemical kinetics. Basically, a shock tube consists of a long tubular reactor which is initially separated by a thin diaphragm into two parts. One of them, the low pressure chamber, is filled with the test gas. The compressed, driver, gas is fed into the second part, the high pressure chamber. At a given time, the diaphragm is rapidly burst and the highly compressed driver gas flows into the low pressure chamber. A shock wave is then propagated through the test gas, while a rarefaction wave travels through the driver gas. The axial pressure and temperature distributions before and after bursting of the diaphragm are shown schematically in Figure 14.

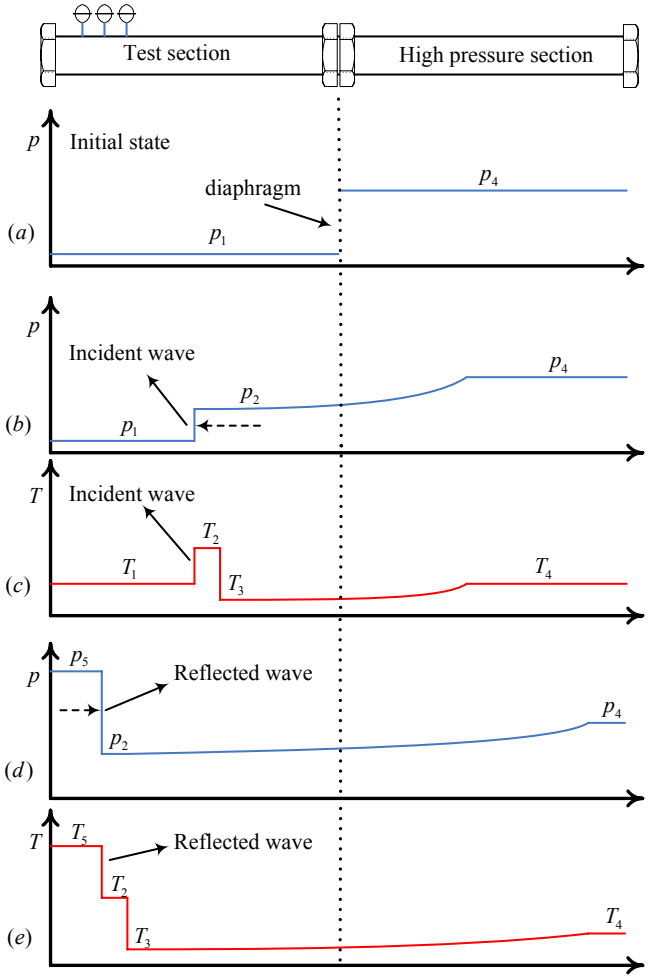

Figure 14. Operation of a shock tube, (a) Initial state, (b) and (c) Propagation of the incident shock wave, (d) and (e) Propagation of the reflected shock wave (Adapted from Zel'dovich et al. 1966a).

Figure 14 shows the axial pressure and temperature distributions, at (a) $t = 0$, and for two intermediate times, (b) and (c) showing the distributions of p and T before the arrival of the incident wave to the end wall, and (d) and (e) showing the axial distribution of p and T after the reflected wave reaches the sample gas. In Figure 14, it can be observed that the incident and reflected shock waves induce two increments of temperature and pressure in the test gas.

Successive longitudinal time-pressure distributions, indicating the shock front position, can be plotted in an x-t diagram, i.e., the typical distance-time diagram, as shown in Figure 15 (Zel'dovich et al. 1966a; Kee et. al., 2000).

At time $t = 0$, the diaphragm is ruptured and a series of compression waves rapidly collapse into a normal shock wave. This wave propagates at supersonic speed in the driven

section and sets up the fluid downstream to it in motion in the direction of the shock, at velocity U_{iw}.

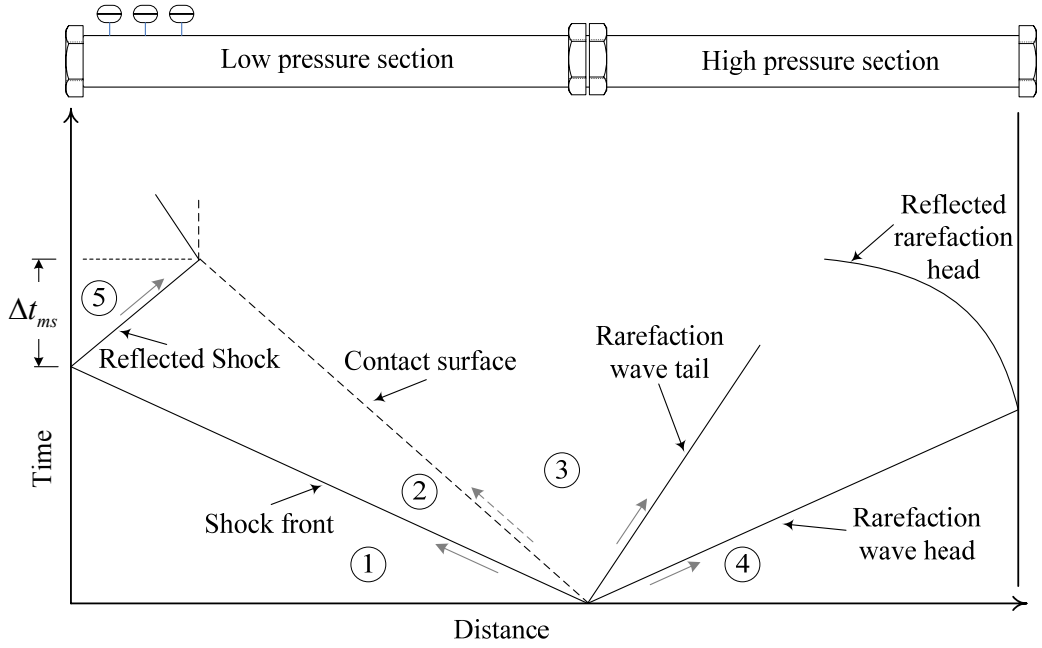

Figure 15. Distance time diagram in shock tube (Adapted from Kee et. al., 2000). Zone 1 – unshocked gas, zone 2 – shocked gas (incident shock), zone 3 – expanded driver gas, zone 4 – unexpanded driver gas, zone 5 – shocked gas (reflected shock).

Downstream the incident wave, the contact surface between the driven and driver gases moves at velocity U_{cs}. The difference between U_{iw} and U_{cs} permits that the test gas achieves the condition of high pressure and temperature (T_5, p_5), required by the experiment when the reflected wave is formed and before the arrival of the contact surface. This is shown as region 5 in Figure 15, where the test gas is under uniform conditions. Simultaneously, at the driver section, a set of rarefaction waves propagate in the opposite direction inside the driver gas. The arrival of the rarefaction waves also disturbs the test gas. The time interval between the arrival of the reflected wave and of the contact surface is the available time for measurements, Δt_{ms}.

2.4.2 Shock wave theory

2.4.2.1 Physics of shock wave

A shock wave is a wave in which the properties of a gas change sharply within a short distance in space. When momentum and energy diffusion is neglected, the shock wave manifests itself in the solution of the conservation equations as a mathematical discontinuity.

When these dissipative processes are taken into account, the net effect is to change the discontinuity into a slightly gradual transition which takes place within a distance of a few molecular mean free paths (Bird et al., 1954; Zel'dovich et al., 1966b).

The mathematical solution of the one-dimensional steady-state flow equations for a viscous and heat conducting gas is given by Bird et al. (1954) and Zel'dovich et al. (1966b). This solution allows to estimate the shock wave thickness for nitrogen at 25 °C, and a pressure ratio p/p_0 of 1.71 at pressures p_0 from 42 to 85 bar, as varying from 1.0×10^{-1} μm to 3.2×10^{-1} μm. Using kinetic theory is possible to estimate the molecular mean free path for given conditions, in this case, taking the molecular mean free path l_0 as 10^{-1} μm, these values correspond to 1.0 to 3.2 molecular mean free paths.

Obviously the shock wave thickness cannot be smaller than the molecular mean free path, since the gas molecules flowing into the discontinuity take at least a few collisions in order to scatter the directed momentum and to convert the kinetic energy of the directed motion into kinetic energy of random motion (temperature). At the same time, the thickness of the shock front in the case of any strong wave cannot include many mean free paths, since the molecules of the incident stream lose, on the average, an appreciate fraction of their momentum during each collision. The relatively small number of molecular collisions that occur within this short distance is, roughly, the minimum number needed to relax the Maxwell-Boltzmann equilibrium velocity distribution from the kinetic conditions upstream to the shock to those prevailing downstream the shock. However, this small number of collisions is not sufficient for the mixture to reach chemical equilibrium. The chemical species concentrations remain frozen across the shock and slowly evolve towards the equilibrium distribution after the shock has passed. This evolution towards equilibrium is controlled by chemical kinetics.

Since the gas undergoes an appreciable change of properties in a length equivalent to a small number of mean free paths, the Navier-Stokes equation, which relies on the continuum approximation, is often insufficiently accurate to describe the structure and thickness of the wave. The macroscopic conservation equations can, however, be used to describe the evolution of the flow properties upstream and downstream to the shock wave, where the continuum hypothesis is applicable. A comprehensive discussion about the shock structure can be found in Zel'dovich et al. (1966b).

2.4.2.2 Boundary layer interaction

When a fluid is set in motion in contact to a solid surface a fluid-dynamic boundary layer is formed. When a shock interacts with a boundary layer, the thickness of the layer is zero at the shock front, increases across the shock wave and contact surface and reaches its free stream value in the expanding driver gas. This thickness falls back to zero again at the trailing rarefaction wave. In an ideal shock tube experiment both the shock and the contact surface are plane sharp discontinuity surfaces, move with constant velocity and the flow between then is uniform. Boundary layer effects, however, are present in shock tube experiments and can modify the expected ideal performance. The presence of a wall boundary layer causes the shock to decelerate (shock attenuation), the contact surface to accelerate and the flow to be non-uniform (Mirels, 1963; Rudinger, 1961)

Figure 16, adapted from Mirels (1963), presents a rendering of (a) the *x-t* diagram and (b) the flow velocity at time t_a for an incident shock wave.

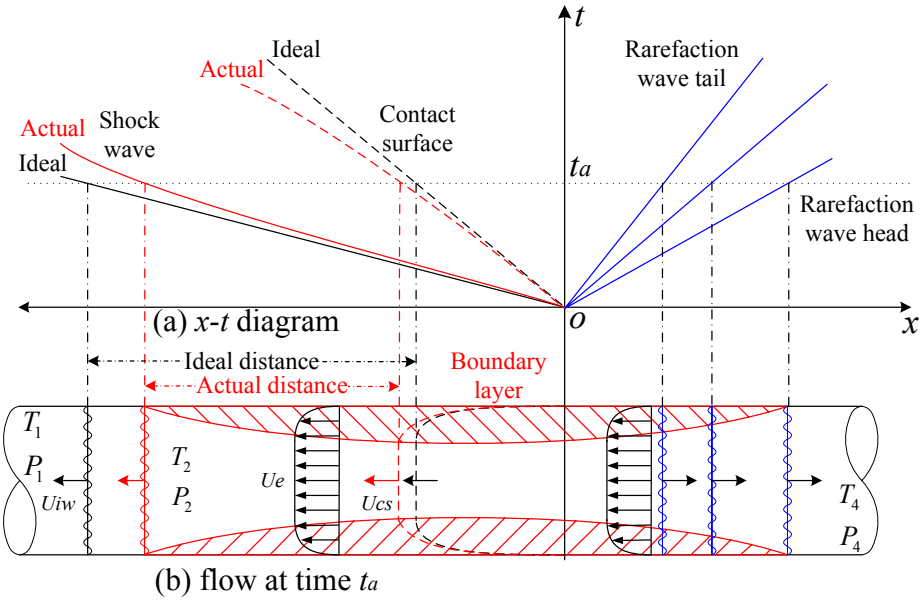

Figure 16. Boundary layer in shock tube (Adapted from Mirels, 1963).

The difference between the ideal and the real positions of the shock and the contact surface can be noticed. It can also be observed that the boundary layer begins at the incident shock wave and ends at the rarefaction wave while its thickness increases with time.

Rudinger (1961) reports the effect of the boundary layer growth on shock reflection from a closed end. It is shown that the pressure behind a propagating shock wave increases slightly with time as a result of the growing of the boundary layer, and that this pressure

increase is significantly magnified by the reflected shock wave. Finally, we note that turbulent eddies wrinkle the contact surface promoting mixing between reactants and driver gases.

Mirels (1963) also provides a relation for the critical Reynolds number for transition from laminar to turbulent regime in the boundary layer in the case of low pressure shock tubes. He shows that transition to turbulent boundary layer becomes more likely as the initial pressure of the shock tube and the shock Mach number increase.

2.4.2.3 1D modeling of flow behind shock waves

The set of equations whose solution describe the concentration, velocity and temperature distributions around the shock wave are derived from the classical conservation laws of mass, linear momentum and energy for gas phase reactive flows. In the CHEMKIN SHOCK package, the flow is assumed to be adiabatic and one-dimensional; mass, heat and linear momentum diffusion are neglected and ideal gas behavior is assumed. Since test times downstream to shock waves are typically of the order of a few hundred microseconds, molecular transport has a negligible effect on the flow field. Initial conditions for the governing equations are derived from the Rankine-Hugoniot relations for flow across a normal shock. The conservation equations for one-dimensional flow through an arbitrary cross-section tube solved in the CHEMKIN SHOCK package are:

Continuity:

$$\rho u A = \text{constant} \ , \qquad [33]$$

Momentum:

$$\rho u \frac{du}{dx} + \frac{dp}{dx} = 0 \ , \qquad [34]$$

Energy:

$$\frac{dh}{dx} + u \frac{du}{dx} = 0 \ , \qquad [35]$$

Mass of chemical species:

$$\rho u \frac{dY_k}{dx} = \dot{\omega}_k W_k \ . \qquad [36]$$

Temperature is related to the specific enthalpy of the gas mixture through the relations:

$$h = \sum_{k=1}^{N} h_k Y_k \ , \qquad [37]$$

and

$$h_k = \left(h_k\right)_0 + \int_{T_0}^{T} c_{p,k} dT \ . \qquad [38]$$

The net molar production rate of each species due to chemical reaction is denoted by $\dot{\omega}_k$. The equation of state relating the intensive thermodynamic properties is:

$$p\bar{W} = \rho \Re T \ , \qquad [39]$$

where the mixture molecular weight, $\bar{W}$, is determined from the local gas concentration using:

$$\bar{W} = \frac{1}{\sum_{k=1}^{N} Y_k / W_k} \ . \qquad [40]$$

In the shock tube experiments, the usual measurable quantities are density, species concentration, velocity and temperature as functions of time. It is therefore desirable to have time as independent variable and not distance. Employing the relation

$$\frac{d}{dt} = u \frac{d}{dx} \ , \qquad [41]$$

and differentiating equations [37], [38], [39] and [40], and combining the results, the following set of coupled, ordinary differential equations are obtained:

$$\frac{d\rho}{dt} = \left(\frac{1}{p + pu^2 / c_p T - pu^2} \right) \left(\frac{\Re \rho}{\bar{W} c_p} \sum_{k=1}^{N} \dot{\omega}_k W_k \left(h_k - \frac{\bar{W} c_p T}{W_k} \right) + \frac{\rho^2 u^3}{A} \left(1 - \frac{\Re}{\bar{W} c_p} \right) \frac{dA}{dx} \right) \ , \qquad [42]$$

$$\frac{dY_k}{dt} = \frac{\dot{\omega}_k W_k}{\rho} \ , \qquad [43]$$

$$\frac{du}{dt} = -\frac{u}{\rho} \frac{d\rho}{dt} - \frac{u^2}{A} \left(\frac{dA}{du} \right) \ , \qquad [44]$$

$$\frac{dT}{dt} = -\frac{u^2}{\rho c_p} \frac{d\rho}{dt} - \frac{1}{\rho c_p} \sum_{k=1}^{N} h_k \dot{\omega}_k W_k + \frac{u^3}{A c_p} \left(\frac{dA}{dx} \right) \ . \qquad [45]$$

The time-histories of the measurable flow quantities should satisfy these relations. The CHEMKIN SHOCK solver uses the set of equations [42], [43], [44] and [45] in order to determine the mass concentration, pressure and temperature time-histories of the system by using the corresponding initial conditions.

Chapter 3: Experiment

3.1 The High Pressure Shock Tube at IVG

The high pressure shock tube at IVG – University of Duisburg Essen is composed by a tubular section of 12.5 m divided by a diaphragm into a driver section of 6.1 m and a driven section of 6.4 m in length.

The device is instrumented at the low pressure section with pressure and quemiluminescense sensors in order to capture the incident and reflected shock waves and the time of ignition in each experiment of ignition delay time. Figure 17 shows a diagram with the basic compounds of the shock tube.

Figure 18 shows a photograph of the high pressure shock tube facility. Several kinetics studies of ignition delay times in pure fuels and gasoline surrogates have been performed in this device (see ref. Firki et al., 2008; Herzler et al., 2005; Hartmann et al. 2009; Herzler et al. 2007).

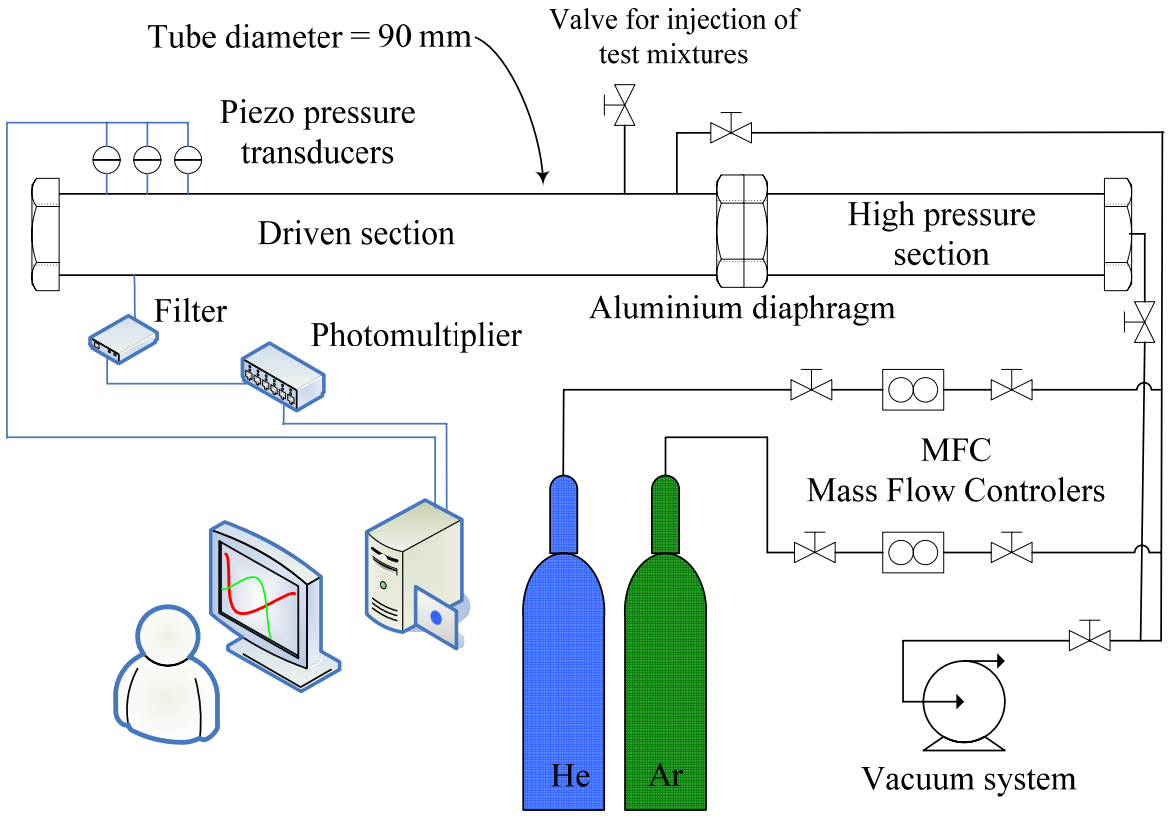

Figure 17. Diagram with the basic compounds of the shock tube at IVG – UDE (Germany).

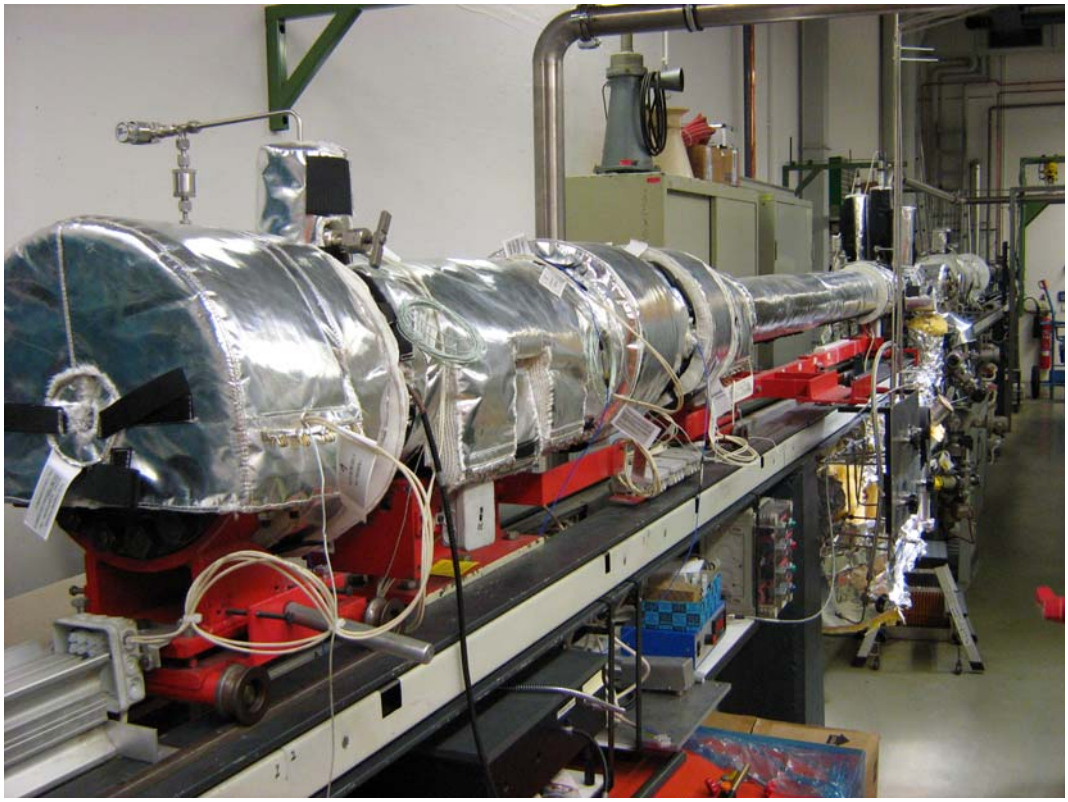

Figure 18. High Pressure Shock Tube at IVG – University of Duisburg-Essen. Maximum Operation Pressure = 500 bar.

3.2 Uncertainties related to the shock tube experiments.

There are several uncertainties associated to the ignition delay time measurements in shock tube experiment. The more representative systematic errors are related to the mixture preparation position of pressure and chemiluminescence devices, formation of boundary layer and optical access of the chemiluminescence sensor to the region of test.

3.2.1 Mixture preparation and injection into shock tube test section.

The pure hydrocarbon fuels were acquired from Merck KGaA, Darmstadt, Germany, with purity ≥ 99.8 %. The liquid mixtures were prepared in clean and haled glass-recipients. The liquid volume of mixture for each set of experiments was dosed at the volumetric composition of each binary (GS-A) and quaternary (GS-B) blends of gasoline surrogates.

The homogenization of the mixture in liquid phase is warranted by manual slow circular movements of the glass recipient during a short period of time of approximately of 3 min. The mixing is done inside a laminar flow cabinet, as shown in Figure 19 (A). The injection of the mixture into the shock tube is done using a syringe HAMILTON CO USA, of 5 ml, as shown in Figure 19 (B) and (C).

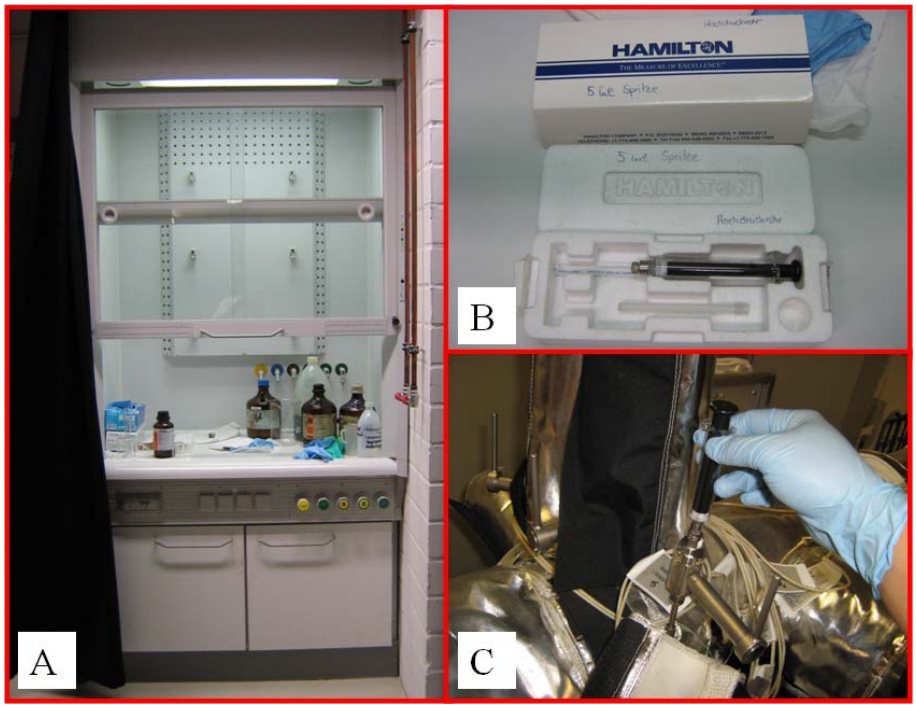

Figure 19. (A) Cabinet for mixture preparation. (B) Syringe used to the injection of the mixture to the shock tube. (C) Injection of the gasoline surrogate into the shock tube.

After injection of the liquid mixture into the shock tube, the mixture begins to evaporate. Usually 1.5 hours later, the pressure reached in the test section is measured and compared to the value calculated theoretically by using Dalton's Law, taking into account all the compounds in the mixture of gasoline surrogates. In this work, in all the valid tests there was no difference between the measured and calculated values of pressure after injection of the mixture into the shock tube test section. This fact was taken as a confirmation that there was total evaporation of the liquid mixture inside the shock tube. Also, it is leave into account the value of the vapor pressure of compounds in the mixture, the vapor pressure of each component have to be greater than the measured/calculated pressure after injection of the mixture into the test section of the shock tube, as shown in Table 7.

After the complete evaporation of the liquid mixture, the test section is filled with synthetic air (Stickstoff 4.6 AIR LIQUID Deutschland GmbH), manometrically, till the pressure reaches the calculated value of p_1 (see Table 7). In this work the synthetic air load was performed carefully and the value of p_1 always match the calculated value. One hour after the synthetic air load process is finished the experiment is performed. The synthetic air load process generates high turbulence levels inside the test section. This fact guarantee two

aspects: (a) the homogenization of the reactive mixture and, (b) it helps to reduce the possibility of stratification due to the density difference among the mixture components.

Table 7. Typical table for shock tube experiments at IVG-UDE

Gasoline Surrogate - B -- Data for P5 = 50 bar -- ø =1.0										
Exp. #	**Pressure (mbar) (after injection)**	**P1A (mbar)**	**P2 (atm)**	**T2 (K)**	**T5 (K)**	**V (m/s)**	**Liquid Mixture (ml)**	**Argon (m^3n/h)**	**Helium (m^3n/h)**	
V	33.880	1022.40	9.74	765.64	1200.00	1021.00	4.430	7.88	200.00	
V	37.236	1123.70	10.04	740.15	1150.00	989.70	4.869	9.44	200.00	
V	41.183	1242.80	10.38	714.66	1100.00	957.70	5.385	11.20	200.00	
V	45.855	1383.80	10.76	689.23	1050.00	925.00	5.996	13.20	200.00	
V	51.466	1553.10	11.19	663.83	1000.10	891.50	6.730	15.40	200.00	
V	58.295	1759.20	11.68	638.42	950.04	857.09	7.623	17.90	200.00	
V	61.360	1851.70	11.90	628.55	930.50	843.45	8.024	19.00	200.00	
V	66.692	2012.60	12.26	613.18	900.07	821.89	8.721	20.00	192.00	
V	77.190	2329.40	12.93	588.06	850.08	785.79	10.093	20.00	165.00	
V	90.584	2733.60	13.72	563.08	800.02	748.70	11.845	20.00	141.00	
V	108.005	3259.30	14.68	538.30	750.00	710.61	14.123	20.00	121.00	
V	136.784	4127.80	16.11	508.84	690.04	663.50	17.886	20.00	99.00	
						Total liquid mixture (ml)	97.700			
Shock tube pre-heated to: 338.15 K - (65 °C)										
Mixture:	**** Gasoline Surrogate B ****									
Ethanol	40.0 % (Volume) -Vapor Pressure (mbar) @ T= 338.15 K ----- P v = 584.41 mbar									
iso-Octane	37.8 % (Volume) - Vapor Pressure (mbar) @ T= 338.15 K ----- P v = 342.50 mbar									
Toluene	12.0 % (Volume) - Vapor Pressure (mbar) @ T= 338.15 K ----- P v = 225.10 mbar									
n-Heptane	10.2 % (Volume) - Vapor Pressure (mbar) @ T= 338.15 K ----- P v = 337.93 mbar									
Brazil - Leonel Dez 18, 2007 IVG - UDE										

The pressure transducers (KELLER Druckmesstechnik type PAA-35XHTC) have an accuracy of 0.5 % FS (Full Span). This value can be used in order to estimate the uncertainties in the stoichiometry, ϕ. Taking the last experiment on Table 7 as an example for error calculations, pressure after injection of 136.78 mbar and fixing p_1 as 4127.80 mbar, the accuracy of the device indicates an error propagation, of about ± 0.009 in the stoichiometry of the mixture, ϕ.

3.2.2 Shock speeds measurements.

Shock speeds were determined by using the signals of three piezopressure transducers placed over the last 1.0 m of the shock tube and extrapolated to the endwall section. Shock attenuations were typically 0.7%/m to 2.5%/m. The measured shock velocities were compared to the initially estimated values of incident shock waves and differences of about ±0.3% were found. Afterward, reflected shock conditions were determined from the standard one-dimensional shock relations and the blended thermodynamic database (Marinov 1999; Curran et al. 1998; Metcalfe et al. 2007; Andrae et al. 2007 and Maurice 1996) for iso-octane, n-

heptane, toluene and ethanol. Using the SHOCK package of CHEMKIN, uncertainties of about ± 0.3% in the incident wave speed yield variations in the calculated T_5 of about ± 7 K and variations in the calculated ignition delay time of about ± 7.5%, in agreement with the experimental uncertainties (temperature and ignition delay time) cited in the literature for shock tube experiments (Davidson et al. 2002; Vasudevan et al. 2005; Dean et al. 2007; Davidson et al. 2000). In this work, the estimated uncertainties in the ignition delay time are in the range of ± 7.5% to ± 10%.

3.2.3 Formation of boundary layer.

As discussed by Davidson and Hanson (2004), in shock tube experiments there are several nonideal effects that influence the measurement of ignition delay time. When modeling ignition delay in shock tubes, Perfectly Stirred Reactor conditions (Zeroth-order approximation model) are used and then, the numerical results are compared to the measurements.

The simulation also assumes that behind the shock wave the spatial and temporal conditions are uniform, i.e., the incident and reflected shock waves travel through the test gas and leave it unperturbed. In a real shock-heated gas ignition process there is the formation of a boundary layer at the tube wall that grows with time the propagation of the shock wave and contact surface, as described in section 2.4.2.2. The observed effect of the of formation and growth of the boundary layer behind the incident shock wave is the generation of a gradual increase in temperature and pressure in the core of the flow (T_2 and p_2). When the shock wave returns as a reflected shock, it sets the temperature and pressure (T_5 and p_5) to values higher than those calculated initially using the Rankine-Hugoniot relations. Also, the displacement of the reflected shock wave also creates a boundary layer behind it, affecting the temperature and pressure (T_5 and p_5).

Petersen and Hanson (2000) proposed a methodology to evaluate this source of systematic error in high pressure shock tubes. They proposed a relation between the relative change of T_5 with reflected shock test time ($dT^*/d\tau$), the expression

$$\frac{dT^*}{d\tau} \approx 10 \ s^{-1} \ , \qquad [46]$$

is proposed for the relative change on temperature T_5 for larger diameter shock tubes (~15 cm). For shock tube diameter less than 10 cm the value of the relative change ($T^* = \Delta T_5 / T_{5\text{initial}}$) increase to values of 20 – 30 s^{-1}. Assuming the boundary layer effect as

major systematic error on temperature, and for shock tube diameter of 9 cm, we can use equation [46] in order to estimate the uncertainties on temperature T_5, as follows:

$$\frac{dT^*}{d\tau} \approx 20\ s^{-1}\ ,$$

$$\int_{T_0^*}^{T^*} dT^* \approx 20\ s^{-1} \times \int_{\tau_0}^{\tau} d\tau\ ,$$

$$T^* \approx 20\ s^{-1} \times (\tau)$$

$$\frac{\Delta T_5}{T_{5\ \text{initial}}} = \frac{T_{5\ \text{final}} - T_{5\ \text{initial}}}{T_{5\ \text{initial}}} \approx 20\ s^{-1} \times (\tau_{ign})\ ,$$

$$T_{5\ \text{final}} \simeq \left[20\ s^{-1} \times (\tau_{ign}) + 1\right] T_{5\ \text{initial}}\ .$$

For example, ignition of ethanol at $T_{5\ \text{initial}}$ = 937 K, with ignition delay time of τ = 1006 μs, the estimated increase on temperature ΔT_5 is about ± 19 K.

3.3 Preparation and measurement procedure

The steps taken to perform a single test can be summarized as follows. The driven section is pumped down to pressures below 10^{-2} mbar. Gas mixtures are prepared by injection of a liquid mixture and subsequent complete evaporation. The measured pressure into the driven section, when the fuel is injected, must be inferior to the vapor pressure of the fuel mixture.

The total amount of fuel and air is controlled manometrically in order to ensure the desired equivalence ratio. The shock speed is measured over two time intervals using three piezo-electric pressure gauges. The data is recorded with a time resolution of 0.1 μs. The temperature and pressure downstream to the reflected shock wave are calculated from the measured incident shock speed and the attenuation using an one-dimensional shock-tube model (CHEMKIN).

The estimated uncertainty, equation [46], in reflected shock temperature is less than ±25 K in the temperature and time range of the measurements. The experiments are carried out in synthetic air containing 79.5% N_2 and 20.5% O_2 by volume.

The model calculations used here are based on an isobaric assumption. The first stage of pre-ignition, however, causes indeed a slight pressure increase, which can expand in the form of a non-stationary wave, thus influencing the ignition behavior. In the crucial case, i.e., long time observation related to low-to-intermediate temperature value, the maximum temperature increase due to this effect was estimated to be 70 K. Moreover, it should be

mentioned that small changes in temperature are most relevant to measurements at low temperature and therefore do not dramatically affect the ignition delay times τ_{ing} in the NTC range. It can be argued that this effect is to some extent fuel-specific and also dependent on how well the driver gas tailoring was chosen.

The driver gas is mixed in-situ by using two high-pressure mass-flow controllers (Bronkhorst Hi-Tec flow meter). Helium is used as the main component and 5 – 20% Argon is added to match the acoustic impedance of the test gas. The acoustic impedance is defined as the ratio of acoustic pressure to acoustics volume flow and it is strongly dependent of the density of the flow.

The composition was calculated for each experimental condition using equations by Oertel (1966) and Palmer and Knox (1961). After rupture of the diaphragm, the ignition is observed downstream the reflected shock waves by measuring the pressure history with a piezo-electric gauge (PCB HM 112 A03) at a side-wall position 15 mm upstream to the endplate. Also, CH* chemiluminescence is measured at the same position.

The spontaneous light emission from the test region is filtered by a band pass filter (431.5 nm, 5 nm HWHM) and detected with a photomultiplier with a time resolution of 1 μs. Then, ignition delay times are determined by extrapolating either the steepest increase of the CH* emission signal to its zero level on the time axis or the pressure increase due to the ignition, as shown in Figure 20. Both procedures yield very similar results (< 5 % deviation). In this work, the data obtained from the chemiluminescence measurement is used.

Figure 21 (A) shows the diaphragm in its initial state. This diaphragm has a thickness of 3.1 mm and depth of the cross groove of 0.8 mm. The groove is used to facilitate an uniform burst of the diaphragm. Figure 21 (B), (C), and (D) show the diaphragm after a typical valid experiment at high pressure and high temperature.

Table 8 shows the main characteristics of the aluminium diaphragms used in this work in order to obtain the desired pressures p_5 in the experiments.

Table 8. Characteristics of the diaphragms used in this work.

Thickness [mm]	**Groove depth [mm]**	**Expected p_5 [bar]**
1.5	0.50	10
3.1	0.80	30
4.1	0.89	50

Figure 20. Definition of ignition delay time from measurements of pressure and CH* signals in the experiments.

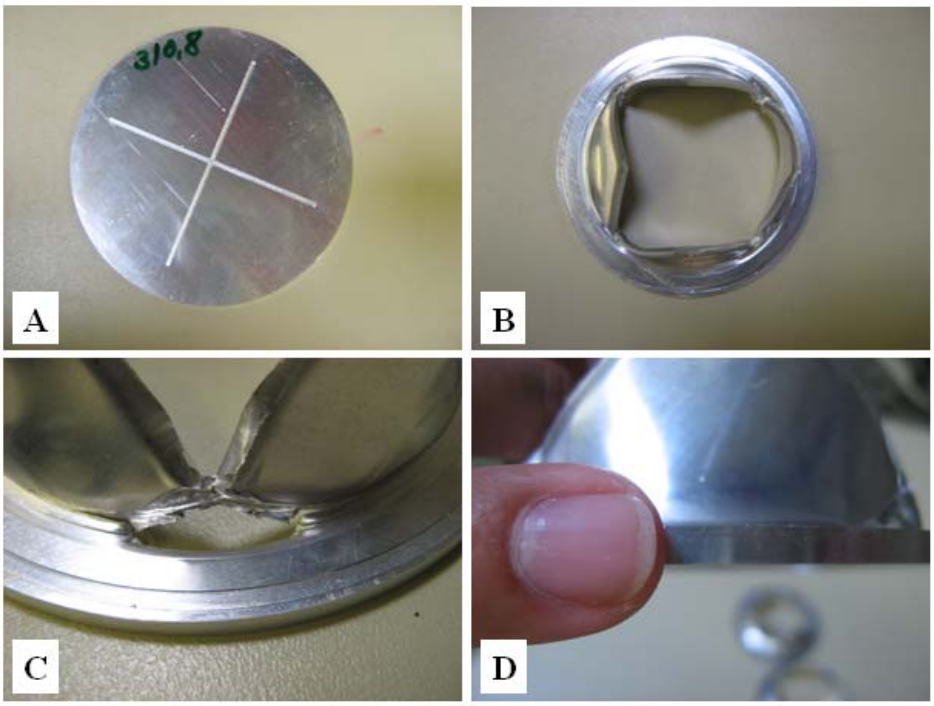

Figure 21. Diaphragms (a) before rupture and (b,c,d) after rupture in a typical valid high pressure shock tube experiment.

3.4 Results

Around 100 tests involving pure ethanol and ethanol containing hydrocarbon fuels (gasoline surrogates) were performed. The experiments were done over the pressure range of 10 – 50 bar, intermediate temperatures covering the range 690 – 1200 K at lean (ϕ = 0.3) and stoichiometric (ϕ = 1.0) compositions. The experimental conditions are comparable to the operating conditions found in combustion chambers of spark-ignition internal combustion engines. Table 9 summarizes the experiments performed at IVG and the composition of the gasoline surrogates analyzed.

Table 9. Experimental conditions of ignition delay time measurements performed in the high pressure shock tube at IVG – UDE.

Mixture	Composition [% by volume]				Oxidizer	Pressure [bar]	Temperature [K]	Equivalence ratio	Octane number
	Ethanol	iso-Octane	n-Heptane	Toluene					
Ethanol pure	100	***	***	***	air	10, 30, 50	690 - 1200	0.3, 1.0	110
Gasoline surrogate A	25	75	***	***	air	30	800 - 1200	1.0	105
Gasoline surrogate B	40	37.8	10.2	12	air	10, 30, 50	690 - 1200	1.0	98.8

Synthetic air containing 79.5% N2 and 20.5% O2 by volume was used

Typical pressure and CH* emission profiles are shown in Figure 22 for an experiment at T = 764 K, p = 31.5 bar and ϕ = 1.0 of surrogate B, comprised of ethanol/iso-octane/n-heptane/toluene at a composition of 40% / 37.8% / 10.2% / 12% by liquid volume.

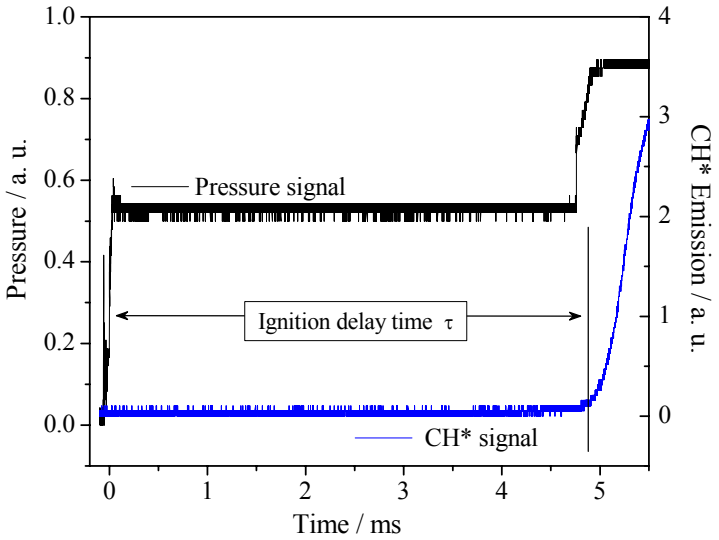

Figure 22. Example of surrogate A/air ignition data showing the determination of the ignition delay time

The two-step increase in pressure is due to the passage of the incident and the reflected shock wave (time zero) followed by a constant pressure for about 4750 μs. The CH* emission (upper part of Figure 22) remains at zero level for 4750 μs, followed by a steep rise that indicates ignition. Ignition delay times shown here are based on an extrapolation of the increase in CH* chemiluminescence emission to the zero level.

In this work, one test was performed for each experimental condition of pressure and temperature (T_5, p_5), except for dispersed experimental results, for which two or three additional tests were performed. Experimental results for gasoline surrogates GS-C, GS-D and GS-E were obtained from the experimental work of Fikri et al., (2008).

3.4.1 Measurements of IDT for ethanol-air system, ϕ = 1.0 , ϕ = 0.3

The ignition delay times evaluated from the CH* emission are listed in Table 10 along with the respective pressures p and temperatures T, for stoichiometric and lean ethanol-air mixture. At temperatures lower than those shown in Table 10 no ignition was observed within the test time of the experiment (15 ms).

Figure 23 shows the experimental results for ignition delay time as a function of temperature (as an Arrhenius plot) for different pressures. The data can be conveniently curve-fitted to an equation of the form

$$\tau = A \exp\left(B/T\right) p^{-x} \qquad [47]$$

where x is the pressure exponent (pressure dependence factor). Multiple linear regression analysis using ln(τ) as the dependent variable and (1/T) and ln(p) as independent variables identified the value of x as 0.83, using the data for ϕ = 1.0 listed in Table 10.
The correlation coefficient, R^2, of the regression was 0.94. An expression of $\tau = \tau_{30}$ (p/30 bar)$^{-0.83}$ was identified for the scaled pressure. For the temperature behavior, an expression of

$$\tau / \mu s = 10^{-1.79} \exp\left(+51.88 \text{ kJ/mol} / \Re T\right)\left(p / \text{bar}\right)^{-0.83}$$

was determined from a fit for the measured range of temperature and for a stoichiometric mixture. The fitting is shown in Figure 23.

The measured ignition delay times decreased for higher temperatures and presented a lower sensitivity to pressure for the higher pressures.

Table 10. Measured ignition delay times of the ethanol – air system.

ϕ	T_5 [K]	p_5 [bar]	τ_{ing} [µs]	ϕ	T_5 [K]	p_5 [bar]	τ_{ing} [µs]
1.0	1223	10.5	70	1.0	1234	53	16
1.0	1190	10.0	140	1.0	1168	52	30
1.0	1145	11.0	252	1.0	1085	48	134
1.0	1096	9.0	409	1.0	1065	52	156
1.0	1049	10.1	738	1.0	999	50	511
1.0	992	9.8	1171	1.0	937	48	1006
1.0	954	10.3	1698	1.0	881	48	2095
1.0	900	10.1	N-I	1.0	841	49	3304
				1.0	781	47	N-I
1.0	1197	30	25	1.0	769	45	N-I
1.0	1152	30	38				
1.0	1138	32	75	0.3	1183	30.2	58
1.0	1116	31	80	0.3	1151	30.8	111
1.0	1045	30	267	0.3	1107	33.7	172
1.0	999	30	547	0.3	1100	37.0	228
1.0	949	30	1244	0.3	1081	35.7	295
1.0	912	31	877	0.3	1042	26.7	621
1.0	881	31	2788	0.3	1024	35.7	686
1.0	848	30	2715	0.3	996	33.5	1029
1.0	801	30	3755	0.3	912	30.9	4759
1.0	789	29	N-I	0.3	868	31.6	13027

N-I: No Ignition within the test time

At the temperature about 910 K and 30 bar the experimental results suggest the possible existence of a negative temperature coefficient (NTC) region. However, due to the scatter exhibited by the measurements additional experiments in this temperature range are necessary in order to elucidate the presence of NTC.

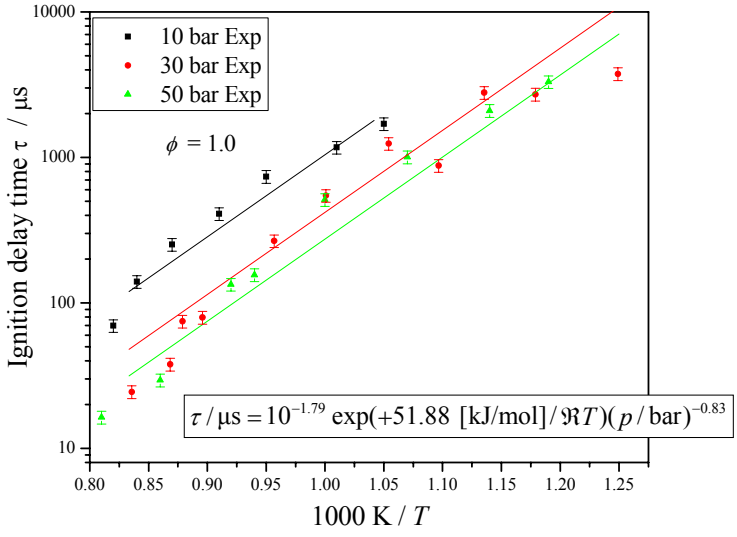

Figure 23. Experimental and curve fitted ignition delay times for ethanol-air system, ϕ = 1.0.

Figure 24 shows the comparison between the experimental results for lean (ϕ = 0.3) and stoichiometric (ϕ = 1.0) mixtures at pressure of 30 bar. The typical negative dependence of the IDT with the concentration of fuel in the mixture, from lean to stoichiometric composition, is evidenced.

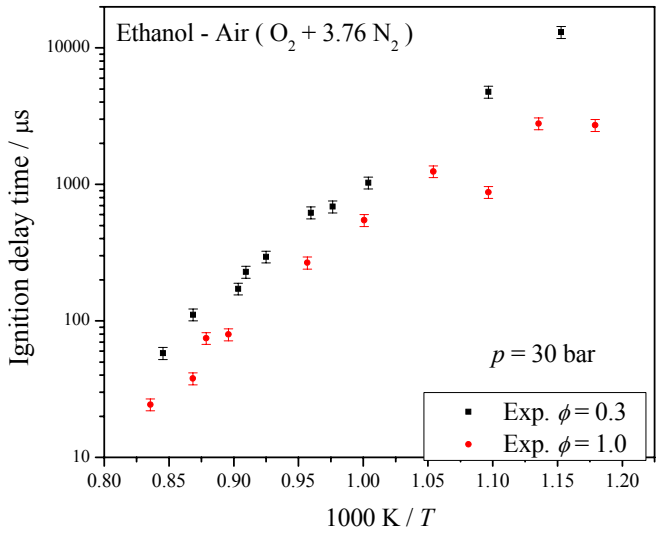

Figure 24. Measured ignition delay times for ethanol-air mixtures for lean mixtures, ϕ = 0.3 and ϕ = 1.0, at pressure of 30 bar.

3.4.2 Measurements of IDT for Gasoline Surrogate A, ϕ = 1.0

The ignition delay times evaluated from the CH* emission are listed in Table 11 along with the respective temperatures T and pressures p, for stoichiometric ethanol/iso-octane (25% / 75%) - air mixture (Surrogate A in Table 9). At temperatures lower than those shown in Table 11 no ignition was observed within the test time of the experiments (15 ms).

Figure 25 shows the measured ignition delay time for the mixture ethanol/iso-octane (25% / 75%) - air mixtures. A regression analysis taking ln(τ) as dependent variable and 1000/T_5 as independent variable, by using equation [47], was performed. The resulting fitted expression

$$\tau / \mu s = 10^{-3.10} \exp\left(+55.53 \text{ kJ/mol} \Big/ \Re T \right),$$

conveys an apparent activation temperature of 13,273 K (E_a ~55.53 kJ/mol). The correlation coefficient, R^2, of the regression was 0.94. The pressure dependency was not measured.

Table 11. Measured ignition delay times for ethanol/iso-octane – air mixtures (25% / 75%) at pressure of 30 bar and stoichiometric composition.

ϕ	T_5 [K]	p_5 [bar]	τ_{ing} [µs]
1.0	1217	30.9	35
1.0	1215	30.8	34
1.0	1169	29.2	58
1.0	1164	30.7	74
1.0	1132	31.9	78
1.0	1059	30.6	404
1.0	1004	30.3	791
1.0	967	31.2	683
1.0	909	30.7	2039
1.0	862	31.1	2097
1.0	809	30.7	N-I

N-I No Ignition

Comparing Figure 25 to Figure 24, it is observed that the presence of iso-octane did not improve the ignition of ethanol at high temperature but provided a small decrease of ignition time at lower temperatures. This small difference is evidenced by the values of the apparent activation energies.

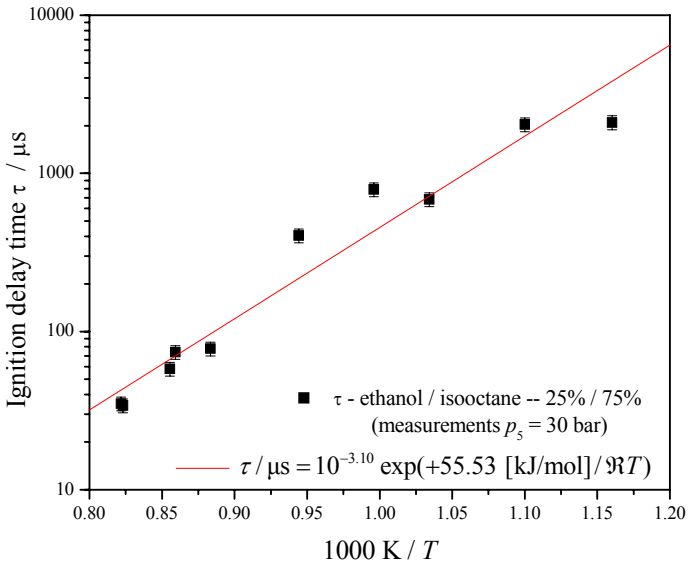

Figure 25. Ignition delay time for mixture ethanol/isooctane (25% / 75% by liquid volume) / air, at pressures of 30 bar and stoichiometric composition.

3.4.3 Measurements of IDT for Gasoline Surrogate B, ϕ = 1.0

Ignition delay times were measured for surrogate B, comprised of ethanol/iso-octane/n-heptane/toluene at a composition of 40% / 37.8% / 10.2% / 12% by liquid volume, which is characterized by a calculated octane number of 98.8 by using a program from Shell (Kalghatgi, 2007). The experiments were carried out with stoichiometric mixtures ϕ = 1.0, temperature range of 690 < T < 1200 K, and pressure of 30 ± 2 bar. The results of the ignition delay time experiments for surrogate B are presented in Table 12 and depicted in Figure 26. For this data set, a flat temperature dependence behavior is observed at around 900 K. Note that, for pressure of 10 bar and temperature below 900 K, no-ignition was observed during the available measurement time. However, contrary to the other mixtures, at p_5 = 30 bar ignition was observed below 800 K Multiple linear regression analyses using ln(τ) as the dependent variable and (1/T) and ln(p) as independent variable identified the value of x as 0.72, using the data for ϕ = 1.0 listed in Table 12. The correlation coefficient, R^2, of the regression was 0.89. An expression of $\tau = \tau_{30}\ (p/30\ \text{bar})^{-0.72}$ was identified for the scaled pressure. For the temperature behavior, an expression of

$$\tau / \mu s = 10^{-1.39} \exp\left({+99.1\ \text{kJ/mol}} \Big/ {\Re T} \right) \left({p} \Big/ {\text{bar}} \right)^{-0.72},$$

was determined from a fit for the measured range of temperature and for a stoichiometric mixture. The fitting is shown in Figure 27. There is considerable scatter from the curve fit at lower and higher temperatures.

Table 12. Measured ignition delay times for gasoline surrogate B at pressures of 10, 30 and 50 bar and stoichiometric composition.

ϕ	T_5 [K]	p_5 [bar]	τ_{ing} [µs]	ϕ	T_5 [K]	p_5 [bar]	τ_{ing} [µs]
1.0	1201	10.1	158	1.0	1016	31	555
1.0	1162	10.3	544	1.0	983	28	774
1.0	1093	9.9	939	1.0	951	30	806
1.0	1058	10.3	1438	1.0	858	31	2795
1.0	1010	10.3	2436	1.0	809	26	6944
1.0	935	9.8	3495	1.0	793	29	6962
1.0	906	10.3	N-I	1.0	764	31	4975
1.0	853	10.2	N-I	1.0	701	30	8731
1.0	806	10.3	N-I				
1.0	758	10.4	N-I	1.0	1191	50	28
1.0	683	9.8	N-I	1.0	1102	51	110
				1.0	985	49	534
1.0	1194	30	50	1.0	930	48	1705
1.0	1168	31	94	1.0	891	49	2296
1.0	1128	32	149	1.0	828	47	3792
1.0	1057	30	314	1.0	788	48	5037

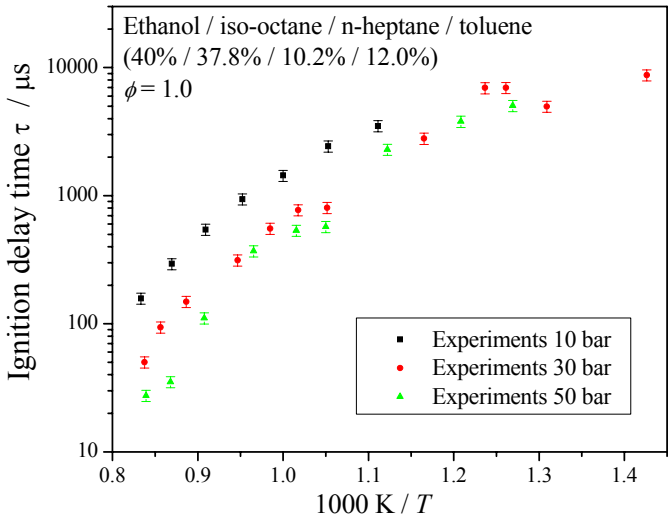

Figure 26. Measured ignition delay times for gasoline surrogate B, at pressures of 10, 30 and 50 bar and stoichiometric composition.

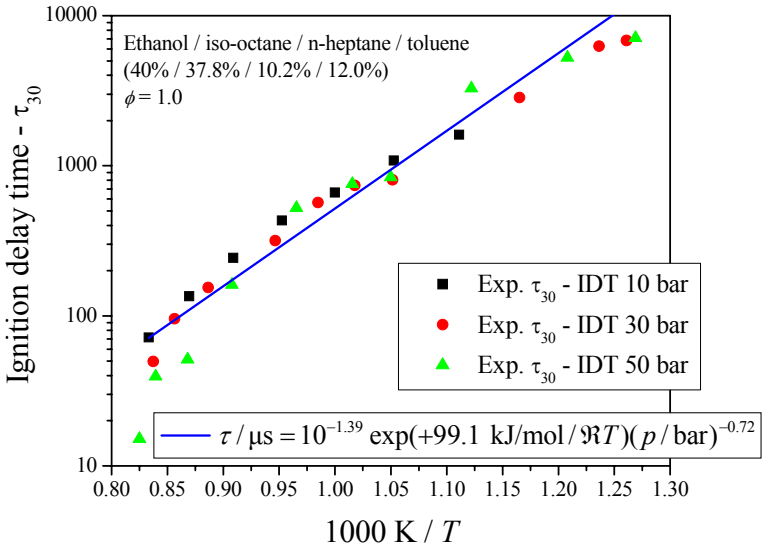

Figure 27. Scaled pressure fitting to pressure p = 30 bar for gasoline surrogate B at stoichiometric composition.

3.4.4 Comparison between ethanol pure, GS-A and GS-B, ϕ = 1.0

Figure 28 shows the measured ignition delay times for ethanol pure, Gasoline surrogate – GS-A and Gasoline surrogate – GS-B at pressure of 30 bar and stoichiometric composition.

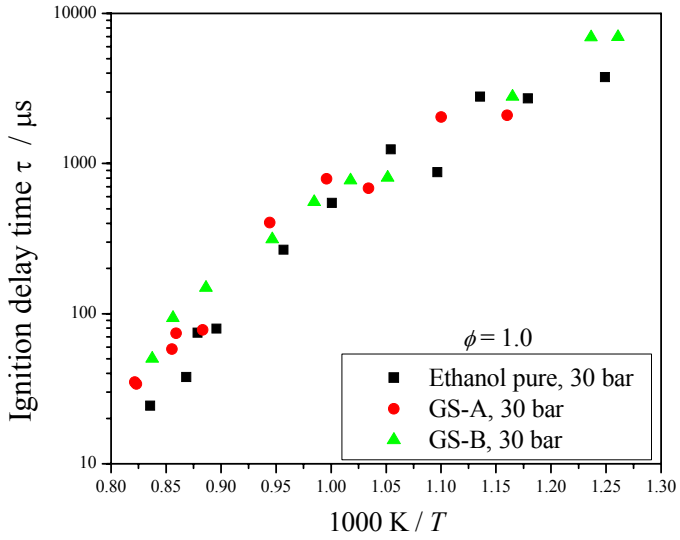

Figure 28. Experimental results of ignition delay time for ethanol pure, Gasoline surrogate – GS-A and Gasoline surrogate GS-B at pressure of 30 bar and stoichiometric condition.

It can be observed that for higher and lowers temperatures (T > 1050 K and T < 850 K), Gasoline surrogate B present more resistance to the autoignition process. For intermediate temperatures (1050 K > T > 850 K), ethanol pure, GS-A and GS-B gives similar results of ignition delay times.

Chapter 4: Modeling and Analysis

The adaptation process of the kinetics models was based on blending the different sub-mechanisms for ethanol and other sub-structures from Marinov (1999), Li (2004) and Lin et al., (2002, 2003, 2004), Cancino et al., (2009b), that were not taken into account by Konnov (2000), Metcalfe et al., (2007), Andrae et al., (2007) and Maurice (1996). Then, the predictions of ignition delay time using the mechanisms formed are compared to the measurements and results from the individual mechanisms, in order to extend the validation of the kinetics model.

The blending of two different mechanisms requires a sequence of steps that can be outlined as:

1. Analyze and potentially adjust the kinetics information of the mechanisms for their use in CHEMKIN.
2. Check the species names in both mechanisms the mechanisms and remove duplicate reactions from the second (minor) mechanism.
3. Add the missing reactions into the major mechanism.
4. Check the thermodynamic data base of the major mechanism and upgrade it with data for the missing species.
5. Test the blended kinetics model with the CHEMKIN interpreter and validate it against measured ignition delay times to ensure/guarantee that the added reactions for an additional fuel component do not change the behavior of the base mechanism in case this component is not present.
6. Determine the rate-controlling route for autoignition via an overall sensitivity analysis and check whether the most sensitive reactions have reliable, i.e., directly measured, kinetics data.

The blending procedure is time consuming. When two chemical species have the same empirical formula, it is necessary to check their thermodynamic databases by comparing the enthalpy h, heat capacity c_p, and entropy s at several temperatures. If their thermodynamic properties return the same (or similar) values, then, both chemical species are considered to be identical despite different names or abbreviations used in the original kinetics models. Productivity increases with the use of computational tools. The programs of Rolland and Simmie (2004) were used to compare the kinetics mechanisms and thermodynamic databases.

4.1 Ethanol-air system

4.1.1 Chemical reaction pathways for thermal oxidation of ethanol

Several authors have qualitatively described the decomposition of ethanol. Recently, Lin et al., (2002, 2003 and 2004) reported 11 different routes for ethanol decomposition involving reactive radical species.

Figure 29 summarizes these major routes. Box I shows the decomposition routes involving methyl radical giving methane as a product in three routes and hydrogen atom in a fourth route. The fifth route gives C_2H_6 (ethane), $CH_3CH_2OCH_3$ (methoxy), CH_3CH_2 (ethyl radical), CH_3OH (Methyl alcohol), CH_2CH_2OH (Ethoxy radical), CH_3CH_2O (Methyl radical, methoxy-), CH_3CHOH (Ethyl radical, 1-hydroxy) and CH_4 (Methane)

Box II depicts H abstraction involving H atoms and producing molecular hydrogen via three routes and additional other unstable species. Box III depicts the H abstraction by a cleavage process involving a third body (bimolecular); all routes giving acetaldehyde, molecular and atomic hydrogen. Box IV shows the decomposition by cleavage involving a third body (bimolecular) of the C–C and C–O bonds and the products are formaldehyde, methane and other unstable species. One can clearly see that the pyrolysis of ethanol proceeds by a chain-branching mechanism.

Kinetics models of ignition of ethanol/O_2 (Borisov et al., 1992) and ethanol/air (Cancino and Oliveira, 2005a; Gardiner, 2000) show that during the induction period ethanol is consumed almost completely. The depletion of the fuel is induced by oxidative pyrolysis. Therefore, the ethanol oxidation model capable of describing accumulation of the products during the induction period and the promoter effect on the ignition process must be based on an ethanol pyrolysis mechanism (Borisov et al., 1992), such as the one described above and depicted in Figure 29.

Since the pathways depicted in Figure 29 proceed at different rates, depending on the range of temperature and pressure considered, a careful analysis and comparison to critical experiments may be able to reveal the most important routes for different pressure and temperature regimes. The mechanistic analysis for temperature can be usually separated in a low temperature regime (below 1000 K) and a high temperature regime (above 1000 K).

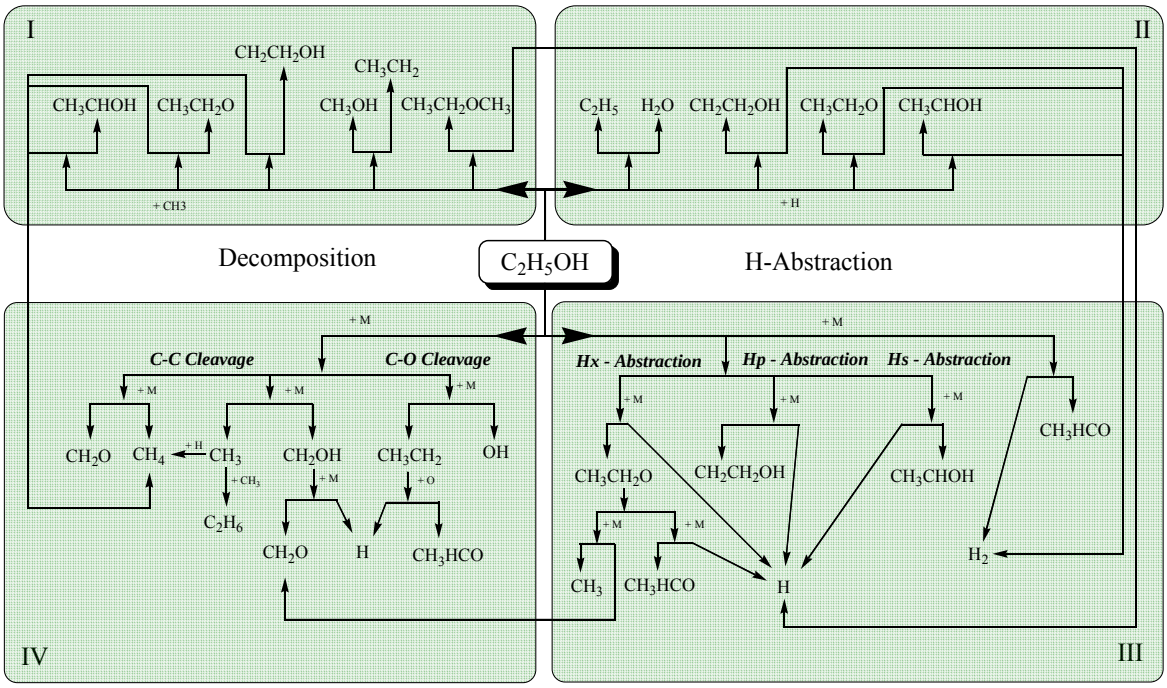

Figure 29. Ethanol decomposition pathways.

4.1.1.1 Low-temperature (T < 1000 K) oxidation of ethanol

Information on low-temperature oxidation of ethanol is scarce. Battin-Leclerc (2008) recently reported an extensive review of kinetics models for low-temperature oxidation of hydrocarbons involving alkanes, alkenes, cycloalkanes and aromatic compounds, but did not include ethanol and other oxygenated hydrocarbons.

Barnard and Hughes (1960) reported experimental results of the ethanol pyrolysis in a reaction vessel for a temperature range from 850 to 900 K and pressures in the range of 6.6×10^{-2} to 4.66×10^{-1} bar. They measured the concentration history of H_2, CO, CH_4, CH_3HCO and C_2 throughout the reaction and revealed that the major pyrolysis products are molecular hydrogen and acetaldehyde (CH_3HCO). They also found that the rate of reaction measured as $-d[C_2H_5OH]/dt$ was of first order with respect to the initial ethanol concentration in the pressure range from 4.66×10^{-2} to 1.0×10^{-1} bar. The fitted global Arrhenius equation for the experimental results was $k_a(T)=10^{10.0(\pm0.4)}\exp[-46200(\pm1700)/RT]$ s^{-1}. Above 0.1 bar the reaction order of the depletion of ethanol was found to be of a higher order.

Borisov et al. (1991) reported experimental results of ethanol pyrolysis in a temperature range of 700 to 1700 K and at pressure of 1 bar in a static vessel. They found that their results agreed fairly well with the T-dependence of the effective rate constant proposed by Barnard and Hughes (1960). The comparison between Borisov´s and Barnard´s results

indicates that the effective rate constant of ethanol is not strongly dependent on the pressure at temperatures below 900 K.

Both Barnard and Hughes (1960) and Borisov et al., (1991) proposed general guidelines for the ethanol pyrolysis at low temperatures, depicted in Figure 30, which are a sub-set of the more complete scheme depicted in Figure 29. They proposed that the pyrolysis starts with a first stage of H-abstraction in the three possible locations: Hx, in the hydroxyl group; Hs, attached to the secondary carbon and Hp, attached to the primary carbon. H atoms are released and three C_nH_pO radicals are formed: CH_3CH_2O, CH_2CH_2OH and CH_3CHOH. In a second stage, these H atoms react with ethanol provoking further H-elimination as H_2 and forming more C_nH_pO radicals (CH_3CH_2O, CH_2CH_2OH and CH_3CHOH). The H atoms released in the first two stages accelerate the ethanol depletion. In a third stage, the C_nH_pO radicals decompose releasing more hydrogen atoms and acetaldehyde. Therefore, the low-temperature ethanol oxidation proceeds basically by H abstraction. The cleavages of the C–C and C–O bonds in the parent molecule are, due to energetic restrictions, unimportant (Borisov et al., 1991).

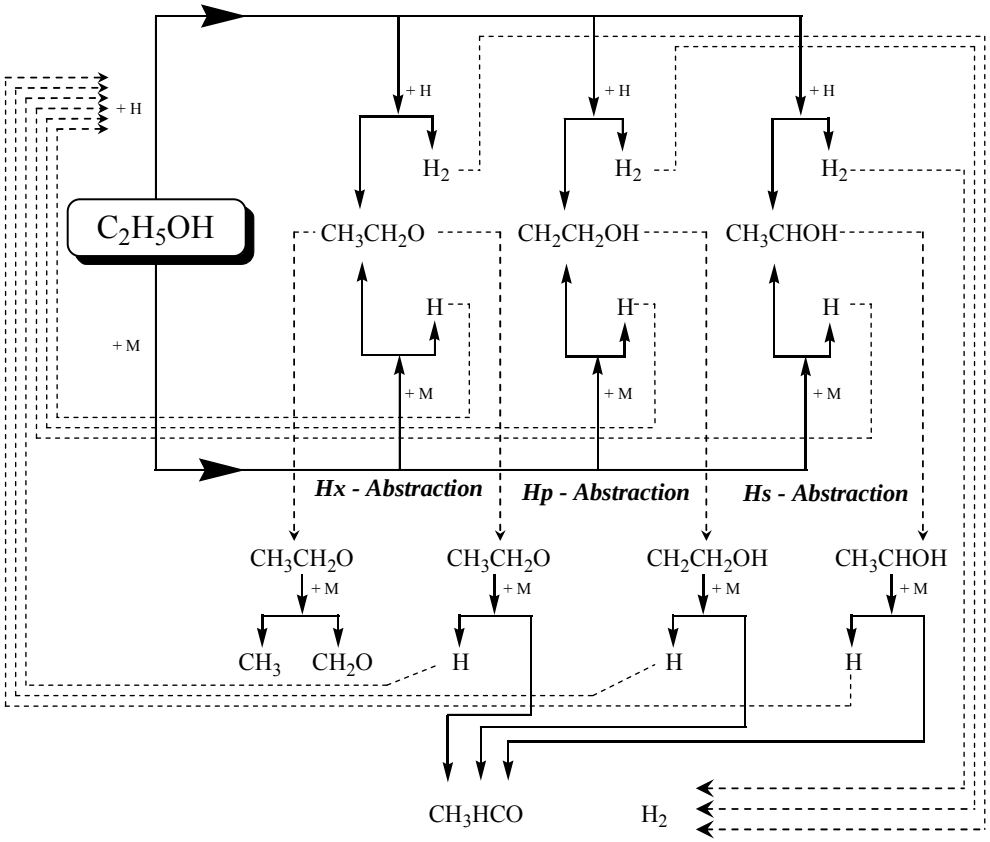

Figure 30. Low-temperature ethanol oxidation routes.

4.1.1.2 High-temperature (T > 1000 K) oxidation of ethanol

Several studies about the high-temperature oxidation of ethanol have been published. Borisov et al. (1989) reported the first data of ignition delay time measurements in a shock tube for mixtures of ethanol and oxygen in a temperature range of 700 to 1550 K and pressures between 0.5 and 6.0 bar. In their study, they also present data for acetaldehyde. Borisov et al., (1991) reported data of ethanol pyrolysis at atmospheric pressure, in a temperature range of 700 to 1700 K in a static reaction vessel. They developed the first detailed kinetics model for ethanol, including pyrolysis and oxidation reactions involving hydrogen, methane, formaldehyde, acetaldehyde, and ethanol. The model was tested for lean, stoichiometric and rich ethanol/O_2 mixtures at atmospheric pressure and temperatures between 900 and 1500 K.

Dunphy and Simmie (1991) reported a survey on shock tube measurements of ignition delay times in ethanol/O_2 mixtures covering equivalence ratios of $0.2 \leq \phi \leq 2.0$, temperatures between 1080 and 1660 K and pressure range of 1.8 to 4.6 bar. Dunphy et al., (1991) developed a detailed kinetics model for the high-temperature ethanol oxidation with molecular oxygen and this model was validated against measurements of Dunphy and Simmie (1991).

Egolfopoulos et al., (1992) reported a detailed kinetics model for the high-temperature oxidation of ethanol/O_2/Ar mixtures that was tested against shock-tube data for 1300 K $\leq T \leq$ 1600 K and 0.8 bar $\leq p \leq$ 1.0 bar.

Similarly, Curran et al., (1992) studied ethanol oxidation in a shock tube by measuring the ignition delay time of ethanol/O_2 mixtures at pressure of 2.3 bar at 1100 K $\leq T \leq$ 1900 K and $0.25 \leq \phi \leq 1.5$. A detailed kinetics model was validated against the obtained experimental results.

Cancino and Oliveira (2005a, 2006) numerically analyzed the performance of the thermal ignition of ethanol/air mixtures using the detailed kinetics models of Marinov (1999) and Konnov (2000) at 1.0 bar $\leq p \leq$ 5.0 bar and temperatures of 1200 and 1400 K. Some key reactions of the ethanol oxidation were analyzed and a detailed kinetics model including NOx kinetics was proposed.

Saxena and Williams (2007) performed a detailed kinetics model for ethanol oxidation and validated it against experimental data of Dunphy and Simmie (1991) for 1300 K $\leq T \leq$ 1700 K and 1.0 bar $\leq p \leq$ 4.6 bar.

Cancino et al. (2007) reported the first high-pressure (30 bar) measurements of ignition delay times in a shock tube for ethanol/air mixtures at 690 K ≤ T ≤ 1200 K and proposed a new tailored detailed kinetics model using the mechanisms of Marinov (1999) and Konnov (2000).

All measurements reported in the literature, in the pressure range of 0.5 bar ≤ p ≤ 5.0, show that an increase in total pressure is accompanied by a decrease in ignition delay time.

From the available kinetics models, the behavior of ethanol oxidation at high temperature can be summarized as follows: In the high-temperature range, the thermal decomposition of ethanol starts with the C–C bond cleavage giving methyl (CH_3) and hydroxymethyl (CH_2OH) radicals (Natarajan and Bhaskaram, 1981; Gardiner, 2000) as products. As the fuel continues to decompose (see box IV in Figure 29) the hydroxymethyl produced in the initiation phase can dissociate due to the low dissociation barrier producing H atoms and formaldehyde (CH_2O).

Methyl also contributes to the build-up of the radical pool composed by O, H and OH that accelerates the depletion of the fuel by ethanol-radical reactions, as depicted in boxes I and II in Figure 29. Stable intermediates like acetaldehyde (CH_3HCO), formaldehyde (H_2CO) and formyl radical (CHO) are mainly responsible for the weakening of the branching reactions and the acetaldehyde concentrations encountered in the ethanol oxidation are found to be higher than of other intermediates (Natarajan and Bhaskaram, 1981).

Excluding a single result at 30 bar, the low temperature data available in the literature has been measured up to 1 bar. High temperature data has been measured up to 5 bar. Thus, the available mechanisms have been only validated for low pressure data and questions remain whether the patterns discussed above are still correct for higher pressures and lower temperatures.

Comparison of results of the mechanisms available in the literature (Cancino et al. 2007) with the data presented in Chapter 3 revealed poor prediction. Therefore, in the following section a new mechanism is proposed and then compared to the available data in the literature and to the data presented in Chapter 3.

4.1.2 Detailed kinetics model for ethanol oxidation

Several detailed kinetics mechanisms for different hydrocarbons are available in the literature. Simmie (2003) presented a comprehensive review of detailed kinetics models for hydrocarbons. The detailed kinetics model by Konnov (2000) was developed for combustion

of small hydrocarbons containing up to 3 carbon atoms in the molecule, including C_1, C_2 and C_3 hydrocarbon sub-kinetics. The mechanism has been validated against several experimental results involving shock tube ignition delay times, flow reactor data, laminar flame species profiles, and laminar flame speeds covering different reactive systems.

This mechanism has not yet been used in the literature for predicting the combustion of ethanol. Nevertheless, Konnov (2005) mentioned that it might be suitable to predict the combustion of ethanol when the additional thermodynamic properties of chemical species not present in the mechanism, are given. The Marinov mechanism (1999), however, was developed exclusively for high-temperature oxidation of ethanol/O_2 mixtures and contains kinetics sub-models for methane and other products in the oxidation of ethanol.

In the present work, the Konnov (2000) and Marinov (1999) detailed kinetics models were taken and tailored to build up the proposed model. Initially, the extensively tested kinetics model for small hydrocarbons of Konnov was extended to the combustion of ethanol by adding the reactions described by Marinov that were missing in Konnov's mechanism.

Then, in order to further improve the predictive capability of the model, a comprehensive review of the literature was performed and new kinetics data was found in Li (2004) and Lin et al. (2002, 2003, 2004).

This procedure allowed for an update of the values of the reaction constants of several elementary reactions involving ethanol. Some elementary reactions that appeared neither in Konnov's nor in Marinov's mechanisms were also added. In summary, the model allows for the following specific reactions for ethanol decomposition:

$$C_2H_5OH \rightarrow C_2H_4 + H_2O \quad (R1)$$
$$\rightarrow CH_3 + CH_2OH \quad (R2)$$
$$\rightarrow CH_3CHO + H_2 \quad (R3)$$
$$\rightarrow C_2H_3OH + H_2 \quad (R4)$$
$$\rightarrow CH_4 + CH_2O \quad (R5)$$
$$\rightarrow CH_4 + CHOH \quad (R6)$$
$$\rightarrow CH_3CH + H_2O \quad (R7)$$
$$\rightarrow C_2H_5 + OH \quad (R8)$$
$$\rightarrow C_2H_5O + H \quad (R9)$$
$$\rightarrow CH_3CHOH + H \quad (R10)$$
$$\rightarrow C_2H_4OH + H \quad (R11)$$

$$H + C_2H_5OH \rightarrow CH_3CHOH + H_2 \quad (R12)$$
$$\rightarrow C_2H_4OH + H_2 \quad (R13)$$
$$\rightarrow C_2H_5O + H_2 \quad (R14)$$
$$\rightarrow C_2H_5 + H_2O \quad (R15)$$

$$CH_3 + C_2H_5OH \rightarrow CH_4 + CH_3CHOH \quad (R16)$$
$$\rightarrow CH_4 + CH_3CH_2O \quad (R17)$$
$$\rightarrow CH_4 + CH_2CH_2OH \quad (R18)$$
$$\rightarrow CH_3OH + CH_3CH_2 \quad (R19)$$
$$\rightarrow H + CH_3CH_2OCH_3 \quad (R20)$$

Lin (2002) determined that, at pressures below 10 bar and temperature range of 700-2500 K, the unimolecular decomposition of ethanol occurs primarily by the dehydration reaction producing $C_2H_4 + H_2O$, represented by reaction (R1) with an energy barrier of 278.65

kJ/mol. At high-pressure limit, and over 1500 K, the production of CH_3 and CH_2OH represented by reaction (R2) becomes dominant.

The H_2-molecular elimination process, represented by reactions (R3) and (R4), is not important throughout the temperature range investigated (700 – 2500 K), Reaction (R5) involves the abstraction of the H atom from the OH group producing CH_4 and CH_2O, the barrier of energy calculated by Lin (2002) was 417.14 kJ/mol. Reaction (R6) also producing methane, has an energy barrier 58.57 kJ/mol lower that (R6). Reaction (R7) analogous to channel of (R1) producing H_2O and CH_3CH, has a dissociation barrier of 346.85 kJ/mol. Reaction (R8) producing hydroxyl radical and C_2H_5 has an energy barrier of 396.64 kJ/mol, 12.55 kJ/mol higher than the prediction of Marinov (1999).

The reactions (R9)-(R11) were not included in the computational chemistry calculation of Lin (2002).

Concerning the chain-propagation reactions by the H atom (reactions R12 to R15) the reaction of dehydration (R15) has a high energy barrier and the probability that reaction (R15) occurs, in the range of temperature investigated in this study, is very low. In this group of reactions, reaction (R14) represents about 10% of the total reaction rate in the temperature range analyzed by Lin (2003). Reactions (R12) and (R13) remain, however, the most important because of their activation energies (energy barrier).

In the CH_3-radical chain-propagation reactions, reactions (R19) and (R20) have higher energy barriers and their feasibility can be ruled out kinetically in the temperature range investigated in this study.

The other reactions forming methane by H abstraction, reactions (R16), (R17) and (R18), remain important because of their values of energy barrier. At higher temperatures ($T >$ ~1200 K), reaction (R18) becomes dominant.

These oxidation routes lead ultimately to the production of methane, formaldehyde and other oxygenated hydrocarbons, as depicted in Figure 29, whose kinetics are well treated in the Konnov (2000) mechanism.

In the proposed detailed kinetics model the most important reactions for the ethanol oxidation were selected and placed in the proposed detailed kinetics model, ruling out those reactions whose energy barriers limitations were noted by the different authors. The final proposed detailed kinetics model is composed by 136 chemical species and 1136 elementary reactions. Table 13 shows the major characteristics of the detailed kinetics mechanism used in this work.

Table 13. Characteristics of the detailed kinetics models

Kinetics model	Elements	Chemical species	Elementary reactions	NOx chemistry	Presure range [bar]	Temperature range [K]	Oxidizer
Konnov	5	127	1200	Yes	0.9 - 7.5	---	O_2 / Air
Marinov	4	54	390	No	1.0 - 4.5	≥ 1000	O_2
Proposed in this work	5	136	1136	Yes	0.9 - 50	700 - 1600	O_2 / Air

4.1.3 Results and comparison to measurements

4.1.3.1 High pressures and intermediate temperatures

Figure 31 shows the experimental results of ignition delay time for ethanol-air mixture at pressure of 30 bar and stoichiometric composition, the figure also shows the numerical response of four detailed kinetics models, the Marinov model, the hybrid Marinov-Konnov model, the Konnov model and the model proposed in this work.

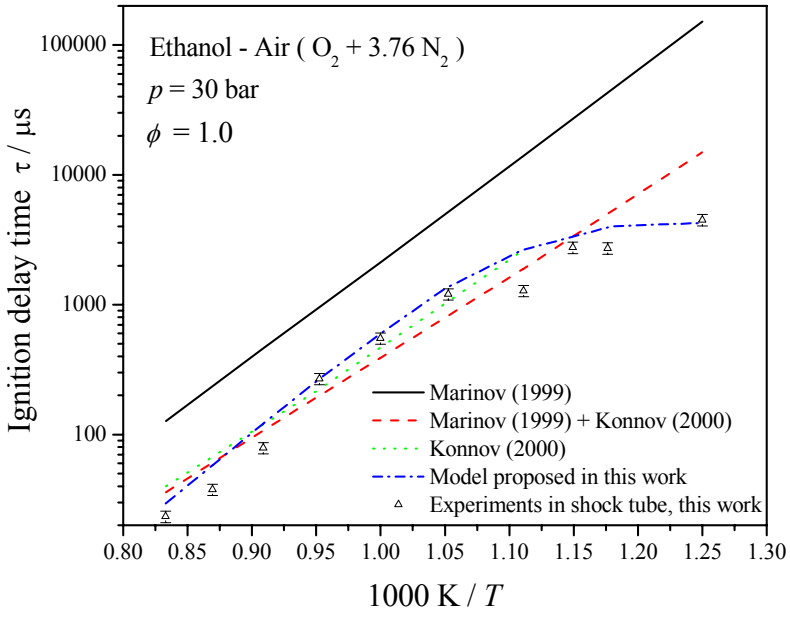

Figure 31. Experimental and numerical results for ethanol-air mixture at pressure of 30 bar and stoichiometric composition.

From Figure 31 one can see that the Marinov model overestimates the ignition delay time for high pressures and over the temperature range investigated in this work. The Konnov model is in agree went with the experimental data but, for temperatures below 900 K the model predicts no-ignition in the reactive mixture. The hybrid model Marinov-Konnov works at temperatures below 900 K, but the prediction of the IDT falls dramatically for lowers

temperatures. The detailed kinetics model proposed in this work captures two important aspects of the experimental data, the apparent activation energy at higher temperatures and the plateau regime at lower temperatures.

Figure 32 shows the comparison between the measured and the predicted ignition delay times by using the proposed detailed kinetics model for ethanol oxidation. The kinetics model is able to predict the general trends with temperature and pressure. The proposed ethanol detailed kinetics model shows good agreement in terms of global activation energy, pre-exponential factor and pressure dependence. The same curve fitting used to approximate the measured ignition delay times was applied to the predicted results. The curve fitted expression obtained is

$$\tau / \mu s = 10^{-1.75} \exp\left(+111.50 \text{ kJ/mol} \Big/ \Re T\right)\left(p \Big/ \text{bar}\right)^{-0.97} \quad , \quad \text{Proposed model, this work.}$$

This is very similar to the curve fit obtained for the measurements, repeated here as,

$$\tau / \mu s = 10^{-1.79} \exp\left(+107.58 \text{ kJ/mol} \Big/ \Re T\right)\left(p \Big/ \text{bar}\right)^{-0.83} \quad , \quad \text{Experimental fit, this work}$$

However, at the pressure of 10 bar, and temperature about 900 K the detailed kinetics model overpredicts the ignition delay time in about ~ 97%. This behavior must be further explored by comparing the predictions to measurements at lower pressures.

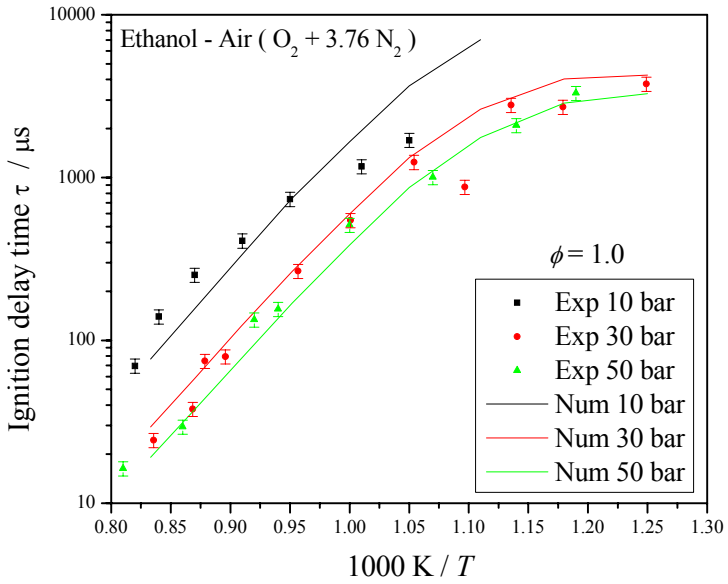

Figure 32. Comparison between predicted and measured ignition delay times for ethanol-air under stoichiometric composition using the proposed model.

Figure 33 shows the comparison between experimental and numerical results for lean (ϕ = 0.3) and stoichiometric (ϕ = 1.0) mixtures at pressure of 30 bar. At stoichiometric conditions there is a tendency of flattening of the ignition delay time dependency with temperature for temperatures below 900 K. The proposed detailed kinetics model is able to predict this effect.

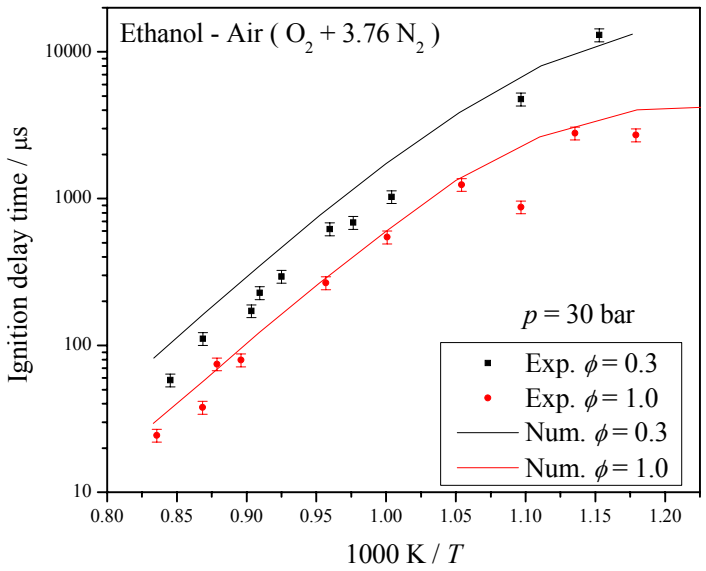

Figure 33. Comparison between predicted and measured ignition delay times of ethanol-air for lean (ϕ = 0.3) and stoichiometric (ϕ = 1.0) mixtures at pressure of 30 bar.

4.1.3.2 Low pressures and high temperatures

Figure 34 shows the comparison between measured (from Dunphy and Simmie, 1991) and predicted ignition delay times of ethanol-O_2 mixtures for equivalence ratios of 0.5, 2.0 and 1.0 at pressures of 3.3, 3.4 and 3.5 bar respectively.

In Figure 34 it is possible to note that the proposed kinetics model reproduces the overall trends of the measurements. However, the measurements show a faster decay at temperatures about 1300 K, indicating that the predictions overestimate the apparent activation energy for the ignition delay in the region around 1300 K. The curve fits obtained by Dunphy and Simmie (1991) are

$$\tau_{OH}/\mathrm{s} = 10^{-12.7}\exp\left(\frac{+14780\ \mathrm{K}}{T}\right)[C_2H_5OH]^{-0.415}[O_2]^{-0.785}[Ar]^{+0.648},$$

$$\tau_{CO-O}/\mathrm{s} = 10^{-14.0}\exp\left(\frac{+15550\ \mathrm{K}}{T}\right)[C_2H_5OH]^{-0.315}[O_2]^{-0.780}[Ar]^{+0.259},$$

$$\tau_{p}/\mathrm{s} = 10^{-14.0}\exp\left(\frac{+16960\ \mathrm{K}}{T}\right)[C_2H_5OH]^{-0.130}[O_2]^{-0.784}[Ar]^{+0.140},$$

with concentrations of ethanol, oxygen and argon in mol cm^{-3}.Note that the values of the global Activation Energy (Activation Temperature × $\Re$) calculated by Dunphy and Simmie (1991) are 122.88 kJ/mol, 129.28 kJ/mol and 141 kJ/mol, for ignition delays obtained from OH, CO-O and pressure methods respectively, for pressures between 1.0 – 4.6 bar, and temperature range of 1300 K – 1700 K. In this work, the global activation energy fitted from experimental data of IDT is about ~108 kJ/mol.

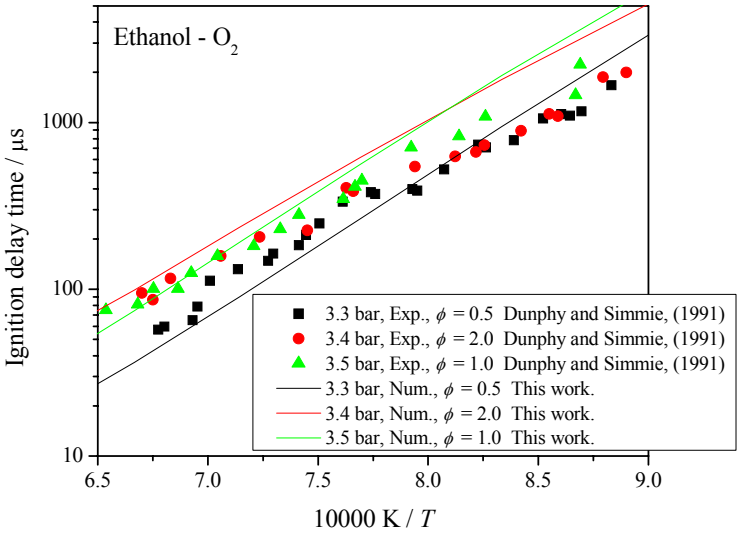

Figure 34. Comparison between measured (from Dunphy and Simmie, 1991) and predicted ignition delay times of ethanol-O_2 mixtures for equivalence ratios of 0.5, 2.0 and 1.0 at pressures of 3.3, 3.4 and 3.5 bar respectively.

Figure 35 shows the comparison between measured (from Dunphy and Simmie, 1991) and predicted ignition delay times of ethanol-O_2 mixtures for equivalence ratio of 0.25 at pressures of 2.0, 3.4 and 4.6 bar.

It can be observed that the proposed detailed kinetics model reproduces the ignition delay time dependence with the pressure for lean ethanol-O_2 mixtures. However, again, the predicted apparent activation energy is higher than the measurements suggest. A multiple regression was performed in the temperature range of 1700 K – 1300 K and pressures of 2.0, 3.4 and 4.6 bar, for a stoichiometric ratio of 0.25, resulting in the fitted expressions:

$$\tau / \mu s = 10^{-2.02} \exp\left(+12.36 \text{ kJ/mol} \Big/ \Re T \right) \left(p \Big/ \text{bar} \right)^{-0.79} \quad , \quad \text{Exp. fit, Dunphy and Simmie (1991).}$$

$$\tau / \mu s = 10^{-3.73} \exp\left(+16.69 \text{ kJ/mol} \Big/ \Re T \right) \left(p \Big/ \text{bar} \right)^{-0.74} \quad , \quad \text{Proposed model, this work.}$$

The proposed model is able to describe the pressure dependence but overestimates the global activation energy in about ~4.2 kJ/mol, for lean ethanol-air mixtures.

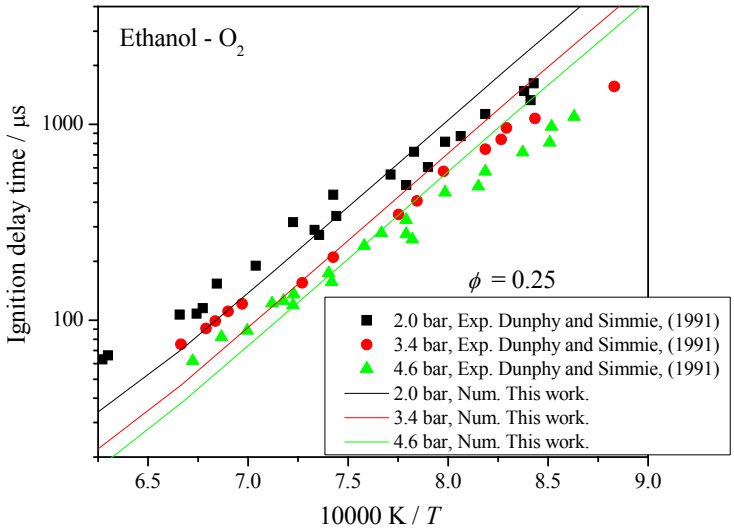

Figure 35. Comparison between measured (from Dunphy and Simmie, 1991) and predicted ignition delay times of ethanol-O_2 mixtures for $\phi = 0.25$ at pressures of 2.0, 3.4 and 4.6 bar.

4.1.4 Sensitivity Analysis

A first-order sensitivity analysis of the effect of each reaction on temperature, OH, H_2O_2, and C_2H_5OH concentrations was performed to find out which reactions dominate the ethanol oxidation at high pressures and also which reaction coefficients need to be systematically improved. For the analysis, we assumed that the combustion process occurred in a perfectly stirred reactor PSR at conditions behind the reflected shock wave starting at time $t = 0$ and ending at $t = \tau_{ing}$.

The conditions for simulations in the PSR were: stoichiometric composition ($\phi = 1.0$), pressures of 10, 30 and 50 bar and temperatures of 1100, 950, and 800 K. The overall sensitivity methodology discussed earlier was generated from the output files from CHEMKIN. For each condition analyzed (pair p,T), the reaction with the largest positive effect on the variables analyzed is denoted as Reaction (+) (largest positive value of sensitivity coefficient), whereas that with the largest negative effect is denoted as Reaction (–) (largest negative value of sensitivity coefficient), i.e., only one level of importance is presented. The results are summarized in Table 14.

Table 14. Sensitivity map for stoichiometric ethanol/air system

50 bar		
1100 K	950 K	800 K
Temperature		
Reaction (+) C2H5OH+HO2 = SC2H5O+H2O2	Reaction (+) C2H5OH+HO2 = SC2H5O+H2O2	Reaction (+) C2H5OH+HO2 = SC2H5O+H2O2
Reaction (-) SC2H5O+O2 = CH3CHO+HO2	Reaction (-) SC2H5O+O2 = CH3CHO+HO2	Reaction (-) SC2H5O+O2 = CH3CHO+HO2
OH		
Reaction (+) C2H5OH+HO2 = SC2H5O+H2O2	Reaction (+) C2H5OH+HO2 = SC2H5O+H2O2	Reaction (+) C2H5OH+HO2 = SC2H5O+H2O2
Reaction (-) C2H5OH+OH = SC2H5O+H2O	Reaction (-) SC2H5O+O2 = CH3CHO+HO2	Reaction (-) SC2H5O+O2 = CH3CHO+HO2
H2O2		
Reaction (+) C2H5OH+HO2 = SC2H5O+H2O2	Reaction (+) C2H5OH+HO2 = SC2H5O+H2O2	Reaction (+) C2H5OH+HO2 = SC2H5O+H2O2
Reaction (-) SC2H5O+O2 = CH3CHO+HO2	Reaction (-) SC2H5O+O2 = CH3CHO+HO2	Reaction (-) SC2H5O+O2 = CH3CHO+HO2
C2H5OH		
Reaction (+) SC2H5O+O2 = CH3CHO+HO2	Reaction (+) SC2H5O+O2 = CH3CHO+HO2	Reaction (+) SC2H5O+O2 = CH3CHO+HO2
Reaction (-) C2H5OH+HO2 = SC2H5O+H2O2	Reaction (-) C2H5OH+HO2 = SC2H5O+H2O2	Reaction (-) C2H5OH+HO2 = SC2H5O+H2O2

30 bar		
1100 K	950 K	800 K
Temperature		
Reaction (+) C2H5OH+HO2 = SC2H5O+H2O2	Reaction (+) C2H5OH+HO2 = SC2H5O+H2O2	Reaction (+) C2H5OH+HO2 = SC2H5O+H2O2
Reaction (-) SC2H5O+O2 = CH3CHO+HO2	Reaction (-) SC2H5O+O2 = CH3CHO+HO2	Reaction (-) SC2H5O+O2 = CH3CHO+HO2
OH		
Reaction (+) C2H5OH+HO2 = SC2H5O+H2O2	Reaction (+) C2H5OH+HO2 = SC2H5O+H2O2	Reaction (+) C2H5OH+HO2 = SC2H5O+H2O2
Reaction (-) C2H5OH+OH = SC2H5O+H2O	Reaction (-) SC2H5O+O2 = CH3CHO+HO2	Reaction (-) SC2H5O+O2 = CH3CHO+HO2
H2O2		
Reaction (+) C2H5OH+HO2 = SC2H5O+H2O2	Reaction (+) C2H5OH+HO2 = SC2H5O+H2O2	Reaction (+) C2H5OH+HO2 = SC2H5O+H2O2
Reaction (-) SC2H5O+O2 = CH3CHO+HO2	Reaction (-) SC2H5O+O2 = CH3CHO+HO2	Reaction (-) SC2H5O+O2 = CH3CHO+HO2
C2H5OH		
Reaction (+) SC2H5O+O2 = CH3CHO+HO2	Reaction (+) SC2H5O+O2 = CH3CHO+HO2	Reaction (+) SC2H5O+O2 = CH3CHO+HO2
Reaction (-) C2H5OH+HO2 = SC2H5O+H2O2	Reaction (-) C2H5OH+HO2 = SC2H5O+H2O2	Reaction (-) C2H5OH+HO2 = SC2H5O+H2O2

10 bar		
1100 K	950 K	800 K
Temperature		
Reaction (+) C2H5OH+HO2 = SC2H5O+H2O2	Reaction (+) C2H5OH+HO2 = SC2H5O+H2O2	Reaction (+) C2H5OH+HO2 = SC2H5O+H2O2
Reaction (-) H+HO2 = H2O+O	Reaction (-) SC2H5O+O2 = CH3CHO+HO2	Reaction (-) SC2H5O+O2 = CH3CHO+HO2
OH		
Reaction (+) C2H5OH+HO2 = SC2H5O+H2O2	Reaction (+) C2H5OH+HO2 = SC2H5O+H2O2	Reaction (+) C2H5OH+HO2 = SC2H5O+H2O2
Reaction (-) C2H5OH+OH = SC2H5O+H2O	Reaction (-) C2H5OH+OH = SC2H5O+H2O	Reaction (-) SC2H5O+O2 = CH3CHO+HO2
H2O2		
Reaction (+) C2H5OH+HO2 = SC2H5O+H2O2	Reaction (+) C2H5OH+HO2 = SC2H5O+H2O2	Reaction (+) C2H5OH+HO2 = SC2H5O+H2O2
Reaction (-) H+HO2 = H2O+O	Reaction (-) SC2H5O+O2 = CH3CHO+HO2	Reaction (-) SC2H5O+O2 = CH3CHO+HO2
C2H5OH		
Reaction (+) H+HO2 = H2O+O	Reaction (+) SC2H5O+O2 = CH3CHO+HO2	Reaction (+) SC2H5O+O2 = CH3CHO+HO2
Reaction (-) C2H5OH+HO2 = SC2H5O+H2O2	Reaction (-) C2H5OH+HO2 = SC2H5O+H2O2	Reaction (-) C2H5OH+HO2 = SC2H5O+H2O2

The sensitivity map shows that reactions

$$C_2H_5OH + HO_2 = SC_2H_5O + H_2O_2 \qquad (R21)$$
$$SC_2H_5O + O_2 = CH_3CHO + HO_2 \qquad (R22)$$
$$C_2H_5OH + OH = SC_2H_5O + H_2O \qquad (R23)$$
$$HO_2 + HO_2 = H_2O_2 + O_2 \qquad (R24)$$

are the most sensitive at high pressures (10, 30, and 50 bar) and for intermediate and high temperatures (800, 950, and 1100 K). It seems that at high pressures the main ethanol oxidation path is dominated by the H-atom abstraction by the hydroperoxy radical (HO_2), producing CH_3CHOH (named SC_2H_5O in this work), one of the three isomers of C_2H_5O.

This route corresponds to reaction (R21) above and is represented schematically in the top part of Figure 36. It leads to the hydrogen peroxide sub-mechanism. In the bottom part of Figure 36, the Hs-abstraction path by collision with a third-body "M" is represented. This path results, also, in the production of CH_3CHOH which is then oxidized forming acetaldehyde, leading to the acetaldehyde sub-mechanism, and HO_2. This corresponds to reaction (R22) above.

The hydroperoxy radical (HO_2) feeds reaction (R21) giving more CH_3CHOH, forming a cycle for the production of CH_3CHOH and HO_2 and depletion of ethanol. (R23) becomes relevant when the pool of HO_2 is formed. The reaction proceeds and more SC_2H_5O is produced. With the increase of the HO_2 concentration, reaction (R24) becomes important.

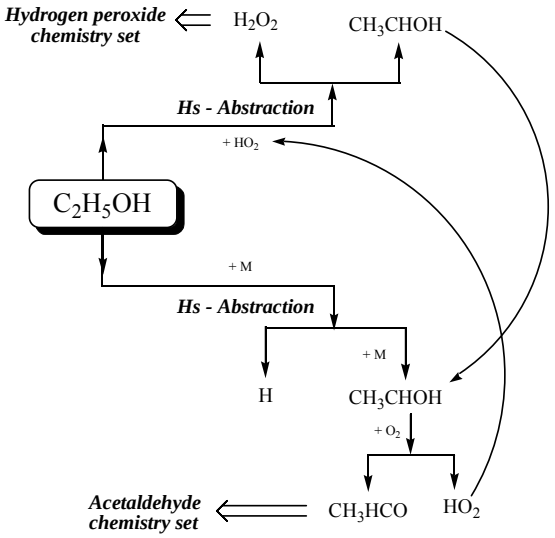

Figure 36. Main ethanol oxidation routes at high pressure.

4.2 Multi-component gasoline surrogates

In this section, detailed kinetics models for several gasoline surrogates are presented. These models are validated against measurements for Gasoline Surrogates A and B and other experimental data of ignition delay time available in the literature. Table 15 summarizes the experimental conditions of the measurements of ignition delay time for gasoline surrogates used in this work for validation purposes.

Table 15. Experimental data for gasoline surrogates.

Mixture	Composition [% by volume]					Oxidizer	Pressure [bar]	Temperature [K]	ϕ	ON **	Ref.
	Ethanol	iso-Octane	n-Heptane	Toluene	DIB*						
Gasoline surrogate A	25	75	***	***	***	air	30	800 - 1200	1.0	105	This work
Gasoline surrogate B	40	37.8	10.2	12	***	air	10, 30, 50	690 - 1200	1.0	98.8	This work
Gasoline surrogate C	20	62	18	***	***	air	10, 30, 50	690 - 1200	1.0	92	Fikri et al. (2008)
Gasoline surrogate D	***	69	17	14	***	air	25, 55	690 - 1200	1.0	87	Gauthier et al. (2004)
Gasoline surrogate E	***	25	20	45	10	air	30, 50	690 - 1200	1.0	90	Fikri et al. (2008)

DIB * = di-isobutylene as 2-4-4 trimethyl-1-pentene
ON ** = Estimated octane number

Five detailed kinetics mechanisms were adapted to simulate the ignition delay time of the different gasoline surrogates given in Table 15. Table 16 summarizes the origin of the sub-mechanisms.

Table 16. Characteristics of the detailed kinetics mechanisms adapted to the surrogate fuels investigated in this work. All mechanisms use the PRF model of Curran et al. (1998) as the base mechanism.

Mechanism		Chemical species	Elementary reactions	Blended mechanism	Reference
Surrogate A	GS-A	1056	4743	ethanol	Cancino et al. (2009)
				PRF	Curran et al. (1998)
Surrogate B	GS-B	1085	4748	ethanol	Marinov (1999)
				toluene	Andrae et al (2007)
				PRF	Curran et al. (1998)
Surrogate C	GS-C	1042	4390	ethanol	Marinov (1999)
				PRF	Curran et al. (1998)
Surrogate D	GS-D	1053	4277	toluene	Maurice (1996)
				PRF	Curran et al. (1998)
Surrogate E	GS-E	1102	4635	toluene	Andrae et al (2007)
				ethanol	Marinov (1999)
				di-isobutylene	Metcalfe et al. (2007)
				PRF	Curran et al. (1998)

The initial kinetics model for the studied surrogates was the PRF model of Curran et al. (1998). In order to simulate the gasoline surrogate A, designed as GS-A model, the PRF model of Curran (1998) was combined with the ethanol kinetics from Cancino et al. (2009b) In order to describe the chemical kinetics of ethanol oxidation in surrogate C, the Marinov (1999) mechanism was used and introduced in the PRF model of Curran, giving the kinetics mechanism GS-C (see Table 16). For the kinetics mechanism GS-B which describes the ignition behavior of surrogate B, the mechanism GS-C was used and upgraded by adding the sub-mechanism for toluene of Andrae et al. (2007). For simulation of gasoline surrogate D, the PRF model of Curran (1998) was combined with the sub-mechanism of toluene of Maurice (1996). Finally GS-E model for the gasoline surrogate E was built by using the kinetics for toluene, ethanol and di-isobutylene from Andrae et al. (2007), Marinov (1999) and Metcalfe et al. (2007) respectively. For abbreviations and references of the used mechanism see Table 15 and Table 16.

The proposed detailed kinetics models in this work were tailored in a progressive form, depending of the availability of the kinetics sub structures at literature, since the gasoline surrogate models GS-B, GS-C, GS-D and GS-E were built in the first stages of the development of this work, they used the Marinov model for ethanol instead of the upgraded model of Cancino et al. (2009)

4.2.1 Detailed kinetics model for ternary gasoline surrogate mixtures

A detailed kinetics model for ternary gasoline surrogate involving ethanol, iso-octane and n-heptane, gasoline surrogate A, is proposed here and named GS-A in Table 15 and Table 16. The chemical species were selected based on the availability of detailed chemistry in the literature, especially, the detailed work by Curran et al. (1998). The starting point was the PRF model of Curran et al. (1998). The chemical kinetics of ethanol oxidation was taken from Cancino et al (2009b), which is an upgraded chemistry of ethanol based on Marinov (1999) and Konnov (2000) kinetics mechanisms.

4.2.1.1 Detailed kinetics model GS-A for Gasoline surrogate A

Figure 37 shows the numerical and experimental results for the binary mixture investigated in section 3.3.2. The PRF model of Curran et al. (1998) overestimates the values of ignition delay time in the temperature range of this study. The GS-A model underestimates

the values of ignition delay time for temperatures about ~1050 K. It presents a slight change in inflection in the range of temperature for which the PRF model presents an NTC behavior (Curran et al., 1998).

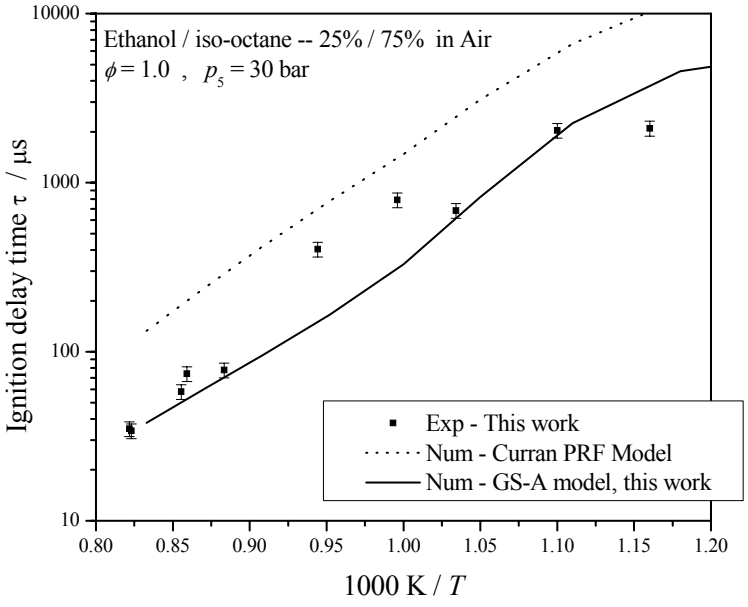

Figure 37. Comparison between the predictions of the PRF model of Curran et al. (1998), the GS-A model and the measurements of ignition delay time for ethanol - iso-octane (25%/75%) in air.

Adding the upgraded ethanol chemistry, the performance of the resulting detailed kinetics model GS-A improves. The improvement can be observed in the values of the apparent pre-exponential factor and in the activation energy predicted by the numerical models when compared to the fitted data from experiments in section 3.3.2. The curve fitted expressions are:

$$\tau / \mu s = 10^{-2.15} \exp\left(+100.77 \text{ kJ/mol} \Big/ \Re T \right) \quad , \quad \text{PRF model Curran et al. (1998).}$$

$$\tau / \mu s = 10^{-3.14} \exp\left(+108.87 \text{ kJ/mol} \Big/ \Re T \right) \quad , \quad \text{GS-A model, this work.}$$

$$\tau / \mu s = 10^{-3.10} \exp\left(+107.96 \text{ kJ/mol} \Big/ \Re T \right) \quad , \quad \text{Experimental fit, this work.}$$

The PRF model of Curran et al. (1998) underestimates the global activation energy in about ~5 kJ/mol and the pre-exponential factor is about ~9 times higher. Comparing the experimental results to the proposed model GS-A, the model underestimates the activation energy in about ~0.6 kJ/mol and the pre-exponential factor is about ~10% lower that the experimental value.

For consistency, the model GS-A is checked against the measurements for pure ethanol. Figure 38 shows the numerical predictions of ignition delay time for ethanol-air mixtures at stoichiometric composition, at pressures of 10, 30 and 50 bar for both the Curran PRF model and the GS-A model, compared to the measurements reported in section 3.3.1.

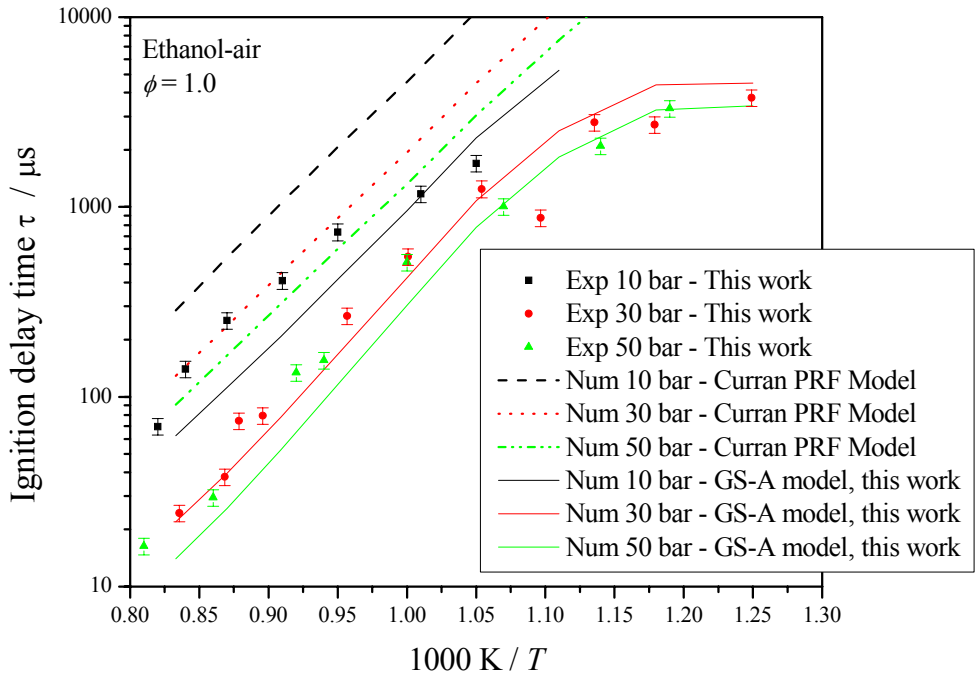

Figure 38. Comparison between the predictions of the PRF model of Curran et al. (1998), the GS-A model and the measurements for pure ethanol.

The Curran PRF model was developed specifically for iso-octane and n-heptane fuels and it was expected that the PRF model would fail in the predictions of ignition delay times for ethanol-air mixtures, especially at temperatures below 1000 K.

A possible explanation of this flaw is based in the small kinetics data-set for ethanol decomposition in the PRF model. Also, the PRF model does not reproduce the flattening of the IDT observed at lower temperatures.

At temperatures above 950 K, however, although it overestimates the measurements, the PRF model is sensitive to the pressure dependence of the ignition delay time and reproduces, approximately, the measured apparent activation energy as shown in the fitted expressions:

$$\tau/\mu s = 10^{-2.90} \exp\left(+131.20\ \text{kJ/mol} \Big/ \Re T\right)\left(p \Big/ \text{bar}\right)^{-0.83} \quad , \text{ Exp., this work, } T > 950 \text{ K}$$

$$\tau/\mu s = 10^{-2.68} \exp\left(+135.96\ \text{kJ/mol} \Big/ \Re T\right)\left(p \Big/ \text{bar}\right)^{-0.87} \quad , \text{ GS-A model, this work, } T > 950 \text{ K.}$$

$$\tau/\mu s = 10^{-3.89} \exp\left(+147.98\ \text{kJ/mol} \Big/ \Re T\right)\left(p \Big/ \text{bar}\right)^{-0.81} \quad , \text{ PRF, Curran et al. (1998), } T > 950 \text{ K.}$$

After adding the ethanol chemistry, the resulting kinetics model is able to reproduce ignition delay times for ethanol-air mixtures.

GS-A model can also be tested against measurements for pure octane. Figure 39 presents the numerical predictions of both, the Curran PRF model and the GS-A model for iso-octane / air mixtures at pressures of 16.8 and 49.4 bar, temperatures between 950 – 1200 K and stoichiometric composition. The measurements were obtained from Davidson et al. (2005).

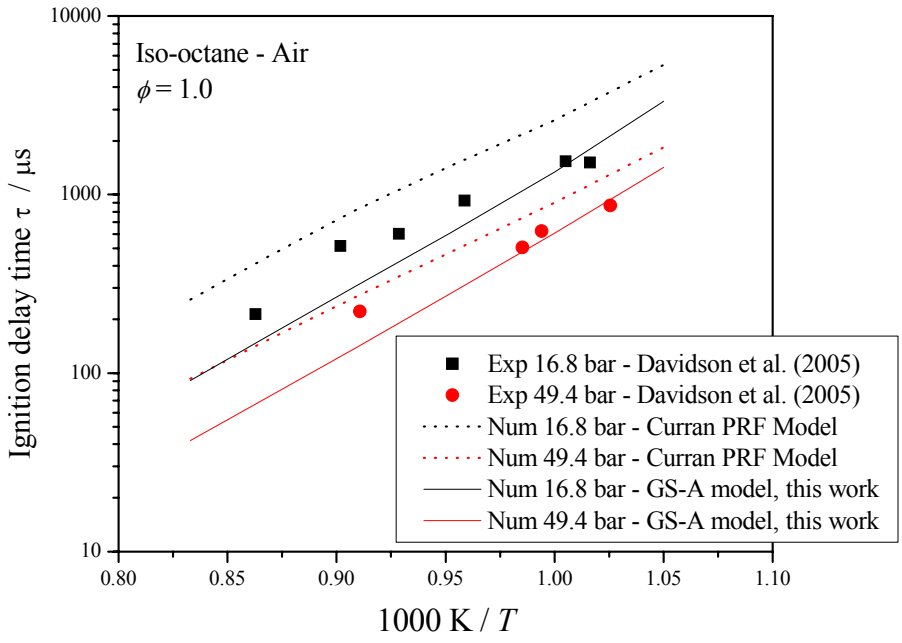

Figure 39. Comparison between the predictions of the PRF model of Curran et al. (1998), the GS-A model and the measurements for pure iso-octane from Davidson et al. (2005).

The fitted equations with the characteristics of global activation energy and pre-exponential factor of the experimental data from Davidson et al. (2005) and for the numerical model of Curran et al. (1998) and GS-A model are:

For pressure of 16.8 bar,

$$\tau/\mu s = 10^{-2.19}\exp\left(+102.35\ \text{kJ/mol}\Big/\Re T\right) \quad , \quad \text{Experimental fit, Davidson et al. (2005).}$$

$$\tau/\mu s = 10^{-2.54}\exp\left(+114.36\ \text{kJ/mol}\Big/\Re T\right) \quad , \quad \text{PRF model Curran et al. (1998).}$$

$$\tau/\mu s = 10^{-4.0}\exp\left(+136.89\ \text{kJ/mol}\Big/\Re T\right) \quad , \quad \text{GS-A model, this work.}$$

For pressure of 49.4 bar,

$$\tau/\mu s = 10^{-2.37}\exp\left(+99.22\ \text{kJ/mol}\Big/\Re T\right) \quad , \quad \text{Experimental fit, Davidson et al. (2005).}$$

$$\tau/\mu s = 10^{-2.96}\exp\left(+113.55\ \text{kJ/mol}\Big/\Re T\right) \quad , \quad \text{PRF model Curran et al. (1998).}$$

$$\tau/\mu s = 10^{-4.24}\exp\left(+134.70\ \text{kJ/mol}\Big/\Re T\right) \quad , \quad \text{GS-A model, this work.}$$

Figure 39 shows that the Curran PRF model overestimates the experimental results, and the discrepancy is more evident at the pressure of 16.8 bar. The GS-A model underestimates the measurements at higher temperatures and also underestimates the apparent activation energy. However, the proposed (GS-A) model captures the general trends of the experiments.

4.2.2 Detailed kinetics models for quaternary gasoline surrogate mixtures

4.2.2.1 Detailed kinetics model GS-B for Gasoline Surrogate B

The base mechanism for GS-B is the primary reference fuel model (PRF) of Curran et al. (1998), and sub-mechanisms were incorporated to account for the effect of ethanol and/or toluene.

The results of the ignition delay time experiments and simulation for surrogate B are depicted in Figure 40. The measurements show the same flattening for temperatures below 900 K observed for the ethanol/iso-octane mixtures.

The predictions using mechanism GS-B results in similar apparent activation energy and reproduces the plateau at low temperatures, especially at high pressures. At higher temperatures (< 1000 K) the fitted equations scaled to 30 bar are:

$$\tau/\mu s = 10^{-3.43}\exp\left(+142.84\ \text{kJ/mol}\Big/\Re T\right)\left(p\Big/\text{bar}\right)^{-0.75} \quad , \quad \text{Experimental fit, } T > 1000\ \text{K}$$

$$\tau/\mu s = 10^{-2.15}\exp\left(+126.08\ \text{kJ/mol}\Big/\Re T\right)\left(p\Big/\text{bar}\right)^{-0.81} \quad , \quad \text{GS-B model, } T > 1000\ \text{K}$$

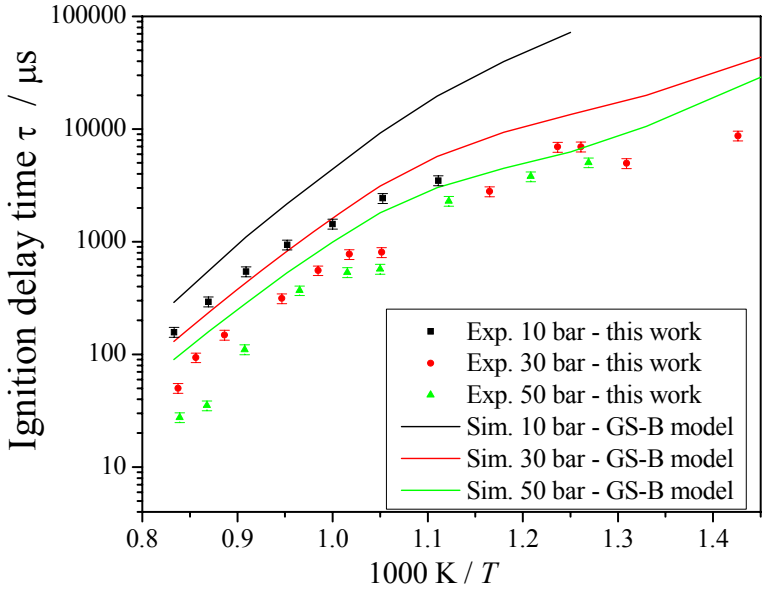

Figure 40. Simulation and measurements for surrogate B ignition delay times in air for ϕ = 1.0, p = 10, 30, and 50 bar (see Table 15 and Table 16 for composition and submechanisms).

The mechanism describing surrogate GS-B was also checked, for its capability in reproducing the ignition delay times of the pure components. The mechanism captured for example quantitatively the results of toluene and the maximum error quoted was about 6 % in relation to the Andrae et al. (2007) model. However, both predictions deviate strongly from the measurements by Davidson et al. (2005). Figure 41 shows the comparison.

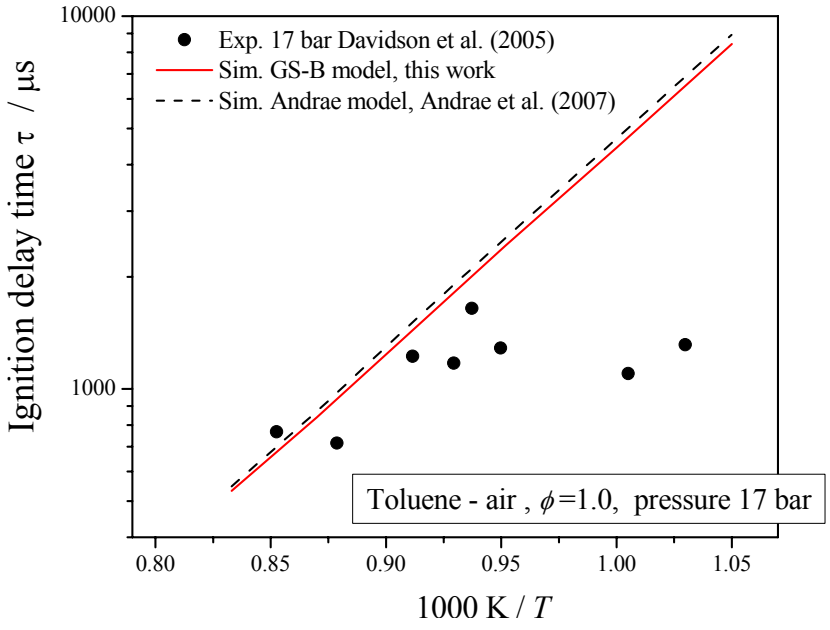

Figure 41. Experimental and numerical data of ignition delay time of toluene-air mixtures at pressure of 17 bar and stoichiometric composition.

In the high temperature range, above 1050 K, the proposed detailed kinetics model GS-B as well as the Andrae et al. (2007) model overestimates the global activation energy in about ~33 kJ/mol, when compared to the experimental data in the same temperature range. The GS-B model and the Andrae model overestimates the pre-exponential factor in about ~28 times the value of the experimental fit from Davidson et al. (2005). The curve fitted equations are:

$$\tau/\mu s = 10^{-0.43}\exp\left(\frac{+73.44\ \text{kJ/mol}}{\Re T}\right) \quad \text{, Exp. fit, Davidson et al. (2005). } (T > 1050\ \text{K}).$$

$$\tau/\mu s = 10^{-1.88}\exp\left(\frac{+106.00\ \text{kJ/mol}}{\Re T}\right) \quad \text{, GS-B model, this work. } (T > 1050\ \text{K}).$$

$$\tau/\mu s = 10^{-1.92}\exp\left(\frac{+107.18\ \text{kJ/mol}}{\Re T}\right) \quad \text{, Toluene, Andrae et al. (2007). } (T > 1050\ \text{K}).$$

The reasons for the discrepancy at lower temperatures were not exploded here.

4.2.2.2 Detailed kinetics model GS-C for Gasoline Surrogate C

Figure 42 combines the simulation results using mechanism GS-C with the measurements reported by Fikri et al. (2008). The GS-C model reproduces most of the trends exhibited by the measurements, especially for the higher pressures.

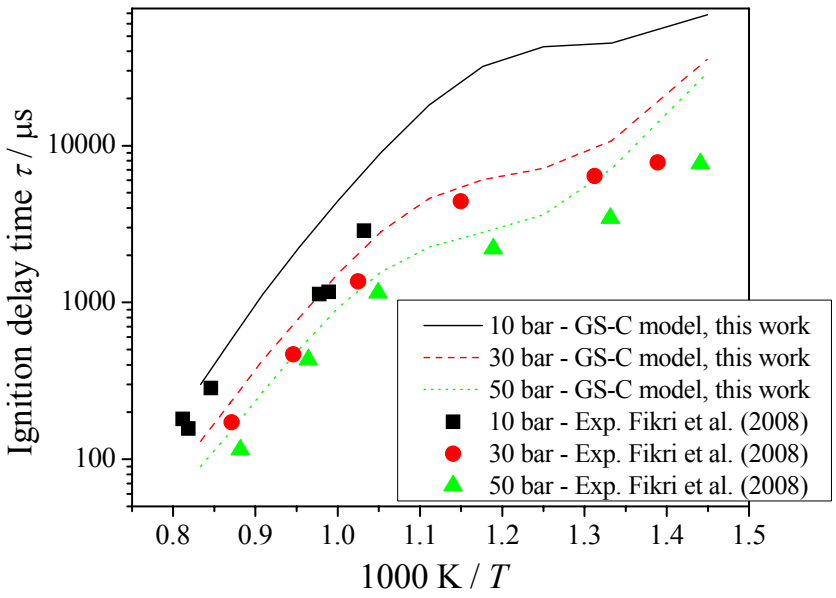

Figure 42. Simulation and experimental results (from Fikri et al., 2008) for surrogate C ignition delay times in air. ϕ = 1.0 (see Table 15 and Table 16 for composition and submechanisms models).

In the high temperature range, above 950 K, the global activation energy and the pre-exponential factor predicted by the GS-C model agree well with the experimental results as shown in the fitted expressions:

$$\tau/\mu s = 10^{-1.37} \exp\left(+100.58\ \text{kJ/mol} \Big/ \Re T\right)\left(p/\text{bar}\right)^{-0.63} \quad , \quad \text{Exp. fit, Fikri et al. (2008), } T > 950\ \text{K}$$

$$\tau/\mu s = 10^{-1.69} \exp\left(+118.72\ \text{kJ/mol} \Big/ \Re T\right)\left(p/\text{bar}\right)^{-0.91} \quad , \quad \text{GS-C model, } T > 950\ \text{K}$$

The GS-C model over predicts the ignition delay at low temperatures. At 10 bar, however, the autoignition delay times is over predicted at intermediate temperatures. Further experimental work including key species time-history measurements of OH (for example from CH_3CH_2OH) is desired to further improve the understanding of the relative effects of the submechanisms used in the blending process.

4.2.2.3 Detailed kinetics model GS-D for Gasoline Surrogate D

Figure 43 presents the comparison between the simulations obtained with the blended mechanism GS-D (Table 16) and the measurements reported by Gauthier et al (2004). The GS-D model overestimates the measured ignition delay, but still represents the pressure dependence.

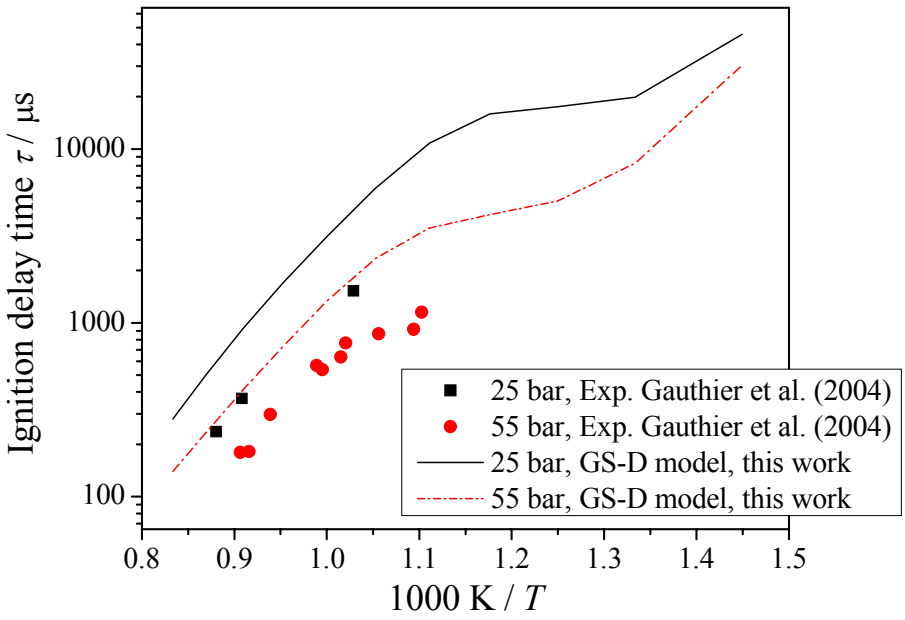

Figure 43. Simulation and experimental results (from Gauthier et al., 2004) for surrogate D ignition delay times in air. ϕ = 1.0 (see Table 15 and Table 16 for composition and submechanisms models)

For temperatures above 950 K, the proposed detailed kinetics model GS-D is able to predict the pressure dependence, and the apparent activation energy is about ~6 kJ/mol higher that the fitted value obtained from experiments, as shown in the fitted expressions:

$$\tau / \mu s = 10^{-0.98} \exp\left(+100.22 \text{ kJ/mol} \Big/ \Re T\right)\left(p \Big/ \text{bar}\right)^{-0.87} \text{, Exp. fit, Gauthier et al. (2004), } T > 950 \text{ K}$$

$$\tau / \mu s = 10^{-0.90} \exp\left(+111.46 \text{ kJ/mol} \Big/ \Re T\right)\left(p \Big/ \text{bar}\right)^{-1.03} \text{, GS-D model, } T > 950 \text{ K}$$

4.2.2.4 Detailed kinetics model GS-E for Gasoline Surrogate E

The kinetics model GS-E is based on the primary reference fuels model (PRF) of Curran et al. (1998) which accounts for the n-heptane/iso-octane chemistry assembled with specific sub-structures for toluene from Andrae et al. (2007), di-isobutylene from Metcalfe et al. (2007), and ethanol from Marinov (1999).

For the validation of the chemical kinetics model GS-E, the results from Fikri et al (2008) of the quaternary gasoline surrogate comprised of toluene / iso-octane / n-heptane / di-isobutylene (45% / 25% / 20% / 10% by liquid volume) were used. Both experimental and simulation results are shown in Figure 44.

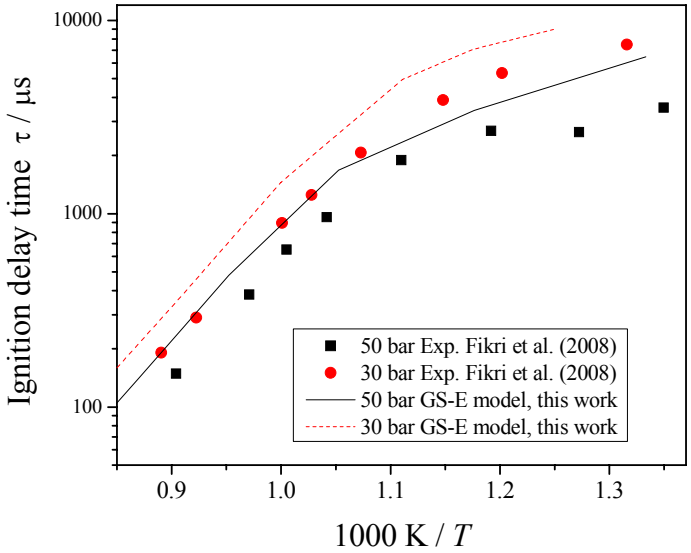

Figure 44. Experimental results from Fikri et al. (2008) and simulation for the gasoline surrogate E comprised of toluene / iso-octane / n-heptane / di-isobutylene at composition of 45% / 25% / 20% / 10% by liquid volume.

The proposed kinetics model renders the trend of the auto-ignition, but it does not capture the absolute values. The fitted expressions,

$$\tau/\mu s = 10^{1.36}\exp\left(+63.66\ \text{kJ/mol}/\Re T\right)\left(p/\text{bar}\right)^{-1.18}, \text{Exp. fit, Fikri et al. (2008), } T > 750\ \text{K}$$

$$\tau/\mu s = 10^{1.19}\exp\left(+64.24\ \text{kJ/mol}/\Re T\right)\left(p/\text{bar}\right)^{-1.10}, \text{GS-E model, } T > 750\ \text{K}$$

show good agreement in the prediction of the global activation energy and pressure dependence. The difference in the pre-exponential factor is a result of the "shift" in the ignition delay time predictions.

4.2.3 Comparison between GS-B, GS-C and GS-D detailed kinetics models.

Using the pressure scaling to p_5 = 30 bar, equation [47], and using the respective scaling factors reported in Fikri et al. (2008), Gauthier et al. (2004) and in this work, all the measurements can be collapsed into a single graph and compared to the predictions using models GS-B, GS-C, and GS-D. This is presented in Figure 45. The figure shows that the predictions over estimate the measurements especially at lower temperatures.

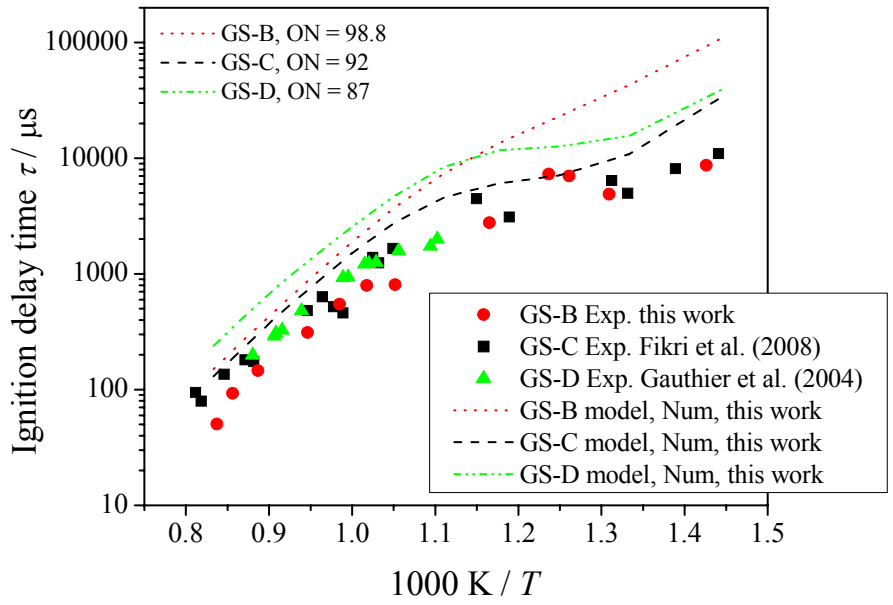

Figure 45. Simulation and experimental results for surrogates B, C and D / air ignition delay times at p_5 = 30 bar. ϕ = 1.0 (see Table 15 and Table 16 for composition and submechanisms models).

Model GS-B reproduces the flattening observed in the experiments in the temperature range between 800 and 690 K. The model GS-C does not reproduce the same trend exhibited by the measurements.

For surrogate D, no experimental data is available in the low-temperature range, whereas GS-D model predicts a flattening of the ignition delay time in the lower temperature range. For temperatures above 1000 K, the expressions:

$$\tau/\mu s = 10^{-1.96}\exp\left(+92.31\ \text{kJ/mol}/\Re T\right)\ ,\ \text{GS-B Exp. fit, this work, } T > 1000\ \text{K.}$$

$$\tau/\mu s = 10^{-3.21}\exp\left(+122.68\ \text{kJ/mol}/\Re T\right)\ ,\ \text{GS-B model, this work, } T > 1000\ \text{K.}$$

$$\tau/\mu s = 10^{-3.73}\exp\left(+126.15\ \text{kJ/mol}/\Re T\right)\ ,\ \text{GS-C Exp. fit, Fikri et al. (2008), } T > 1000\ \text{K.}$$

$$\tau/\mu s = 10^{-3.30}\exp\left(+126.22\ \text{kJ/mol}/\Re T\right)\ ,\ \text{GS-C model, this work, } T > 1000\ \text{K.}$$

$$\tau/\mu s = 10^{-2.93}\exp\left(+114.03\ \text{kJ/mol}/\Re T\right)\ ,\ \text{GS-D Exp. fit, Gauthier et al. (2004), } T > 1000\ \text{K.}$$

$$\tau/\mu s = 10^{-2.73}\exp\left(+117.98\ \text{kJ/mol}/\Re T\right)\ ,\ \text{GS-D model, this work, } T > 1000\ \text{K.}$$

show that GS-B model overestimates the global activation energy in about ~20 kJ/mol, and also overestimates the pre-exponential factor. The GS-C and GS-D models are in good agreement in relation to the apparent activation energy and pre-exponential factor.

Further comparison with measurements from Andrae et al. (2007) show that this mechanism does not work well, see Cancino et al. (2009a).

Therefore, further improvement of this mechanism is required, by validating it against experimental data for wider range of temperature and pressure. Also, the ethanol sub-mechanism of Marinov (1999) does not give satisfactory results at high pressures and intermediate temperatures as shown in Figure 31, and further refinements are needed.

An analysis of the important reactions may help to the optimization of the mechanism. The kernel of the ignition chemistry for hydrocarbon fuels is centered around three elementary reactions (Risberg, 2006; Westbrook, 2000):

$$H^{\bullet} + O_2 + M \rightarrow HO_2^{\bullet} + M \qquad \text{(R25)}$$

$$RH + HO_2^{\bullet} \rightarrow R^{\bullet} + H_2O_2 \qquad \text{(R26)}$$

$$H_2O_2 + M \rightarrow 2OH^{\bullet} + M \qquad \text{(R27)}$$

In these reactions, RH denotes an alkane, $R^{\bullet}$ denotes an alkyl radical. The reactions (R25) and (R26) are chain propagating reactions and (R27) is a chain branching reaction, and the most important reaction for the promotion of the hydroxyl radical ($OH^{\bullet}$) which is a key species to promote ignition. Reaction (R28):

$$H + O_2 \rightarrow OH^{\bullet} + O \qquad \text{(R28)}$$

also plays a significant role for the ignition delay time at temperatures above 1200 K. Below this temperature, and at measured temperatures and pressures, the chemistry is dominated by the termination reaction (R25).

Accordingly, and to explain the non-consensus of the simulations performed in this work, the hydrogen peroxide (H_2O_2) production could be eventually underestimated in the presented mechanisms.

The approach of blending sub-mechanisms used in this work, does not consider cross reactions in which a free radical generated from one of the fuels "abstracts" hydrogen from the other fuel. Andrae et al. (2007) presents a detailed kinetics model for Toluene Reference Fuels (TRF) in which cross reactions between toluene and PRF and between iso-octane and n-heptane are contemplated.

Therefore, the detailed kinetics model of Andrae et al. (2007) was also used to simulate the gasoline surrogates GS-B, GS-C and GS-D investigated in this work. Figure 46 shows the corresponding results.

Figure 46 shows that the TRF model does not present a clear distinction between the ignition delay times for the gasoline surrogates GS-B, GS-C and GS-D, at temperatures above ~ 950 K. The experiments, however, indicate a difference in this temperature range. The detailed kinetics mechanisms tailored in this work, in contrast, are able to reproduce the experimentally observed difference of the ignition delay times as shown, for instance in Figure 45. Also, the proposed blended mechanisms show that, at low temperatures, the ignition delay times increase with increasing the octane number calculated using a blending program from Shell, (Kalghatgi, 2007), as shown in Figure 45.

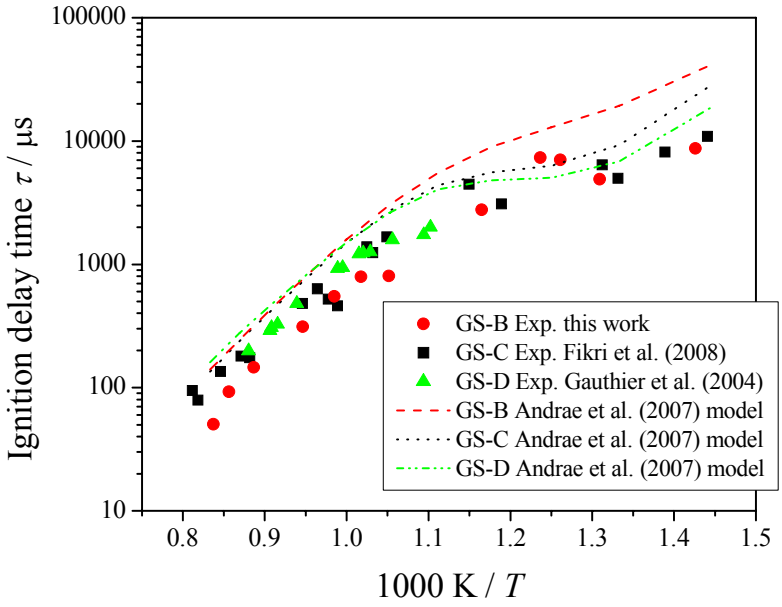

Figure 46. Simulation and experimental results for surrogates B, C and D / air ignition delay times at $p_5 = 30$ bar at $\phi = 1.0$ – Comparison with the results of the toluene fuel reference mechanism (TRF) of Andrae et al. (2007).

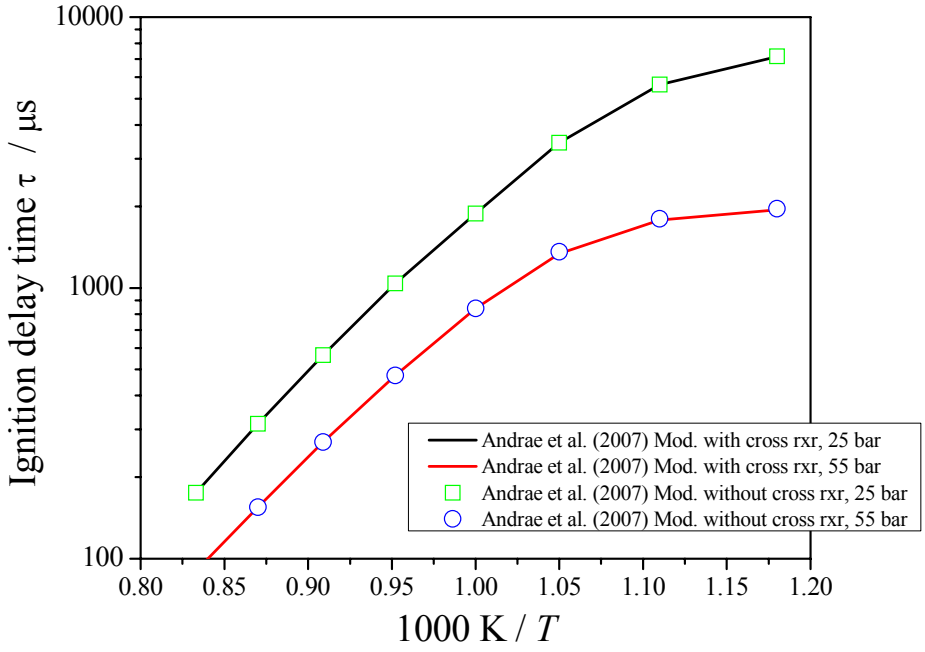

Figure 47. Effect of cross reactions in the ignition delay times using the model of Andrae et al. (2007)

Figure 47 compares the simulated ignition delay times with and without considering the cross-reactions from the Andrae model. One can clearly see that under these conditions cross reactions effects are insignificant, which agrees with the observations by Andrae et al. (2007).

Chapter 5: Conclusions and Recommendations

Several conclusions and recommendations can be done at the end of this work. The mayor objective focused to the development and application of detailed chemical kinetics mechanisms for pure ethanol and ethanol containing multi-component gasoline surrogates was reached. The proposed detailed kinetics models were validated against experimental results of ignition delay times for ethanol pure and gasoline surrogates GS-A and GS-B. The experiments were performed in the Laboratory for Combustion and Gasdynamic – IVG at University of Duisburg-Essen, Germany. The conclusions and recommendations of this work are listed separately for each reactive system investigated in this work.

5.1 Ethanol/air system

The final proposed detailed kinetics model for pure ethanol is formed by 136 chemical species and 1136 elementary reactions. Table 13 shows the major characteristics of the detailed kinetics mechanism proposed in this work. The detailed kinetics model predicts the reduced pressure sensitivity of the ignition delay time at higher pressures. Additionally, it predicts the global trend with temperature. No negative temperature coefficient region was detected in the temperature and pressure range analyzed. From the detailed kinetics modeling, a possible main oxidation route for ethanol oxidation at high pressures is suggested, see Figure 36. This route involves the H-atom abstraction from the secondary carbon of the ethanol molecule by reaction with hydroperoxy radical, giving CH_3CHOH and H_2O_2 as major products

The sensitivity analysis (discussed in section 2.5.1) revealed that reaction $C_2H_5OH + HO_2 = SC_2H_5O + H_2O_2$ has the largest sensitivity on temperature, OH, H_2O_2 and C_2H_5OH concentrations in the whole temperature interval tested. To improve the predictive capability of the kinetics model, the original Arrhenius parameters of this reaction in the Konnov mechanism were altered. The total reaction rate constant for this reaction in the proposed mechanism was formed by the sum of three constants: $k_a = 1.01\times10^{+18}\ \exp(+41351/RT)$, $k_b = 4.65\times10^{+129}T^{-41.37}$ and $k_c = 2.45\times10^{+23}T^{-4.97}$. A similar expression for this rate constant was not found in the literature and this is advanced here as a way of better predicting the measurements for higher pressure and lower temperature.

A more complete comparison of predictions with this reaction mechanism against measurements is recommended, as well as, a more thorough study of the reactions pointed as the most sensitive, especially the reaction $C_2H_5OH + HO_2 = SC_2H_5O + H_2O_2$.

5.2 Multi-component Gasoline surrogates/air systems

In this work, five detailed kinetics models for multi-component gasoline surrogates are proposed.

The first one, named GS-A, was created for ternary mixtures and validated for binary mixtures of iso-octane and ethanol (75% / 25%, by liquid volume). The blended mechanisms were the PRFs (iso-octane and n-heptane) and ethanol based on the kinetics schemes from Curran (1998) and Cancino et al. (2009b) respectively. The proposed detailed kinetics model, GS-A, was validated against experimental results from this work, and against experimental results of ignition delay times in shock tube for the pure fuels available at literature. The numerical results of ignition delay time show good agreement to the experimental data of ethanol and iso-octane available in the literature.

For iso-octane/air mixtures, the Curran PRF model overestimates the experimental results, and the discrepancy is more evident at pressures of 16.8 bar. The GS-A model underestimates the experimental results. However, it captures the general trends of the experiments. For the binary mixture analyzed in this work, the PRF model overestimates the values of ignition delay time in the temperature range of this study. Adding the upgraded ethanol chemistry (Cancino et al. 2009b), the performance of the resulting detailed kinetics model improves. The proposed model underestimates the values of ignition delay time for temperatures about ~1050 K.

The GS-B model was developed and validated for quaternary mixtures. The model was and built by using the PRF model of Curran et al. (1998), the ethanol kinetics from Marinov (1999) and the Toluene kinetics from Andrae et al. (2007). The mechanism GS-B for the surrogate B (ethanol / iso-octane / n-heptane / toluene – 40% / 37.8% / 10.2% / 12% by liquid volume) predicts similar apparent activation energies for the ignition delay times as the experimental data. It shows, similarly to the experimental data a flattening trend in activation energy at low temperatures especially at high pressures. The mechanism describing surrogate GS-B was also checked against ignition delay times of the pure components. The mechanism captured quantitatively the results of toluene and the maximum error quoted was about 6%.

The GS-C model was developed and tested for ternary mixtures. The kinetics model was built by tailoring the PRF model from Curran et al. (1998) and ethanol kinetics from Marinov (1999). The mechanism GS-C, for gasoline surrogate C (ethanol / iso-octane / n-heptane – 20% / 62% / 18%, by liquid volume), results in relative good prediction of the autoignition delay time of surrogate GS-C at three different pressures. The agreement is good in the high-temperature range for the results at 30 and 50 bar but the model overpredicts the ignition delay at low temperatures. At 10 bar, the autoignition delay times is over predicted even at high temperature. However, it can be clearly seen that the mechanism GS-C gives the closest agreement from all mechanisms with respect to the experimental data.

The GS-D detailed kinetics model was developed and tested for the gasoline surrogate D (iso-octane / n-heptane / toluene – 69% / 17% / 14%, by liquid volume). The kinetics model was built by tailoring the PRF model of Curran et al. (1998) and toluene kinetics from Maurice (1996).

The GS-E detailed kinetics model was developed for quinary mixtures and tested for quaternary mixtures. The kinetics model is based on the primary reference fuels model (PRF) of Curran et al. (1998) which accounts for the n-heptane/iso-octane chemistry assembled with specific sub-structures for toluene from Andrae et al. (2007), di-isobutylene from Metcalfe et al. (2007), and ethanol from Marinov (1999).

The ignition delay times are “shifted” in all results for GS-B, GS-C, GS-D and GS-E compared to the experimental results to longer times. Further comparisons of simulated ignition delay times based on the mechanism with the added toluene reactions with experimental data from Andrae et al. (2007) show that this mechanism causes some disagreement in the 900–1200 K range. Therefore, further improvement of this mechanism is required, by validating it against experimental data for wider range of temperature and pressure. Also, the ethanol sub-mechanism of Marinov does not give satisfactory results for the higher pressures. Further experimental work including key species time-history measurements of OH (for example from CH_3CH_2OH) is desired to further improve the understanding of the relative effects of the submechanisms used in the blending process.

References

Andrae J.C.G. "Development of a detailed kinetics model for gasoline surrogate fuels" Fuel 87, 2013–2022, (2008).

Andrae J.C.G., Björnbom P., Cracknell R.F., Kalghatgi G.T. "Autoignition of toluene reference fuels at high pressures modeled with detailed chemical kinetics." Combust. Flame 149, 2–24, (2007).

Andrae J.C.G., Johansson D., Björnbom P., Risberg P., Kalghatgi G.T. "Co-oxidation in the auto-ignition of primary reference fuels and n-heptane/toluene blends." Combust. Flame 140, 267–286, (2007).

Andrae J.C.G., Brinck T. and Kalghatgi G.T. "HCCI experiments with toluene fuels modeled by a semidetailed chemical kinetics model" Combustion and Flame 155, 696–712, (2008).

Barnard J.A. and Hughes H.W.D. "The Pyrolysis of ethanol" Trans. Faraday Soc. 56, 55 – 63, (1960).

Battin-Leclerc F. "Detailed chemical kinetics models for the low-tempeature combustion of hydrocarbons with application to gasoline ans diesel surrogates" Progress in Energy and Combustion Science 34, 440–498, (2008).

Bendtsen A.B., Glarborg P. and Dam-Johansen K. "Visualization methods in analysis of detailed chemical kinetics modelling" Computers and Chemistry 25, 161–170, (2001).

Bird R.B., Hirschfelder J.O. and Curtis C.F. "Molecular Theory of Gases and Liquids". John Wiley & Sons, Inc. USA. (1954).

Borisov A.A., Zamanskii V.M., Konnov A. A., Lisyanskii V.V., Rusanov S.A., and Skachkov G. I. "High temperature ignition of mixtures of ethanol and acetaldehyde with oxygen" Sov. J Chem. Phys., Vol 4(11), pp.2561–2575, (1989).

Borisov A.A., Zamanskii V.M., Konnov A.A., Lisyanskii V.V., Rusanov S.A., and Skachkov G.I. "A mechanism of high-temperature ethanol ignition." Sov. J Chem. Phys., Vol 9(11), pp.2527–2537, (1992).

Borisov A.A., Zamanskii V.M., Konnov A.A., Lisyanskii V.V., Rusanov S.A., and Skachkov G. I. "High-temperature pyrolysis of ethanol." Sov. J Chem. Phys., Vol 8(1), pp.121–141 (1991).

Bourque G., Healy D., Curran H. J., Zinner C., Kalitan D., J. de Vries, Aul C., and Petersen E. "Ignition and Flame Speed Kinetics of Two Natural Gas Blends with High Levels of Heavier Hydrocarbons", Proc. ASME Turbo Expo., 3, 1051–1066, (2008).

Cancino L.R. and Oliveira A.A.M. "Analysis and comparison of two detailed kinetic models for the thermal oxidation of ethanol-oxygen mixtures in high temperatures.", Proceedings of the 11th Brazilian Congress of Thermal Sciences and Engineering., Paper CIT06–0456., Brazil, (2006).

Cancino L.R. and Oliveira A.A.M. "Analysis of the thermal ignition and induction time of premixed ethanol and air combustion.", 18th International Congress of Mechanical Engineering., Paper COBEM2005–0959, Brazil, (2005a).

Cancino L.R., "Análise de equilibrio, cinética química da ignição termica e propagação de chama plana laminar de misturas de hidrocarbonetos leves com ar." Master Dissertation. Federal University of Santa Catarina., Florianopolis, Brazil. (2004).

Cancino L.R., Fikri M., Oliveira A.M.M., Schulz C., "Autoignition of gasoline surrogate mixtures at intermediate temperatures and high pressures: Experimental and numerical approaches.", Proceedings of the Combustion Institute Volume 32, Issue 1, Pages 501–508, (2009a)

Cancino L.R., Fikri M., Oliveira A.M.M., Schulz C., "Autoignition of Binary Mixtures of Gasoline Surrogates, Ethanol – Isooctane Blends in Air: Numerical and Experimental Study in High Pressure Shock Tube". 20th International Congress of Mechanical Engineering., November 15–20, Gramado, RS, Brazil, (2009c)

Cancino L.R., Fikri M., Oliveira A.M.M., Schulz C., "Autoignition of ethanol: analysis and experiment of ethanol ignition in shock tube.", 12th Brazilian Congress of Thermal Engineering and Sciences., Brazil. (2008a).

Cancino L.R., Fikri M., Oliveira A.M.M., Schulz C., "Detailed chemical modeling of the autoignition of mult-component gasoline surrogates at intermediate temperatures and high pressures." 32th International Symposium on Combustion, Montreal, Canada.. WIPP01–31. (2008b).

Cancino L.R., Fikri M., Oliveira A.M.M., Schulz C., "Shock-tube study of the Ignition delay times of ethanol at high pressures and intermediates temperatures Experimental and

numerical approaches.", Eastern State Fall Technical Meeting Chemical & Physical Processes in Combustion University of Virginia October 21–25, (2007).

Cancino L.R., Fikri M., Oliveira A.M.M., Schulz C., "Thermal Oxidation of Ethanol: Experimental and Numerical Analysis of Ignition Chemistry of Ethanol-Air Mixtures in Shock-Heated Gases", Paper 30074, 27th International Symposium on Shock Waves, St. Petersburg, Russia, (2009b).

Cataluña R and Silva R., "Development of a device to valuate the effect of ethanol on the vapor pressure and vaporization enthalpy of fuel gasoline." Quim. Nova. Vol 29, No 3, 580-585, (in Portuguese), (2006).

Curran H.J., Dunphy M., Simmie J.M, Westbrook C.K, Pitz W.J. "Shock tube ignition of ethanol, isobutene and MTBE: Experiments and modelling" Twenty-Fourth Symposium (International) on Combustion/The Combustion Institute, pp. 769–766, (1992)

Curran H.J., Gaffuri P, Pitz W.J., Westbrook C.K., "A Comprehensive Modeling Study of iso-Octane Oxidation.", Combustion and Flame 129, 253–280 (2002).

Curran H.J., Gaffuri P., Pitz W.J., and Westbrook C.K. "A Comprehensive Modeling Study of n-Heptane Oxidation." Combustion and Flame 114, 149–177, (1998b).

Curran H.J., Pitz W.J., Westbrook C.K., Callahan C.V., Dryer F.L. "Oxidation of automotive primary reference fuels at elevated pressures.", Proc. Combust. Inst. 27, 379–387 (1998).

Dagaut P., Pengloan G. and Ristori A. "Oxidation, ignition and combustion of toluene: Experimental and detailed chemical kinetic modeling" Phys. Chem. Chem Phys., 4, 1846–1854, (2002).

Davidson D.F. and Hanson R.K., "Interpreting Shock Tube Ignition Data". Int. J Chem. Kinet 36: 510–523, (2004)

Davidson D.F., Horning D.C., Herbon J.T., and Hanson R.K. "Shock tube measurements of JP-10 ignition" Proceedings of the Combustion Institute, Volume 28, pp. 1687–1692, (2000).

Davidson D.F., Gauthier B.M., Hanson R.K., "Shock tube ignition measurements of iso-octane/air and toluene/air at high pressures.", Proc. Combust. Inst. 30, 1175–1182, (2005).

Davidson D.F., Oehlschlaeger M.A., Herbon J.T., Hanson R.K., "Shock tube measurements of iso-octane ignition times and oh concentration time histories.", Proc. Combust. Inst. 29, 1295–1301, (2002).

Dean A.J., Penyazkov O.G., Sevruk K.L., Varatharajan B. "Autoignition of surrogate fuels at elevated temperatures and pressures" Proceedings of the Combustion Institute, Volume 31 Pages 2481–2488. (2007).

Dunphy M.P. and Simmie J.M. "High temperature oxidation of ethanol. Part 1. –Ignition Delays in Shock Waves." J. Chem. Soc. Faraday Trans. 87, 1691–1696, (1991).

Dunphy M.P., Patterson P.M., Simmie J.M. "High-temperature oxidation of ethanol. Part 2. – Kinetic Modelling." J. Chem. Soc. Faraday Trans. 87, 2549–2559, (1991).

Egolfopulos, F.N., Du D.X., Law C.K. "A estudy on ethanol oxidation kinetics in laminar premixed flames, flow reactors and shock tubes" Twenty-Fourth Symposium (international) on Combustion/The Combustion Institute. pp. 833–841. (1992)

Favre A. Statistical equations of turbulents gases. In *Problems of hydrodynamics and continuum mechanics*, pp. 231–266 (1969).

Fikri M., Herzler J., Starke R., Schulz C., Roth P., Kalghatgi G.T., "Autoignition of Gasoline Surrogates Mixtures at Intermediate Temperatures and High Pressures" Combust. Flame 152, 276–281. (2008).

Fischer S.L., Dryer F.L., and Curran H.J., "The Reaction Kinetics of Dimethyl Ether. I: High-Temperature Pyrolysis and Oxidation in Flow Reactors." Int. J. Chem. Kinet. 32: 713–740, (2000).

Fisher E.M., Pitz W.J., Curran H.J. and Westbrook C.K. "Detailed Chemical Kinetic Mechanisms for Combustion of Oxygenated Fuels" Proceedings of the Combustion Institute 28, p. 1579–1586, (2000).

Gardiner W.C. "Gas-Phase Combustion Chemistry". Springer-Verlag New York Inc. USA. (2000).

Gauthier B.M., Davidson D.F., Hanson R.K. "Shock tube determination of ignition delay times in full-blend and surrogate fuel mixtures" Combust. Flame 139, 300–311. (2004).

Gilbert RG., Luther K. and Troe J. "Theory of thermal unimolecular reactions in the fall-off range. II. Weak collision rate constants"., Ber Bunsenges Phys Chem, 87, 169–77 (1982)

Gregory P. Smith, David M. Golden, Michael Frenklach, Nigel W. Moriarty, Boris Eiteneer, Mikhail Goldenberg, C. Thomas Bowman, Ronald K. Hanson, Soonho Song, William C. Gardiner, Jr., Vitali V. Lissianski, and Zhiwei Qin "GRI-Mech 3.0". http://www.me.berkeley.edu/gri_mech/

Griffiths J.F., "Reduced kinetic models and their application to practical combustion systems" Progress in Energy and Combustion Science, 21 (1), p.25–107. (1995).

Gulder Ö. "Laminar burning velocities of Methanol, ethanol ans iso-octane-air mixtures" Nineteenth Symposium (internatinal) on Combustion/The Combustion Institute, 1982/pp. 275–281

Hartmann M., Tian K., Hofrath C., Fikri M., Schubert A., Schießl R., Starke R., Atakan B., Schulz C., Maas U., Jäger F.K. and Kühling K. "Experiments and modeling of ignition delay times, flame structure and intermediate species of EHN-doped stoichiometric n-heptane/air combustion" Proceedings of the Combustion Institute Volume 32, Issue 1, Pages 197–204, (2009).

Herbinet O., Pitz W.J., and Westbrook C.K., "Detailed Chemical Kinetic Oxidation Mechanism for a Biodiesel Surrogate" Combust. Flame 154 507–528 (2008). http://dx.doi.org/10.1016/j.combustflame.2008.03.003

Herzler J., Fikri M., Hitzbleck K., Starke R., Schulz C., Roth P. and Kalghatgi G.T. "Shock-tube study of the autoignition of n-heptane/toluene/air mixtures at intermediate temperatures and high pressures". Combustion and Flame Volume 149, Issues 1-2, Pages 25–31, (2007).

Herzler J., Jerig L. and Roth P. "Shock tube study of the ignition of lean n-heptane/air mixtures at intermediate temperatures and high pressures" Proceedings of the Combustion Institute Volume 30, Issue 1, Pages 1147–1153, (2005).

Kalghatgi G.T., "Personal communication", (2007).

Kasper T.S., Oßwald P., Kamphus M., Kohse-Höinghaus K. "Ethanol flame structure investigated by molecular beam mass spectrometry." Combustion and Flame 150, 220 – 231, (2007).

Kee R.J., Rupley F.M., Miller J.A., Coltrin M.E., Grcar J.F., Meeks E., Moffat H.K., Lutz A.E., Dixon-Lewis G., Smooke M.D., Warnatz J., Evans G.H., Larson R.S., Mitchell R.E., Petzold L.R., Reynolds W.C., Carcotsios M., Stewart W.E., Glarborg P., Wang C. and

Adigun O., "CHEMKIN Collection, Release 3.7.1", Reaction Design, Inc., San Diego, CA, 2000

Konnov A. "Development and validation of a detailed reaction mechanism for the combustion of small hydrocarbons.", 28-th Symposium (Int.) on Combustion, Edinburgh,. Abstr. Symp. Pap. p. 317. (2000).

Konnov A.A.. "Personal Communication" (2005)

Kuo K. "Principles of Combustion", Jhon Wiley & Sons, USA, (1986)

Laude P.A., Pitz W.J., and Thomson M.J., "Chemical Kinetic Modeling of Dimethyl Carbonate in an Opposed-Flow Diffusion Flame" Proceedings of the Combustion Institute 30, pp. 1095–1102 (2004).

Li J., Kazakov A., Dryer F.L. "Experimental and Numerical Studies of Ethanol Decomposition Reactions" J. Phys. Chem. A., 108(38), 7671–7680, (2004).

LLNL – Lawrence Livermore National Laboratory available at < http://www-cmls.llnl.gov/?url=science_and_technology-chemistry-combustion-mechanisms >

Marinov N.M. "A detailed chemical kinetic model for high temperature ethanol oxidation.", Int. J. Chem. Kinet 31, 183–220, (1999).

Marinov N.M., Pitz W.J., Westbrook C.K., Hori M. and Matsunaga N. "An Experimental and Kinetic Calculation of the Promotion Effect of Hydrocarbons on the NO-NO2 Conversion in a Flow Reactor" Proceedings of the Combustion Institute, Volume 27, pp. 389–396, (1998).

Marinov N.M., Pitz W.J., Westbrook C.K., Vincitore A.M., Castaldi M.J., Senkan S.M., "Aromatic and Polycyclic Aromatic Hydrocarbon Formation in a Laminar Premixed n-Butane Flame" Combustion and Flame 114, 192–213 (1998).

Maurice L.Q., "Detailed chemical kinetic models for aviation fuels" Ph.D Thesis. Imperial College, London, (1996).

Metcalfe W.K., Pitz W.J., Curran H.J., Simmie J.M., Westbrook C.K. "The development of a detailed chemical kinetic mechanism for diisobutylene and comparison to shock tube ignition times." Proceedings of the Combustion Institute 31 377–384, (2007).

Mirels H. "Test Time in Low-Pressure Shock Tubes.", The Physics of Fluids. Volume 6, Number 9. (1963).

NASA Glenn thermodynamic database. Available at http://cea.grc.nasa.gov/

Natarajan K., Bhaskaram K.A. "An experimental and analytical investigation of high temperature ignition of ethanol." Proc 13th Int. Shock Tube Symp., Niagara Falls, pp. 834. (1981).

O'Connaire M., Curran H.J., Simmie J.M., Pitz W.J., and Westbrook C.K., "A Comprehensive Modeling Study of Hydrogen Oxidation" Int. J. Chem. Kinet., 36:603–622, (2004).

Oertel H., "Stoßrohre", Springer Verlag, Wien, New York, 1966.

Palmer H. B., Knox B.E., ARS Journal 31 826–828. (1961).

Park J., Zhu R.S. and Lin M.C., "Thermal decomposition of ethanol. I. Ab Initiomolecular orbital/Rice–Ramsperger–Kassel–Marcus prediction of rate constant and product branching ratios". Journal of Chemical Physics. Vol 117, Number 7 – (2002).

Park J., Xu Z.F. and Lin M.C. "Thermal decomposition of ethanol. II. A computational study of the kinetics and mechanism for the H+C2H5OH reaction" Journal of Chemical Physics. Vol 118, Number 22 – (2003).

Park J., Xu Z.F. and Lin M.C. "Thermal decomposition of ethanol. III. A computational study of the kinetics and mechanism for the CH3+C2H5OH reaction" Journal of Chemical Physics. Vol 120, Number 14 – (2004).

Peters N. "Turbulent combustion" Cambridge University Press, (2000).

Petersen E.L. and Hanson R.K., "Nonideal effects behind reflected shock waves in a high-pressure shock tube" Shock Waves, 10; 405 – 420, (2001).

Petersen E.L., D.M. Kalitan, S. Simmons, G. Bourque, H.J. Curran, J.M. Simmie "Methane/Propane Oxidation at High Pressures: Experimental and Detailed Chemical Kinetic Modelling" Proceedings of the Combustion Institute, 31: 447–454, (2007).

Pitz W.J., Naik C.V., Mhaolduin T.N., Westbrook C.K., Curran H.J., Orme J.P. and Simmie J.M., "Modeling and experimental investigation of methylcyclohexane ignition in a rapid compression machine" Proc. Combust. Inst. 31 (1) (2007) 267–275, http://dx.doi.org/10.1016/j.proci.2006.08.041

Poinsot T and Veynante Denis. "Theoretical and Numerical Combustion" Edwars, USA (2001).

Risberg P., "Describing the Auto-Ignition Quality of Fuels in HCCI Engines" Ph.D. Thesis, School of Industrial Engineering and Management Royal Institute of Technology. Stockholm, (2006).

Rolland S., Simmie J.M., "The comparison of detailed kinetic mechanisms: Application to the combustion of methane" Int. J. Chem. Kinet. 36, 467–471 (2004).

Rudinger G. "Effect of Boundary Layer Growth in a Shock Tube on Shock Reflection from a Closed End." The Physics of Fluids. Volume 4, Number 12. (1961).

Saad M.A. "Compressible Fluid Flow" 2nd Ed. Prentice Hall. USA.(1993)

Salvi G., "La Combustión, Teoría y aplicaciones", Ed. S.A. Dossat, Madrid, (1975)

Saxena P., Williams F. "Numerical and experimental studies of ethanol flames". Proceedings of the Combustion Institute 31 1149–1156, (2007).

Seiser H., Pitsch H., Seshadri K., Pitz W.J., and Curran H.J., "Extinction and Autoignition of n-Heptane in Counterflow Configuration" Proceedings of the Combustion Institute 28, p. 2029–2037, (2000).

Silke E.J., Pitz W.J. and Westbrook C.K. "Detailed Chemical Kinetic Modeling of Cyclohexane Oxidation" J. Phys. Chem. A ASAP Article, DOI: 10.1021/jp067592d (2007).

Simmie J.M., "Detailed chemical kinetic models for the combustion of hydrocarbon fuels" Progress in Energy and Combustion Science, 29 (6), p.599–634. (2003).

Sivaramakrishnan R., Tranter R.S. and Brezinsky K. "A high pressure model for the oxidation of toluene" Proceedings of the Combustion Institute 30 1165–1173 (2005).

Stewart P.H., Larson C.W. and Golden D.M. "Pressure and temperature dependence of reactions proceeding via a bound complex. 2. Application to 2CH3 → C2H5 + H" Combustion and Flame, Volume 75, Issue 1, Pages 25–31, (1989).

Vasudevan V., Davidson D.F., Hanson R.K. "Shock tube measurements of toluene ignition times and OH concentration time histories" Proceedings of the Combustion Institute, Volume 30, Pages 1155–1163. (2005).

Warnatz J. Mass U., Dibble R.W. "Combustion Physical and Chemical Fundamentals, Modeling and Simulation, Experiments, Pollutant Formation." 2nd Edition, Springer, (1999).

Westbrook C. K., Pitz W.J., Herbinet O., Curran H.J., and Silke E.J., "A Detailed Chemical Kinetic Reaction Mechanism for n-Alkane Hydrocarbons from n-Octane to n-Hexadecane" Combustion and Flame 156 181–199 (2009).

Westbrook C.K and Dryer F. "Simplified Reaction Mechanisms for the Oxidation of Hydrocarbon Fuels in Flames" Combustion Science and Technology, Vol. 27. pp. 31–43. (1981).

Westbrook C.K. "Chemical kinetics of hydrocarbon ignition in practical combustion systems", Proceedings of the Combustion Institute, Volume 28, pp. 1563–1577, (2000).

Westbrook C.K., Mizobuchi Y., Poinsot T.J., Smith P.J., Warnatz J., "Computational combustion." Proc. Combust. Inst. 30, 125–157 (2005).

Wilcox D.C. "Turbulence Modeling for CFD". DCW Industries, Inc. La Cañada, California, (1994).

Zel'dovich Ya.B., Raizer Yu.P., Hayes W.D., Probstein R.F. "Physics of Shock Waves and High-Temperature Hydrodynamic Phenomena" Volume I. Academic Press, New York and London (1966a).

Zel'dovich Ya.B., Raizer Yu.P., Hayes W.D., Probstein R.F. "Physics of Shock Waves and High-Temperature Hydrodynamic Phenomena" Volume II. Academic Press, New York and London (1966b).

Appendix

Appendix A:

Autoignition of gasoline surrogate mixtures at intermediate temperatures and high pressures: Experimental and numerical approaches.
Cancino L.R., Fikri M., Oliveira A.A.M., Schulz C.
Proceedings of the Combustion Institute, 32 (1), p.501-508, Jan 2009.

Appendix B:

Thermal Oxidation of Ethanol: Experimental and Numerical Analysis of Ignition Chemistry of Ethanol-Air Mixtures in Shock-Heated Gases.
Cancino L.R., Fikri M., Oliveira A.A.M., Schulz C.
27th International Symposium on Shock Waves, St. Petersburg, Russia, 19…24 July 2009.
Paper 30074 pag. 137-142.

Apendix C:

Autoignition of binary mixtures of gasoline surrogates, ethanol – iso-octane blends in air: Numerical and experimental study in a high-pressure shock tube.
Cancino L.R., Fikri M., Oliveira A.A.M., Schulz C.
20th International Congress of Mechanical Engineering. Proceedings of COBEM 2009.
November 15-20, 2009, Gramado, RS, Brazil. Paper COB09-0355.

Available online at www.sciencedirect.com
ScienceDirect
Proceedings of the Combustion Institute 32 (2009) 501–508
Proceedings of the Combustion Institute
www.elsevier.com/locate/proci

Autoignition of gasoline surrogate mixtures at intermediate temperatures and high pressures: Experimental and numerical approaches

L.R. Cancino [a,b,*], M. Fikri [b], A.A.M. Oliveira [a], C. Schulz [b]

[a] *Laboratório de Combustão e Engenharia de Sistemas Térmicos, Universidade Federal de Santa Catarina, Campus Universitário, Trindade, 88040-900 Florianópolis, SC, Brazil*
[b] *IVG, University of Duisburg-Essen, Duisburg, Germany*

Abstract

Ignition-delay times were measured in shock-heated gases for a surrogate gasoline fuel comprised of ethanol/iso-octane/*n*-heptane/toluene at a composition of 40%/37.8%/10.2%/12% by liquid volume with a calculated octane number of 98.8. The experiments were carried out in stoichiometric mixtures in air behind reflected shock waves in a heated high-pressure shock tube. Initial reflected shock conditions were as follows: Temperatures of 690–1200 K, and pressures of 10, 30 and 50 bar, respectively. Ignition delay times were determined from CH^* chemiluminescence at 431.5 nm measured at a sidewall location. The experimental results are compared to simulated ignition delay times based on detailed chemical kinetic mechanisms. The main mechanism is based on the primary reference fuels (PRF) model, and sub-mechanisms were incorporated to account for the effect of ethanol and/or toluene. The simulations are also compared to experimental ignition-delay data from the literature for ethanol/iso-octane/*n*-heptane (20%/62%/18% by liquid volume) and iso-octane/*n*-heptane/toluene (69%/17%/14% by liquid volume) surrogate fuels. The relative behavior of the ignition delay times of the different surrogates was well predicted, but the simulations overestimate the ignition delay, mostly at low temperatures.

Keywords: Detailed kinetic model; Gasoline surrogates; Shock tube; Autoignition; Ignition delay time

1. Introduction

In the development of future fuels for internal combustion (IC) engines the interest currently shifts towards increasing the concentration of biomass-derived and synthetic components. Special emphasis is set on ethanol, because of its high availability. It has also been used as an octane-boosting, pollution-reducing additive for gasoline [1]. Countries like Brazil have a long history in

* Corresponding author. Address: Laboratório de Combustão e Engenharia de Sistemas Térmicos, Universidade Federal de Santa Catarina, Campus Universitário, Trindade, 88040-900 Florianópolis, SC, Brazil. Fax: +55 48 3234 3131.
E-mail address: leonel@labcet.ufsc.br (L.R. Cancino).

1540-7489/$ - see front matter Crown copyright © 2009 Published by Elsevier Inc. on behalf of The Combustion Institute. All rights reserved.
doi:10.1016/j.proci.2008.06.180

using ethanol for IC engines and automotive fuel is commercially available in mixture with ethanol at about 25% or as 100% ethanol. So-called flex engines have been developed to cope with strongly varying fuel compositions [2]. Nevertheless, fundamental studies of the ignition properties of ethanol-containing model fuels are scarce [3].

For the characterization of fuels the autoignition delay is a significant observable and is a critical parameter for IC engines. It influences the performance of both compression-ignition (CI) and spark-ignition (SI) engines. In CI and homogeneous-charge compression-ignition (HCCI) engines, the combustion process is initiated by autoignition. Therefore, it is crucial to know "when" ignition will occur. In SI engines, autoignition causes knock which limits the accessibility of the most efficient engine operation regimes. Therefore, again, it is necessary to know after which residence time a fuel ignites at specific temperatures and pressures.

Several methodologies can be applied to determine ignition delay times (IDTs). Experiments were carried out in shock tubes, rapid-compression machines (RCM), or perfectly stirred reactors (PSR) [3–6]. Here, we study the ignition delay in a shock tube using undiluted homogeneous mixtures of fuel and synthetic air in order to generate validation data for comparison with the results of chemistry models.

Practical fuels are a complex mixture of various hydrocarbons. Their ignition characteristics are typically described by comparison to those of reference fuels. The traditional comparison to two-component fuels (*n*-heptane/iso-octane defining the octane number ON) has shown weaknesses for the operating conditions of modern IC engines. Therefore, more complicated surrogate fuels have been developed. Detailed chemical mechanisms for ignition and combustion of reference fuels can then be included in engine simulations.

Validation and optimization of such models depend on the availability of experimental data, particularly on IDTs. Recently, models have been developed for fuel surrogates such as *n*-heptane/toluene [7]. Yahyaoui et al. studied the oxidation of iso-octane/toluene/1-hexane/ETBE mixtures in a jet stirred reactor [8]. The experimental data have been used to validate a new detailed chemical kinetics mechanism including cross-reactions [5,7]. The same group studied the autoignition of a binary mixture of 1-hexene and toluene in a shock tube in the 750–1860 K temperature and 2–10 bar pressure range [9]. Studies of other relevant mixtures containing aromatics, olefins and ethanol are just appearing [5,7]. Recently, Fikri et al. [3] measured the ignition delay times for various shock-heated mixtures of two multi-component model fuels in air. The fuels were comprised of *n*-heptane/iso-octane/ethanol and *n*-heptane/toluene/iso-octane/diisobutylene (18%/62%/20% and 20%/45%/25%/10% by liquid volume, respectively). The fuels have similar research octane numbers (RON 95) and motor octane numbers (MON 85) that correspond to the standard European gasoline. Gauthier et al. [4] investigated the ignition-delay time of gasoline behind reflected shock waves and compared them to the results of two gasoline surrogates comprised of iso-octane/toluene/*n*-heptane by keeping the *n*-heptane fraction constant and varying the iso-octane/toluene proportion. The optimized surrogates showed a good agreement to real gasoline in terms of IDTs.

The previous studies have thus focused on hydrocarbon-based fuels with *either* toluene *or* ethanol. Surrogates containing both components have not yet been studied. Therefore, the main purpose of this study was to provide experimental data for fuel surrogates containing ethanol *as well as* toluene for the development of chemical kinetic models for gasoline/ethanol mixtures. We therefore studied the behavior of a four-component fuel (called "Surrogate A" in this paper) of ethanol/iso-octane/*n*-heptane/toluene (40%/37.8%/10.2%/12% by liquid volume) behind reflected shock waves. Our model results are additionally compared to the literature data for surrogate fuels based on a primary reference fuel containing ethanol [3] or toluene [4] (called "Surrogate B" and "Surrogate C" in this paper, resp.). Table 1 summarizes the composition of the three surrogates. The respective octane numbers have been calculated using a blending program from Shell [10].

The numerical simulations were done using the SHOCK package of CHEMKIN [11]. The detailed kinetic models tailored in this work use the PRF model of Curran et al. [6] for iso-octane/*n*-heptane chemistry as a "kernel". This PRF model is the result of the improvement and of several detailed kinetics models developed for hydrocarbons containing up to eight carbon atoms in the molecular structure [6]. The PRF

Table 1
Composition of the gasoline surrogates (GS) investigated in this study

Gasoline surrogate	Composition liquid volume (%)				Octane number
	Ethanol	Iso-octane	*n*-Heptane	Toluene	
Surrogate A	40.0	37.8	10.2	12.0	98.75 [10]
Surrogate B [3]	20.0	62.0	18.0	**	92.0 [10]
Surrogate C [4]	**	69.0	17.0	14.0	87.0 [10]

kinetic model has been tested and validated against various experimental data [6]. Sub-mechanisms for toluene and/or ethanol were embedded into the PRF mechanism to expand its applicability to a larger variety of fuels. The blending procedure that carefully adds selected additional reactions to the base mechanisms is described in the section "chemistry modeling". This work is the first contribution for the optimization process of kinetic models involving ethanol, iso-octane, *n*-heptane, and toluene.

2. Experimental

The experiments were carried out in a high-pressure shock tube with an internal diameter of 90 mm. It is divided by an aluminum diaphragm into a driver section of 6.1 m and a driven section of 6.4 m in length. The driven section was pumped down to pressures below 10^{-2} mbar. Gas mixtures were prepared by injection of a liquid mixture and subsequent complete evaporation in a stainless-steel mixing vessel. The total amount of fuel and air was controlled manometrically in order to ensure the desired equivalence ratio. The shock speed was measured over two intervals using three piezo-electric pressure gauges. The data were recorded with a time resolution of 0.1 μs. The temperature and pressure behind the reflected shock wave were computed from the measured incident shock speed and the attenuation using a one-dimensional shock-tube model (CHEMKIN [11]). The estimated uncertainty in reflected shock temperature is less than ±25 K in the temperature and time range of our measurements. The experiments were carried out in synthetic air containing 79.5% N_2 and 20.5% O_2 by volume.

The model calculations used here are based on an isochoric assumption. The first stage of pre-ignition, however, causes indeed a slight pressure increase, which can expand in the form of a non-stationary wave thus influencing the ignition behavior. In the crucial case (long time observation related to low-to-intermediate temperature) the maximum temperature increase was estimated to be 20 K which is within the error estimated in the uncertainty. Moreover, we should mention that small changes in temperature are most relevant to measurements at low temperature and therefore do not dramatically affect the ignition delay times τ_{ing} in the NTC range. We believe that this effect is to some extent fuel-specific and also dependent on how well the driver gas tailoring was chosen.

The ignition was observed behind the reflected shock waves by measuring temporal pressure profiles with a piezo-electric gauge (PCB HM 112 A03) at a side-wall position 15 mm upstream of the endplate. Also, CH^* chemiluminescence was measured at the same position. It was selected by a bandpass filter (431.5 nm, 5 nm HWHM) and detected with a photomultiplier with a time resolution of 1 μs. Ignition delay times were determined by extrapolating either the steepest increase of the CH^* emission signal to its zero level on the time axis or the pressure increase due to the ignition. Both procedures yield very similar results (<5% deviation). Here, we use the data obtained from the chemiluminescence measurement. Bifurcation effects are not observed.

We used driver gas tailoring to extend the observation time to a maximum of 15 ms to allow for measurements of the IDTs at low temperatures. The driver gas was mixed in situ by using two high-pressure mass-flow controllers (Bronkhorst Hi-Tec flow meter). Helium was used as the main component and 5–20% argon was added to match the acoustic impedance of the test gas. The composition was calculated for each experimental condition using equations by Oertel [12] and Palmer and Knox [13].

3. Chemistry modeling

Several detailed kinetic mechanisms for different hydrocarbons and blends of primary reference fuels (PRF) are available in the literature [6,14,15]. In this work, three different mechanisms were taken into account and tailored for the specific gasoline surrogates. The "adaptation process" of the kinetic models is based on blending of different sub-mechanisms for the different fuel compounds. This process requires a sequence of steps to construct the final detailed kinetic model that are outlined for the combination of two mechanisms below:

1. Analyze and potentially adjust the kinetic information of both mechanisms for their use in CHEMKIN.
2. Check the species names in both mechanisms and remove duplicate reactions from the second (minor) mechanism.
3. Add the missing reactions into the major mechanism.
4. Check the thermodynamic data base of the major mechanism and upgrade it with data for the missing species.
5. Test the blended kinetic model with the CHEMKIN interpreter and validate it against measured IDTs. To make sure that the added reactions for an additional fuel component do not change the behavior of the mechanism in case this component is not present.
6. Optimize the blended kinetic mechanism: Determine the rate-determining route for autoignition via a sensitivity analysis and figure out whether the major reactions have reliable (directly measured) kinetic data.

Table 2
Characteristics of the detailed kinetic mechanisms adapted to the surrogate fuels investigated in this work

	Mechanism	Blended mechanism	Reference
Surrogate A	GS-A	Ethanol	[1]
		Toluene	[18]
Surrogate B	GS-B	Ethanol	[1]
Surrogate C	GS-C	Toluene	[17]

The adopted mechanisms used for the surrogates A, B, and C were tailored by incorporating the mechanisms given in the third column into the PRF mechanism [6].

The blending procedure is time consuming. If two chemical species have the same chemical formula, it is necessary to check their thermodynamic databases by comparing the enthalpy h, heat capacity c_p, and entropy s at several temperature values. If their thermodynamic properties return the same (or similar) values, then both chemical species are identical despite different names or abbreviations used in the original kinetic models.

These steps require the utilization of computational tools. In this work the programs of Rolland and Simmie [16] were used to compare the kinetics mechanisms and thermodynamic databases.

3.1. Tailored kinetic models for gasoline surrogates

Three detailed kinetic mechanisms were adapted to simulate the IDTs of different gasoline surrogates with the compositions and characteristics given in Table 1. Table 2 summarizes the origin of the sub-mechanisms. The full mechanisms are available as Supplementary material from the combustion symposium website.

The initial kinetic model tailored for the studied surrogates was the PRF model of Curran et al. [6]. To describe the chemical kinetics of ethanol oxidation, the Marinov mechanism was used [1] and introduced in the PRF model of Curran, giving the kinetic mechanism GS-B to simulate the ignition delay times of surrogate B (see Table 2). For the elaboration of the kinetic mechanism GS-A which describes the ignition behavior of surrogate A, the mechanism GS-B was used and upgraded by adding the sub-mechanism for toluene of Andrae et al. [18]. Finally, to simulate the gasoline surrogate C, the kinetic model GS-C was designed. Here, the PRF model of Curran was combined with the sub-mechanism of toluene of Maurice [17]. For abbreviations and references of the used mechanism see Tables 1 and 2.

4. Results and discussion

This work combines experimental and simulated ignition delay times for gasoline surrogates that contain toluene and/or ethanol. The simulations are based on different blended mechanisms. Thus, the comparison to experimental data allows to choose the most appropriate modeling approaches. The results are parceled in groups and presented in the following order: (i) presentation of the new experimental results for surrogate A and comparison with simulations, (ii) simulation of the IDTs of surrogate B, and (iii) ignition delay results for gasoline surrogate C in comparison to experimental data from the literature [3,4].

4.1. Results for surrogate A

The temperature range of the present study was $690 < T < 1200$ K and target pressures were 10 ± 2, 30 ± 2 and 50 ± 2 bar. All measurements were carried out at $\phi = 1$. Typical pressure and CH^* emission profiles are shown in Fig. 1 for an experiment at $T = 764$ K, $p = 31.5$ bar and $\phi = 1.0$. The two-step increase in pressure is due to the incident and reflected shock wave (time zero) followed by a constant pressure for about 4750 μs. The CH^* emission (lower part of Fig. 1) remains at zero level for 4750 μs, followed by a steep rise that indicates ignition. Ignition delay times shown here are based on an extrapolation of the increase in CH^* chemiluminescence emission to the zero level.

The results and simulations of the IDT experiments for surrogate A are presented in Table 3 and depicted in Fig. 2. For this data set the onset

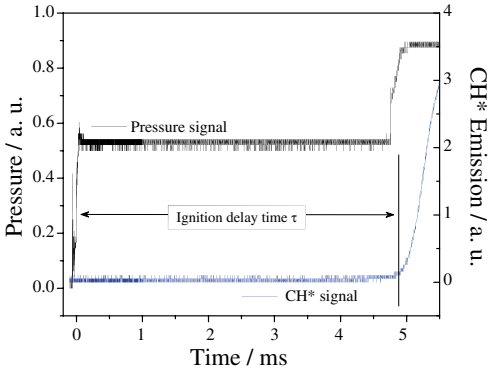

Fig. 1. Example of surrogate A/air ignition data showing the determination of the ignition delay time.

Table 3
Measured ignition delay times for surrogate A in air

Φ	T_5 (K)	P_5 (bar)	τ_{ing} (μs)
1.0	1201	10.1	158
1.0	1162	10.3	544
1.0	1093	9.9	939
1.0	1058	10.3	1438
1.0	1010	10.3	2436
1.0	935	9.8	3495
1.0	906	10.3	N-I
1.0	853	10.2	N-I
1.0	806	10.3	N-I
1.0	758	10.4	N-I
1.0	683	9.8	N-I
1.0	1194	30	50
1.0	1168	31	94
1.0	1128	32	149
1.0	1057	30	314
1.0	1016	31	555
1.0	983	28	774
1.0	951	30	806
1.0	858	31	2795
1.0	809	26	6944
1.0	793	29	6962
1.0	764	31	4975
1.0	701	30	8731
1.0	1191	50	28
1.0	1102	51	110
1.0	985	49	534
1.0	930	48	1705
1.0	891	49	2296
1.0	828	47	3792
1.0	788	48	5037

N-I, no ignition.

of a weak negative temperature coefficient (NTC) regime at around 900 K is observed.

The mechanism GS-A for the surrogate A predicts a similar activation energy for IDTs as the experimental data. It shows similarly to the experimental data a roll-off trend in activation energy at low temperatures especially at high pressures.

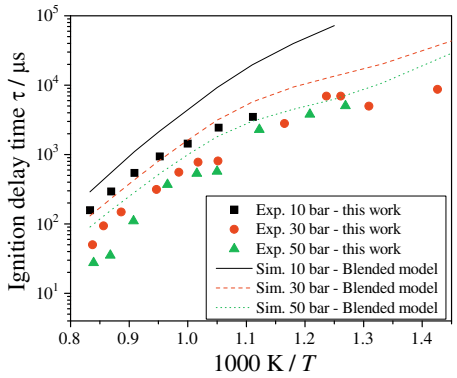

Fig. 2. Simulation and experimental results for surrogate A ignition delay times in air. $\phi = 1.0$, $p = 10$, 30, and 50 bar (see Tables 1 and 2 for composition and sub-mechanisms models).

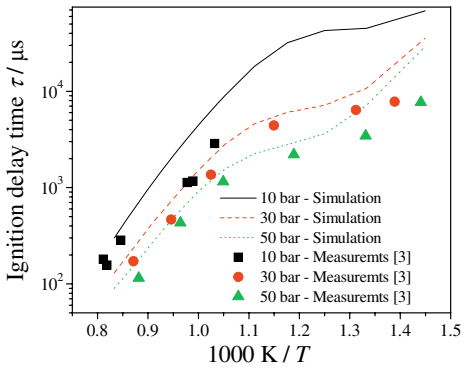

Fig. 3. Simulation and experimental results (from [3]) for surrogate B ignition delay times in air. $\phi = 1.0$ (see Tables 1 and 2 for composition and sub-mechanisms models).

The mechanism describing surrogate GS-A was also checked, whether it still reproduces the IDTs of the pure components. The mechanism captured for example quantitatively the results of toluene and the maximum error quoted was about 6%.

4.2. Results for surrogate B

Figure 3 combines our simulation results with the experimental data reported by Fikri et al. [3]. The lines depict the results of the simulation using the primary reference fuel mechanism of Curran in combination with the Marinov mechanism describing the ethanol oxidation. The new model does a relatively good job in predicting the autoignition delay time of surrogate B at three different pressures. The agreement is good in the high-temperature range for the results at 30 and 50 bar. The model over predicts the ignition delay at low temperatures. At 10 bar, however, the autoignition delay times is over predicted even at high temperature. The model does not capture the experimental results obtained from the shock tube at this pressure.

It can be clearly seen that the mechanism GS-B gives the closest agreement from all mechanisms with respect to the experimental data. Further experimental work including key species time-history measurements of OH (for example from CH_3CH_2OH) is desired to further improve the understanding of the relative effects of the sub-mechanisms used in the blending process.

4.3. Results for surrogate C

Figure 4 shows the simulations obtained with the blended mechanism GS-C (Table 2) and the experimental data reported by Gauthier et al.

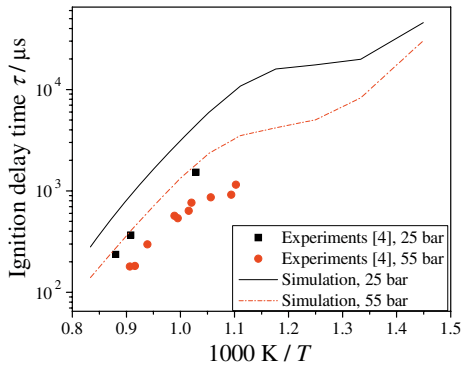

Fig. 4. Simulation and experimental results (from [4]) for surrogate C ignition delay times in air. $\phi = 1.0$ (see Tables 1 and 2 for composition and sub-mechanisms models).

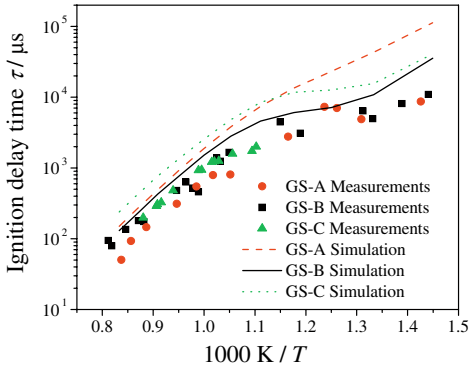

Fig. 5. Simulation and experimental results for all surrogates/air ignition delay times at $p_5 = 30$ bar. $\phi = 1.0$ (see Tables 1 and 2 for composition and sub-mechanisms models).

[4]. It is clearly seen, that the model also overestimates the measured ignition delay, but is still sensitive to the pressure dependence.

All detailed kinetic models GS-A, GS-B, and GS-C overestimate the IDTs. Figure 5 shows the experimental data scaled to $p_5 = 30$ bar using their respective scaling factors reported in [3,4] and the numerical simulation for the same pressure level for all surrogates. The data show a slight NTC behavior between 800 and 690 K for surrogates B which is also predicted by the simulation. For surrogate A the experiments indicate a weak NTC effect which is not shown by the simulation. Further experimental data are required to investigate this discrepancy.

For the surrogate GS-C no experimental data are available in the low-temperature range, however, the detailed kinetic model for this surrogate predicts a negative temperature behavior in this temperature range (dotted line). Despite these discrepancies in ignition delay times, the models capture the trends of the experiments. The ignition delay times are "shifted" in all cases compared to the experimental results to longer times. Further comparisons of simulated ignition delay times based on the mechanism with the added toluene reactions with experimental data from [18] show that this mechanism causes some disagreement in the 900–1200 K range. Therefore, further improvement of this mechanism is required, by validating it against experimental data for wide range of temperature and pressure.

Also, the ethanol sub-mechanism of Marinov does not give satisfactory results in our application and further refinements are needed. A sensitivity analysis of the two mechanisms is in progress. The results will shed light onto the key reactions which have the largest impact on the autoignition.

The kernel of the ignition chemistry is centered around three elementary reactions [19]:

$$H^{\cdot} + O_2 + M \rightarrow HO_2^{\cdot} + M \quad (R1)$$

$$RH + HO_2^{\cdot} \rightarrow R^{\cdot} + H_2O_2 \quad (R2)$$

$$H_2O_2 + M \rightarrow 2OH^{\cdot} + M \quad (R3)$$

In these reactions, RH denotes an alkane, R denotes an alkyl radical. The reactions (R1) and (R2) are chain propagating reactions and (R3) is a chain branching reaction, and the most important reaction for the promotion of the hydroxyl radical (OH) which is a key species to promote ignition [20]. The reaction (R4):

$$H + O_2 \rightarrow OH^{\cdot} + O \quad (R4)$$

also plays a significant role for the IDT at temperatures above 1200 K. Below this temperature and at measured temperatures and pressures the chemistry is dominated by (R1). Accordingly, and to explain the non-consensus of the simulations in this work, the hydrogen peroxide (H_2O_2) production could be eventually underestimated in the presented mechanisms.

Our approach of blending sub-mechanisms does not consider cross-reactions in which a free radical generated from one of the fuels "abstracts" hydrogen from the other fuel [18]. Andrae et al. [18] present a detailed kinetic model for toluene reference fuels (TRF), in which cross-reactions between toluene and PRF and between iso-octane and *n*-heptane are contemplated. Therefore, the detailed kinetic model of Andrae et al. [18] was also used to simulate the three gasoline surrogates investigated in this work. Figure 6 shows the results. Figure 7 compares the simulated ignition delay times with and without considering the cross-reactions from the Andrae model. One can clearly see that under these conditions cross-reactions are insignificant which agrees with the observation by Andrae et al. [18]. The TRF model does not show a clear difference

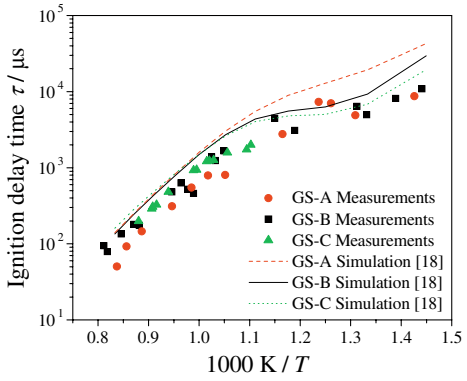

Fig. 6. Simulation and experimental results for all surrogates/air ignition delay times at $p_5 = 30$ bar. $\phi = 1.0$ – comparison with the results of the toluene reference fuel mechanism (TRF) of Andrae et al. [18].

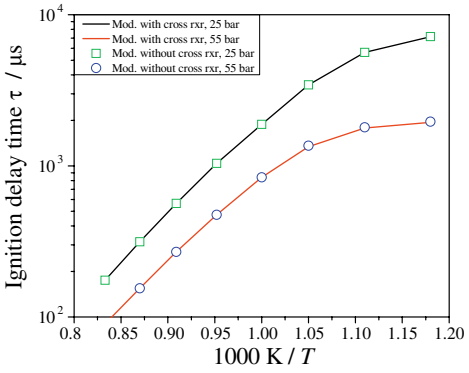

Fig. 7. Effect of cross-reactions in the ignition delay times using the model from [18].

between the ignition delay times for the three gasoline surrogates at temperatures above ~950 K. The experiments, however, indicate a difference in this temperature range. The detailed kinetic mechanisms tailored in this work in contrast are able to reproduce the experimentally observed difference of the ignition delay times (see Fig. 5). Also, our blended mechanism shows that at low temperature the ignition delay times increase with increasing the octane number calculated using a blending program from Shell [10].

5. Summary and conclusions

In this work, ignition delay times of a gasoline surrogate A (ethanol/iso-octane/*n*-heptane: 40%/37.8%/10.2%/12% by liquid volume) have been studied using the Duisburg high-pressure shock tube facility. The investigated post-reflected-shock temperature range was 690–1200 K. For investigations at low temperature, tailoring of the driver gas was necessary to extend the observation time. The experiments were carried out at stoichiometric ($\phi = 1$) conditions at pressures of 10, 30 and 50 bar. IDTs were evaluated using side-wall detection of CH^* chemiluminescence ($\lambda = 431.5$ nm).

Detailed kinetics modeling was used to simulate the autoignition of surrogate A and two other gasoline surrogates (surrogate B: ethanol/iso-octane/*n*-heptane: 20%/62%/18% by liquid volume, surrogate C: iso-octane/*n*-heptane/toluene: 69%/17%/14% by liquid volume) based on experimental data from the literature [2,3]. The model was developed by incorporating sub-mechanisms for ethanol and/or toluene oxidation into the primary reference fuel model of Curran et al. [6]. The resulting model shows the right trend but fails to capture absolute values of the ignition delay times, especially at low temperatures. All kinetics models over estimate the ignition delay times.

Acknowledgments

The authors gratefully acknowledge the Conselho Nacional de Desenvolvimento Científico e Tecnológico – CNPq – Brazil, N. Schlösser for help in conducting the experiments, G.T. Kalghatgi for discussions, and Deutscher Akademischer Austausch Dienst (DAAD), and the German Research Foundation (DFG) for financial support.

Appendix A. Supplementary material

Supplementary data associated with this article can be found, in the online version, at doi:10.1016/j.proci.2008.06.180.

References

[1] N.M. Marinov, *Int. J. Chem. Kinet.* 31 (1999) 183–220.
[2] R.C.O.B. Delgado, A.S. Araujo, V.J. Fernandes, *Fuel Process. Technol.* 88 (2007) 365–368.
[3] M. Fikri, J. Herzler, R. Starke, C. Schulz, P. Roth, G.T. Kalghatgi, *Combust. Flame* 152 (2008) 276–281.
[4] B.M. Gauthier, D.F. Davidson, R.K. Hanson, *Combust. Flame* 139 (2004) 300–311.
[5] C.V. Naik, W.J. Pitz, C.K Westbrook et al., SAE Technical Paper Series 2005-01-3741, 2005.
[6] H.J. Curran, W.J. Pitz, C.K. Westbrook, C.V. Callahan, F.L. Dryer, *Proc. Combust. Inst.* 27 (1998) 379–387.
[7] J. Andrae, D. Johansson, P. Björnbom, P. Risberg, G.T. Kalghatgi, *Combust. Flame* 140 (2005) 267–286.
[8] M. Yahyaoui, N. Djebaili-Chaumeix, P. Dagaut, C.-E. Paillard, S. Gail, *Proc. Combust. Inst.* 31 (2007) 385–391.
[9] M. Yahyaoui, N. Djebaili-Chaumeix, P. Dagaut, C.-E. Paillard, B. Heyberger, G. Pengloan, *Int. J. Chem. Kinet.* 39 (2007) 518–538.

[10] G.T. Kalghatgi, personal communication, 2007.
[11] R.J. Kee, F.M. Rupley, J.A. Miller et al., CHEMKIN Collection, Release 3.7.1 Reaction Design, Inc., San Diego, CA, 2000.
[12] H. Oertel, *Stoßrohre*, Springer, New York, 1966.
[13] H.B. Palmer, B.E. Knox, *ARS J.* 31 (1961) 826–828.
[14] A. Konnov, 28th Symposium (Int.) on Combustion, Edinburgh, 2000. Abstr. Symp. Pap. p. 317.
[15] Combustion Chemistry Centre, Chemistry Department, National University of Ireland, Mechanism download, available at http://www.ucg.ie/chem/combust.htm.
[16] S. Rolland, J. Simmie, *Int. J. Chem. Kinet.* 36 (2004) 467–471.
[17] L.Q. Maurice, *Detailed Chemical Kinetic Models for Aviation Fuels*, Ph.D. thesis, Imperial College, London, 1996.
[18] J.C.G. Andrae, P. Björnbom, R.F. Cracknell, G.T. Kalghatgi, *Combust. Flame* 149 (2007) 2–24.
[19] P. Risberg. *Describing the Auto-Ignition Quality of Fuels in HCCI Engines*, Ph.D. thesis, School of Industrial Engineering and Management Royal Institute of Technology. Stockholm, 2006.
[20] G. Salvi, La Combustión, Teoría y aplicaciones, S.A. Dossat (Ed.), Madrid, 1975.

Thermal Oxidation of Ethanol: Experimental and Numerical Analysis of Ignition Chemistry of Ethanol-Air Mixtures in Shock-Heated Gases

L.R. Cancino [*] **, A.A.M. Oliveira**
LabCET, Federal University of Santa Catarina, Campus Trindade, Florianopolis, 88040-900, Brazil
M. Fikri, C. Schulz
IVG, University of Duisburg-Essen, Duisburg, 47057, Germany

Key words: Ethanol,Ignition Delay Time, Shock Tube, Detailed Kinetic Model

Abstract:

The present work proposes a detailed kinetic model for the thermal oxidation of ethanol/air mixtures at intermediate temperatures and high pressures, validated against ignition delay times measured in a shock tube behind reflected shock waves. Ignition delay times were measured under stoichiometric conditions at 10, 30, and 50 bar and from 650 to 1220 K. From a multiple linear regression analysis using $\ln(\tau)$ as the dependent variable and $(1/T)$ and $\ln(p)$ as independent variables an expression of $\tau/\mu s = 10^{-1.79} \exp(+12400\ \mathrm{K}/T)\ (p/\mathrm{bar})^{-0.83}$ was curve fitted for the measured range of temperature, pressure and stoichiometric mixture. The kinetic model was built up by incorporating available submechanisms for ethanol chemistry (Marinov) as well as C_3-chemistry (Konnov), taken as central kernel. Additionally, other key reactions obtained from computational chemistry and available on the literature (Lin) were included. For improvement of the model, the sensitivity of each reaction on temperature, OH, H_2O_2, and C_2H_5OH concentrations was determined using a perfectly-stirred-reactor assumption for temperatures of 1100, 950, and 800 K at all pressures and stoichiometric mixture. The sensitivity analysis identified a set of important reactions involving the H-atom abstraction from the ethanol molecule by the hydroperoxy radical (HO_2), giving CH_3CHOH, acetaldehyde and H_2O_2. The model predicts the global trend with temperature and pressure as well as the lower sensitivity of the ignition delay time with pressure at higher pressures.

1. Introduction

There are several motivations to investigate and learn about the combustion of ethanol. In summary, there is a need of a) alternatives to conventional hydrocarbon fuels, especially from renewable sources, b) reduction of pollutant and carbon emissions from energy and power, and c) additives to control engine knock (Curran et al. (1992)). These needs are grounded on economic and environmental considerations. In the last sixty years, several authors have focused on ethanol oxidation. As results of these efforts a limited quantity of experimental and numerical investigations about ethanol kinetics involving different experimental setup and numerical models is available. From the pioneering works, using a well-stirred reaction vessel, Barnard and Hughes. (1960) showed that the pyrolysis of ethanol at temperatures between 849 and 897 K can be described as a homogeneous reaction of first order. Gulder. (1982) measured laminar burning speed of ethanol-air in lean and rich mixtures in a constant pressure bomb at pressure of 1 bar and room temperature. More recently, Borizov et al. (1991) used a reaction vessel to experimentally analyze the pyrolysis of ethanol at 1 bar and a temperature range of 700 - 1700 K. These results where later complemented by detailed laminar flame and shock tube data. Egolfopoulos et al. (1992) measured laminar burning speed, ignition delay time and chemical species in ethanol/(air/O_2) mixtures by using a shock tube, a counter-flow twin flame and a flow reactor. Kohse-Höinghaus et al. (2007) reported chemical species measurements and flame structure of ethanol/O_2 mixtures at 298 K and low pressures (0.05 bar). Natarajan and Bhaskaram (1981) reported ignition delay time measurements in a shock tube for pressures of 1.0 and 2.0 bar and high temperatures. Borizov et al. (1989) measured ignition delay times in ethanol/O_2 mixtures by using the shock tube at pressures between 0.5 and 6 bar. Dunphy and Simmie (1991) measured ignition delay times in a shock tube of ethanol/O_2 mixtures at high temperatures and pressures of 1.8 to 4.6 bar. Curran et al. (1992) measured ignition delay times of ethanol/O_2 mixtures in a shock tube at high temperatures and a pressure of 2.3 bar for lean and rich mixtures. Li et al. (2007) report measurements of stable species in the ethanol oxidation in a variable pressure flow reactor. The measured species were C_2H_5OH, H_2O, C_2H_4, CH_4, CH_3CHO, CO and CO_2, at pressure range of 3 to 12 bar, initial temperatures from 800 to 950 K and equivalence ratio from 0.3 to 1.4. Recently, the available data was extended to higher pressure. Cancino et al. (2007) reported measurements of ignition delay times in a high pressure shock tube from 690 to 1200 K and pressure of 30 bar. To the author's knowledge, these are the highest pressures reported so far for ethanol oxidation. Detailed chemical kinetic mechanisms have also been developed using these experimental results as guidance. Natarajan and Bhaskaram (1981) reported a detailed kinetic model for the high-temperature oxidation of ethanol containing 56 elementary reactions, including the bimolecular decomposition

[*]Leonel R. Cancino, e-mail: leonel@labcet.ufsc.br

reaction $C_2H_5OH + M \rightleftharpoons CH_2OH + CH_3 + M$, in other words, proposing the C-C cleavage of ethanol. Validation against experimental data of ignition delay time in a shock tube at pressures of 1.0 and 2.0 bar and temperatures between 1300 and 1700 K resulted in good agreement with the pressure dependence. Borizov et al. (1989) and Borizov et al. (1992) reported another detailed kinetic model for the high-temperature ignition of ethanol involving 94 elementary reactions. This kinetic mechanism was built starting from the Natarajan and Bhaskaram (1981) model, adding reactions that describe the pyrolysis of ethanol and some reactions representing the thermal oxidation by active radicals, not considered in the Natarajan model. The model was validated against experimental results of ignition delay time in shock tubes for stoichiometric, lean and rich compositions at pressure of 1 atm and a good agreement was found. In the nineties, Marinov (1999) developed a comprehensive model composed by 383 elementary reactions among 57 chemical species for the high-temperature ethanol oxidation. It included an accurate kinetic data-set for ethanol oxidation, reaction routes involving H-abstraction, C-C and C-O cleavage were proposed and computational chemistry methods were used in order to determine the Arrhenius parameters. It was validated against experimental results of ignition delay time in shock tube, laminar flame speed in counterflow twin flame and chemical species concentrations in jet-stirred reactor. Good agreement was found in general with all measurements. More recently, Saxena and Williams (2007) reported a kinetic model with 288 elementary reactions among 57 chemical species. This model is about 100 elementary reactions smaller than Marinov's and also predicts the nitrogen oxidation chemistry. It was validated against experimental results of ignition delay time in a shock tube at high temperatures (1300 to 1700 K) and pressures of 1.0 and 2.0 bar for stoichiometric, lean and rich ethanol/O_2/Ar mixtures. The Saxena model was also validated against laminar burning velocity data from Egolfopoulos et al. (1992). Marinov's and Saxena and William's models were also tested by Li et al. (2007). They proposed an improved detailed kinetic model for pyrolysis and oxidation of ethanol based mostly on their previous work (see references in Li et al. (2007)). Their model consists of 39 chemical species and 238 reversible elementary reactions and was developed in a hierarchical manner. The final mechanism was validated against the experimental results of shock tube from Curran et al. (1992) and Natarajan and Bhaskaram (1981), laminar flame from Gulder. (1982) and Egolfopoulos et al. (1992) (from 300 to 450 K), and their own variable pressure flow reactor (temperature from 800 to 950 K, pressure from 3 to 12 bar and equivalence ratio from 0.3 to 1.4). An agreement better than previous models (Marinov (1999) and Saxena and Williams (2007)) was obtained. The comparison with shock tube ignition delay from 2 to 4.5 bar resulted in the same trend of reduction of ignition delay time as presure increases. But, there was a tendency of overpredicting the ignition delay in the lower temperature range at higher pressure. Numerical studies on ethanol decomposition using computational chemistry have also been reported. They have been useful in completing the gaps on thermodynamic and chemical kinetic parameters as well as in pointing out important reactions and reactions with a very high reaction barrier. Marinov (1999) used RRKM theory to analyze the multichannel decomposition of ethanol. In this study, he determined the reaction rate parameters of the thermal decomposition of ethanol at high temperatures, involving new degradation routes like H-abstraction. These new data permitted to increase the accuracy of the kinetic modeling resulting in a good comparison to a host of experimental data. Recently, Li et al. (2004) found that Marinov's model underestimates the production rate of H_2O and C_2H_4 as well as the overall ethanol consumption. He then presented a new set of Arrhenius parameters for the decomposition reactions; $C_2H_5OH \rightleftharpoons C_2H_4 + H_2O$ and $C_2H_5OH \rightleftharpoons CH_3 + CH_2OH$. Finally, Lin et al. (2002), Lin et al. (2003) and Lin et al. (2004) published the most recent kinetic data obtained from computational chemistry for the thermal oxidation of ethanol. They provided a new kinetic database allowing for thermal decomposition of ethanol and ethanol-radical reactions. High barrier reactions are detected and critical reactions are identified.

This work has two objectives: (1) to report experimental results of shock tube experiments at high pressures and intermediate temperatures for ethanol, which have not been covered in the literature so far, and (2) to propose a detailed kinetic model for the ethanol oxidation obtained by using and improving available kinetic models.

2. Chemical reaction pathways for thermal oxidation of ethanol

The oxidation of hydrocarbons proceeds either by hydrogen atom abstraction or by cleavage of C-C bonds at primary or secondary carbon atoms. In the case of aliphatic alcohol hydrocarbons, the hydroxyl group plays a very important role for the oxidation and as a third pathway the cleavage of the C-O bond can occur. Any of the three paths follows after a temperature activated perturbation of the energy field of the molecule and proceed either by intramolecular (isomerization), giving several sub-structures, or as a result of collision with active radical species. Several authors have qualitatively described the decomposition of ethanol. Recently, Lin et al. (2002), Lin et al. (2003) and Lin et al. (2004) reported 11 different routes for ethanol decomposition involving reactive radical species. Figure 1 summarizes these major routes. Box I shows the decomposition routes involving methyl giving methane and hydrogen atoms as a product in three routes. Box II depicts H abstraction involving H atoms and producing molecular hydrogen via three routes and additional other unstable species. Box III depicts the H abstraction by a unimolecular self-cleavage process; all routes giving acetaldehyde, molecular and atomic hydrogen. Box IV shows the decomposition process

by unimolecular self-cleavage, involving the C-C and C-O bonds and the products are formaldehyde, methane and other unstable species. One can clearly see that the pyrolysis of ethanol proceeds by a chain-branching mechanism where free radical species like methyl and H atoms produced in boxes III and IV feed the active radical species for pathways of boxes I and II. Kinetic models of ignition of ethanol/O_2, Borizov et al. (1992) and ethanol/air, Cancino and Oliveira (2006), Gardiner (2000) show that during the induction period ethanol is consumed almost completely. The depletion of the fuel is induced by oxidative pyrolysis. Therefore, the ethanol oxidation model capable of describing accumulation of the products during the induction period and the promoter effect on the ignition process must be based on an ethanol pyrolysis mechanism, such as the one described above. Since the pathways depicted in

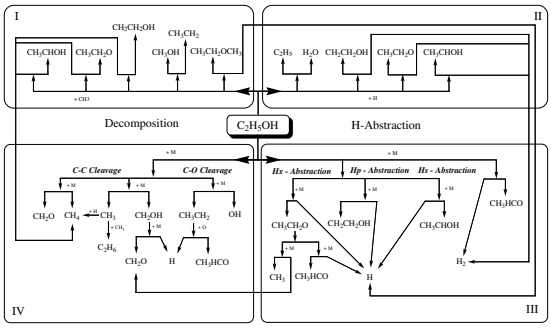

Figure 1. Ethanol decomposition pathways

Figure 1 proceed at different rates depending on the range of temperature and pressure, a careful analysis and comparison to critical experiments may be able to reveal the most important routes at different pressure and temperature regimes. Excluding a single result at 30 bar, the low temperature data has been measured up to 4.5 bar and high temperature data has been measured up to 12 bar. Using the available chemical mechanisms, it has been observed that the predictions overestimate the shock tube ignition delay data at higher pressures. Therefore, questions remain whether the patterns discussed above are still correct for higher pressures and also how the rates of the different paths behave as pressure is increased. In the following, new measurements of ignition delay are presented and compared to an improved detailed chemical kinetic model.

3. Experiments

3.1. Experimental set-up

The experiments were carried out in the high-pressure shock tube at the University of Duisburg-Essen. This facility, depicted in Figure 2, has an internal diameter of 90 mm, divided by an aluminum diaphragm into a driver section of 6.1 m and a driven section of 6.4 m in length. The driven section is pumped down to pressures below 10^{-2} mbar in between the experiments. Gas mixtures were prepared by injecting liquid ethanol into a stainless-steel mixing vessel and subsequent complete evaporation and mixing. The total amount of fuel and air was controlled manometrically in order to ensure the desired equivalence ratio. The shock tube was heated to 348 K . The shock speed was measured over two intervals using three piezo-electric pressure gauges. Pressure data were recorded with a time resolution of 0.1 μs. The temperature and pressure behind the reflected shock wave were computed from the measured incident shock speed and the speed attenuation using a one-dimensional shock-tube model (shock-tube code of the CHEMKIN package Kee et al. (2000)). The estimated uncertainty in reflected shock temperature is less than 25 K. The experiments were carried out with synthetic air containing 79.5% N_2 and 20.5% O_2. The ignition was observed by side-wall measurement of pressure profiles with a piezo-electric gauge (PCB HM 112 A03) located 15 mm upstream of the end flange. Also, the CH* emission at 431.5 nm from a side wall was selected by a narrow band pass filter (5 nm HWHM) and detected with a photomultiplier. All ignition delay times shown in this work were determined by extrapolating the steepest increase of the CH* chemiluminescence emission signal to its zero level on the time axis. The driver gas was mixed in-situ by using two high-pressure mass-flow controllers (Bronkhorst Hi-Tec flow meter F-136AI-FZD-55-V and F-123MI-FZD-55-V). Helium was used as the main component and Argon was added to match the acoustic impedance of the test gas. The required driver gas composition was calculated by a spreadsheet analysis prior to the experiments using equations by Oertel (1996) and Palmer and Knox. (1961). Concentrations of 5 to 20% Ar in He were required to generate tailored shock waves.

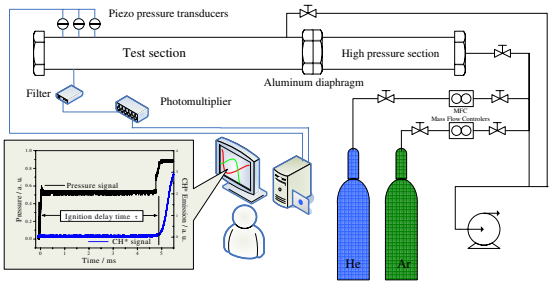

Figure 2. Experimental setup of the high-pressure shock tube facility

3.2. Measured ignition delay times

The ignition delay times evaluated from the CH* emission are listed in Table 1 along with the respective pressures p and temperatures T, for stoichiometric ethanol-air mixture. At temperatures lower than those shown in Table 1 no ignition was observed within the test time of our experiment (15 ms). Figure 3 shows the experimental results for ignition delay time as a function of temperature (as an Arrhenius plot) for different pressures and stoichiometric composition. All data was curve-fitted to an equation of the form $\tau = A \exp(B / T) p^{-x}$, where x is the pressure exponent. Multiple linear regression analyses

Table 1. Measured ignition delay times in shock tube for stoichiometric ethanol-air mixture

ϕ	T_5 [K]	p_5 [bar]	τ [μs]
1.0	1223	10.5	70
1.0	1223	10.5	70
1.0	1190	10.0	140
1.0	1145	11.0	252
1.0	1096	9.0	409
1.0	1049	10.1	738
1.0	992	9.8	1171
1.0	954	10.3	1698
1.0	900	10.1	N-I
1.0	1197	30	25
1.0	1152	30	38
1.0	1138	32	75
1.0	1116	31	80
1.0	1045	30	267
1.0	999	30	547
1.0	949	30	1244
1.0	912	31	877
1.0	881	31	2788
1.0	848	30	2715
1.0	801	30	3755
1.0	789	29	N-I
1.0	1234	53	16
1.0	1168	52	30
1.0	1085	48	134
1.0	1065	52	156
1.0	999	50	511
1.0	937	48	1006
1.0	881	48	2095
1.0	841	49	3304
1.0	781	47	N-I
1.0	769	45	N-I

N-I - No ignition

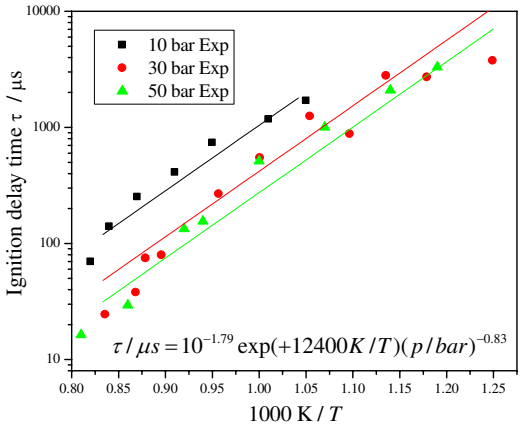

Figure 3. Experimental and curve fitted ignition delay times for stoichiometric ethanol/air mixture

using $\ln(\tau)$ as the dependent variable and $(1/T)$ and $\ln(p)$ as independent variables identified an expression of $\tau = 10^{-1.79}\ \exp(+12400/T)\ p^{-0.83}$, with T in K, p in bar and τ in μs, for the measured range of temperature and for a stoichiometric mixture. The curve fitting suggests an apparent activation energy of 24.6 kcal/mol. The fitting is shown in Figure 3. The measurements exhibit a decrease in ignition delay time as the pressure increases. There is also a smaller sensitivity to pressure at higher pressures. The variation with temperature at higher temperature tends to become smaller but the data does not indicate the existence of a negative temperature coefficient (NTC) region. These results are next used as a basis to extend current detailed chemical kinetic models for ethanol oxidation.

4. Detailed chemical kinetic modeling

4.1. Model development

In the present work, the Konnov (2000) and Marinov (1999) detailed kinetic models were taken and tailored to build up the proposed model. Initially, the extensively tested kinetic model for small hydrocarbons of Konnov was extended to the combustion of ethanol by adding the reactions described by Marinov that were missing in Konnov's mechanism. Then, in order to further improve the predictive capability of the model, a comprehensive review of the literature was performed and new kinetic data was found in Li et al. (2004), Lin et al. (2002), Lin et al. (2003) and Lin et al. (2004). They allowed for an update of the values of the reaction constants of several elementary reactions involving ethanol. Some elementary reactions that appeared neither in Konnov's nor in Marinov's mechanisms were also added. The adaptation process of the kinetic model was based on blending the different sub-mechanisms for ethanol and other sub-structures from Marinov, Li and Lin et al., that were not taken into account by Konnov, calculating ignition delay times with the subsequently formed mechanisms and comparing the results generated by the modified and base mechanisms. In summary, the model allows the specific reactions for ethanol decomposition of Figure 4. Lin et al. (2002) found that at pressures below

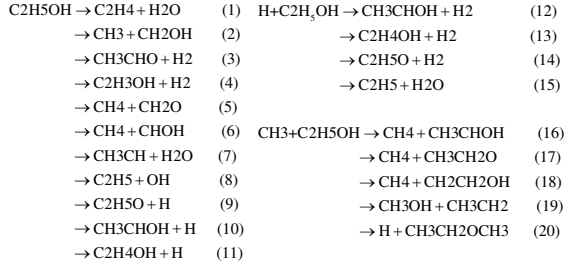

Figure 4. Specific reactions for ethanol decomposition

10 bar, the unimolecular decomposition of ethanol occurs primarily by the dehydration reaction producing C_2H_4 + H_2O, represented by reaction (1). At high-pressure limit and over 1500 K the production of CH_3 and CH_2OH becomes dominant, represented by reaction (2). The H_2-molecular elimination process, represented by reactions (3) and (4), is not important throughout the temperature range investigated (700 - 2500 K). Concerning the chain-propagation reactions by the H atom (reactions 12 to 15) the reaction of dehydration (15) has a high energy barrier and the possibility

that the reaction (15) proceeds is very low. In this group of reactions, reaction (14) represents about 10% of the total reaction rate in the temperature range analyzed by Egolfopoulos et al. (1992). Reactions (12) and (13) remain, however, the most important. In the CH_3-radical chain-propagation reactions, reactions (19) and (20) have higher energy barriers and their feasibility can be ruled out kinetically. The other reactions forming methane by H abstraction, reactions (16), (17) and (18), remain important and, at higher temperatures ($T > \sim$1200 K), reaction (18) becomes dominant. These oxidation routes lead ultimately to the production of methane, formaldehyde and other oxygenated hydrocarbons, as depicted in Figure 1, whose kinetics are well treated in the Konnov mechanism. In the proposed detailed kinetic model the most important reactions for the ethanol oxidation were selected and placed, ruling out those reactions whose energy barriers limitations were noted by the different authors. The final proposed detailed kinetic model is composed by 136 chemical species and 1136 elementary reactions. Table 2 shows the major characteristics of the detailed kinetic mechanism used in this work. The sensitivity analysis (discussed below) revealed that reaction $C_2H_5OH + HO_2 \rightleftharpoons SC_2H_5O + H_2O_2$ has the largest sensitivity on temperature, OH, H_2O_2 and C_2H_5OH concentrations in the whole temperature interval tested. To impove the predictive capability of the kinetic model, the original Arrhenius parameters of this reaction in the Konnov mechanism were altered. The total reaction rate constant for this reaction in the proposed mechanism was formed by the sum of three constants: $k_a = 1.01 \times 10^{+18} \exp(+41351/RT)$, $k_b = 4.65 \times 10^{+129} T^{-41.37}$ and $k_c = 2.45 \times 10^{+23} T^{-4.97}$. A similar expression for this rate constant was not found in the literature and this is advanced here as a way of better predicting the measurements for higher pressure and lower temperature.

Table 2. Characteristics of the detailed kinetic models

Kinetic model	Konnov	Marinov	Proposed in this work
Elements	5	4	5
Chemical Species	127	54	136
Elementary reactions	1200	390	1136
NOx chemistry	Yes	No	Yes
Presurre Range [atm]	0.9 - 7.5	1.0 - 4.5	0.9 - 50
Temperature Range [K]	—	$\geq$ 1000	700 - 1200

4.2. Results and comparison to measurements

Figure 5 shows the comparison between the measured and the predicted ignition delay times. The kinetic model is able to predict the general trends with temperature and pressure, including the smaller dependence with pressure for higher pressures and a smaller dependence with temperature for lower temperatures. At the pressure of 10 bar, the detailed kinetic model over predicts the ignition delay time for higher temperature.

4.3. Sensitivity analysis

A first-order sensitivity analysis of the effect of each reaction on temperature, OH, H_2O_2, and C_2H_5OH concentrations was performed to find out which reactions dominate the ethanol oxidation at high pressures and also which reaction coefficients need to be systematically improved. For the analysis, we assumed that the combustion process occurs in a perfectly stirred reactor starting at time $t = 0$ s and ending at $t = \tau_{ing}$. The conditions of the reactor were set at stoichiometric composition, pressures of 10, 30, and 50 bar and temperatures of 1100, 950, and 800 K. The sensitivity map was generated from the output files from CHEMKIN and shows the more sensitive reactions for the entire kinetic evolution of the system. The sensitivity map shows that reactions $C_2H_5OH + HO_2 \rightleftharpoons SC_2H_5O + H_2O_2$ (R1), $SC_2H_5O + O_2 \rightleftharpoons CH_3CHO + HO_2$ (R2), $C_2H_5OH + OH \rightleftharpoons SC_2H_5O + H_2O$ (R3) and $HO_2 + HO_2 \rightleftharpoons H_2O_2 + O_2$ (R4) are the more sensitive reactions at high pressures (10, 30, and 50 bar) and for intermediate and high temperatures (800, 950, and 1100 K). It seems that at high pressures the main ethanol oxidation path is dominated by the H-atom abstraction by the hydroperoxy radical (HO_2), producing CH_3CHOH (named SC_2H_5O in this work), one of the three isomers of C_2H_5O. This route corresponds to reaction R1 above and is represented schematically in the top part of Figure 6. This path leads to the hydrogen peroxide sub-mechanism. In the bottom part of Figure 6, is represented the H_s-abstraction path by collision with a third-body M. This path results also in the production of CH_3CHOH which is then oxidized forming acetaldehyde, leading to the acetaldehyde sub-mechanism, and HO_2. This corresponds to reaction R2 above. The hydroperoxy radical (HO_2) feeds reaction R1 giving more SC_2H_5O, forming a cycle for the production of SC_2H_5O and HO_2 and depletion of ethanol. R3 becomes relevant when the pool of HO_2 is formed. The reaction proceeds and more SC_2H_5O are produced. With the increase of HO_2 concentration, reaction R4 becomes important.

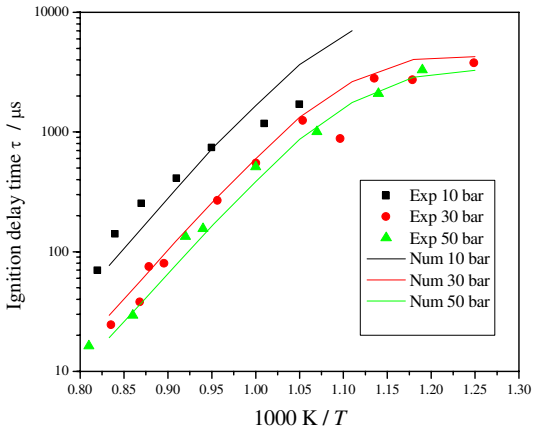

Figure 5. Comparison between predicted and measured ignition delay times for ethanol/air stoichiometric mixture

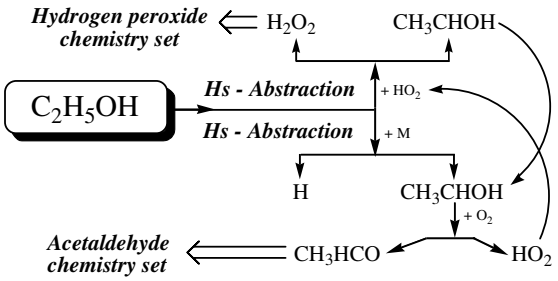

Figure 6. Main ethanol oxidation route at high pressure

5. Conclusions

In this paper we proposed a detailed kinetic model for the thermal oxidation of ethanol/air mixtures at higher pressures and intermediate and high temperatures. The model results from a combination and tailoring of the Konnov (2000) and Marinov (1999) models. Initially, the extensively tested kinetic model for small hydrocarbons of Konnov (suitable for hydrocarbons with up to 3 carbon atoms) was extended to include the combustion of ethanol by adding the reactions described by Marinov. Then, in order to further improve the predictive capability of the model, a comprehensive review of the literature was performed and new kinetic data was added from Li et al. (2004), Lin et al. (2002), Lin et al. (2003) and Lin et al. (2004). There data enabled us to update the values of the reaction rate constants of several elementary reactions involving ethanol. Some elementary reactions that appeared neither in Konnov's nor in Marinov's mechanisms were also added. A first-order sensitivity analysis revealed that reaction $C_2H_5OH + HO_2 \rightleftharpoons SC_2H_5O + H_2O_2$ had the largest sensitivity on temperature, OH, H_2O_2 and C_2H_5OH concentrations in the whole temperature interval tested. Then, the rate constants for this reaction were modified in order to better predict the measurements for higher pressure and lower temperatures. The final mechanism is composed of 136 chemical species and contains 1136 elementary reactions. The model was then validated against experimental data of ignition delay time from shock-tube measurements in the pressure range of $10 \leq p \leq 50$ bar and temperature range of $750 \leq T \leq 1200$ K. The detailed kinetic model predicts the reduced pressure sensitivity of the ignition delay time at higher pressures. Additionally, it predicts the global trend with temperature. No negative temperature coefficient region was detected in the temperature and pressure range analyzed. From the detailed kinetic modeling, a possible main oxidation route for ethanol oxidation at high pressures is suggested. This route involves the H-atom abstraction from the secondary carbon of the ethanol molecule by reaction with hydroperoxy radical, giving CH_3CHOH and H_2O_2 as major products. It is recommended a more complete comparison of predictions with this reaction mechanism against previous measurements and also a more thorough study of the reactions pointed as the most sensitive, especialy the reaction $C_2H_5OH + HO_2 \rightleftharpoons SC_2H_5O + H_2O_2$.

Acknowledgements

The authors gratefully acknowledge the Conselho Nacional de Desenvolvimento Cientfico e Tecnolgico - CNPq - Brazil, Deutscher Akademischer Austausch Dienst - DAAD - Germany, and the German Research Foundation (DFG) for the support given in the development of this work. The help of N. Schlösser in conducting the experiments is also greatly appreciated.

References

Barnard J.A. and Hughes H.W.D. (1960), The pyrolysis of Ethanol, Trans Faraday Soc,56,p55.

Borizov A.A., Zamanskii V., Konnov A.A., Lisyanskii V., Rusanov S., Skachkov G., (1989), Sov. J Chem. Phys., Vol 4(11), pp.2561

Borizov A.A., Zamanskii V. ,Konnov A.A. ,Lisyanskii V. ,Rusanov S., Skachkov G., (1991), Sov. J Chem. Phys., Vol 8(1),pp.121

Borizov A.A., Zamanskii V., Konnov A.A., Lisyanskii V., Rusanov S., Skachkov G., (1992), Sov. J Chem. Phys.,Vol 9(11), pp.2527

Cancino L.R., Oliveira A.A.M. (2006), Proc. of the 11th ENCIT 2006. ABCM, Brazil.

Cancino L.R., Fikri M, Oliveira A.A.M., Schulz C. (2007), Eastern State Fall Technical Meeting. U. of Virginia. October 21-25.

Curran H., Dunphy M., Simmie J., Westbrook C., Pitz W. (1992), Twenty-Fourth Symposium (International) on Combustion, pp.769

Dunphy M.P., Simmie J.M. (1991), J. Chem. Soc. Faraday Trans., 87(11), 1691-1696.

Egolfopoulos, F.N., Du, D.X., Law, C.K. (1992), 24^{th} Symposium (Int.) on Combustion, pp.833

Gardiner W.C. (2000), Gas Combustion Chemistry, Springer-Verlag - USA.

Gulder Ö. (1982), Nineteenth Symposium (Internatinal) on Combustion, pp. 275.

Kee R.J., et al, (2000). CHEMKIN Collection, Release 3.7.1 R&D, Inc., San Diego, CA.

Konnov. A.A (2000), 28-th Symp. (Int.) on Comb., Edinburgh, Abstr. Symp. Pap. p.317.

Kohse-Höinghaus K., T.S. Kasper, P. Oβwald, M. Kamphus. (2007), C&F 150 p.220.

Li J., Kazakov A., Dryer F.L.J., (2004), Phys. Chem. A. (Article),108(38) 7671-7680.

Li J., Kazakov A., Chaos M., Dryer F.L. (2007), 5^{th} US Comb. Meeting, San Diego, March 25-28 Paper C26.

Lin M.C., Park J., and Zhu R.S. (2002), Journal of Chemical Physics. Vol 117, Number 7

Lin M.C.,Park J., and Xu Z.F. (2003), Journal of Chemical Physics. Vol 118, Number 22

Lin M.C., Xu Z.F. and Park J. (2004), Journal of Chemical Physics. Vol 120, Number 14

Marinov. N.M. (1999), Int. J Chem. Kinet. 31. p.183

Natarajan K. and Bhaskaram K.A. (1981), Proc 13th Int. Shock tube Sym. Niagara Falls,pp.834.

Oertel H. (1966), Stoβrohre, Springer-Verlag,Wien/New York.

Palmer H.B., Knox B.E. (1961), ARS J. 31 826-828.

Saxena P., Williams F.A. (2007), Proc. Comb. Ins. 31 p.1149.

AUTOIGNITION OF BINARY MIXTURES OF GASOLINE SURROGATES, ETHANOL – ISO-OCTANE BLENDS IN AIR: NUMERICAL AND EXPERIMENTAL STUDY IN A HIGH-PRESSURE SHOCK TUBE

Leonel R. Cancino, leonel@labcet.ufsc.br
Laboratorio de Combustão e Engenharia de Sistemas Térmicos – LABCET
Universidade Federal de Santa Catarina, Brazil

Mustapha Fikri, mustapha.fikri@uni-due.de
Institut für Verbrennung und Gasdynamik – IVG
Universität Duisburg Essen, Germany.

Amir A M Oliveira, amir@emc.ufsc.br
Laboratorio de Combustão e Engenharia de Sistemas Térmicos – LABCET
Universidade Federal de Santa Catarina, Brazil

Christof Schulz, christof.schulz@uni-due.de
Institute for Combustion and Gasdynamics – IVG
University of Duisburg-Essen, Duisburg, Germany.

Abstract. *Ignition delay times were measured in shock-heated gases for a two-component gasoline surrogate comprised of ethanol and iso-octane at a composition of 25% / 75% by liquid volume, with calculated RON/MON numbers of 109/101. The experiments were carried out in stoichiometric mixtures in synthetic air (oxygen 21% - nitrogen 79%) behind reflected shock waves in a high-pressure shock tube. The temperature ranged between 750 – 1200 K, at a pressure of 30 bar. Ignition delay time was determined from CH* chemiluminescence at 431.5 nm measured at a side-wall location. An activation temperature of ~13,272 K was found for the experimental conditions of the shock tube experiments. A detailed chemical kinetics model is proposed for ternary mixtures of gasoline surrogates involving ethanol and primary reference fuels. The kinetics model was obtained by blending the available detailed kinetics models. The qualitative behavior of the ethanol-isooctane mixture investigated in this work was well predicted as well as the behavior of other ignition delay time measurements for pure fuels available in the literature.*

Keywords*: Gasoline surrogates, autoignition, shock tube, detailed kinetics model, ethanol.*

1. INTRODUCTION

Presently, the combustion of practical fuels can only be investigated by experimental approaches. However, the scientific community is moving towards more in-depth numerical approaches as computational resources, numerical methods and chemical knowledge increases. As mentioned by Westbrook et al. (2005), computer modeling has grown rapidly to play a major role in virtually every field of science and engineering. Today it is common to find numerical models attempting to represent combustion process of single hydrocarbon fuels, and depending on the desired quality or target of the results, using either global or detailed kinetics mechanisms. In this direction, many researchers have devoted considerable time studding and proposing global and detailed kinetics models. For example, Griffiths (1995) and Simmie (2003) present reviews for oxidation of pure hydrocarbons.

The number of chemical species that can be present in a real gasoline can be, however, at the order of hundreds, involving saturated and unsaturated hydrocarbons including alkanes, cycloalkanes, alkenes, cycloalkenes, aromatic, ethers and esters, components whose identity and amounts are often unknown (Metcalfe et al. (2007)). The modeling for even a pure component requires reasonable computational resources. The well-known kinetics model for pure iso-octane oxidation of Curran et al (2002) is composed by 857 chemical species allowing 3606 elementary reactions. To think about a detailed kinetics model for a practical fuel involving hundreds of chemical species demands a dramatically increase in the number of elementary reactions, making the problem intractable with current computational capabilities.

Being mindful of the dimension of the problem the scientific community uses a host of methods to have a reliable approach of the problem. One of these is the modeling the combustion of surrogate mixtures.

A surrogate fuel consists of a small number of components that can be used to represent the practical fuel and still predict characteristics of the real fuel. These desirable characteristics may include ignition behavior, burning velocity, viscosity, vaporization, and emission such as carbon monoxide, hydrocarbons, soot and nitrogen oxides (Metcalfe et al. (2007)). The development and modeling of fuel chemistry of gasoline surrogates started with Curran et al. (1998) and Curran et al. (2002). They reported detailed chemical kinetics models of n-heptane and iso-octane covering the parameters used to qualified fuel ignition the Research Octane Number (RON) and the Motor Octane Number (MON). The RON and MON scales are both based on Primary Reference Fuels (PRF); n-heptane (RON = MON = 0) and iso-

octane (RON = MON = 100). Here, the use of surrogate fuels is an approach to make the development of chemical kinetics mechanisms for practical fuels tractable. These kinetics models have been compared to, ignition delay time measurements and other quantities.

Several experimental results of ignition delay time in shock tube have been reported involving PRFs and ethanol. Davidson et al. (2002) reported shock-tube measurements of iso-octane/O_2 mixtures in a temperature range of 1177 to 2009 K, a pressure range of 1.18 to 8.17 bar and equivalence ratios form 0.25 to 2. Hydroxyl radical concentration time histories were reported. Gauthier et al. (2004) reported ignition delay times for n-heptane/air at pressures between 15 – 60 bar, temperatures of 800 – 1350 K and stoichiometric mixture composition. Natarajan and Bhaskaran (1981) reported ignition delay time measurements in a shock tube of mixtures of ethanol/O_2, for pressures of 1.0 and 2.0 bar at higher temperatures of 1300 – 1700 K and equivalence ratios of 0.5, 1.0 and 2.0. Dunphy and Simmie (1991) reported ignition delay times of ethanol/O_2 mixtures at high temperatures (1080 – 1660 K), pressures between 1.8 – 4.6 bar and equivalence ratios between 0.25 – 2.0. Cancino et al. (2009) reports measurements of ignition delay times measured in a high-pressure shock tube for a temperature range of 690 – 1200 K at pressures of 10, 30 and 50 bar for stoichiometric composition of ethanol/air mixtures. More information about experimental results involving ethanol in different experimental results can be found in Cancino et al. (2008).

Concerning numerical studies of binary gasoline surrogate mixtures involving PRFs, Curran et al. (1998) proposed the first detailed kinetics model for n-heptane and iso-octane blends at elevated pressures. This kinetics model was validated against experimental results in a high-pressure flow reactor using both the pure components and their mixtures in a temperature range of 550 – 850 K and at pressures of 12.5 bar. The Curran et al. (1998) PRF model was validated against measured ignition delay times in shock tubes over the temperature range of 690 – 1220 K and at pressure of 40 bar, Good agreement was observed between experimental and simulation results for both pure PRF and their mixtures. Concerning ethanol oxidation, Marinov (1999) proposed the often cited detailed kinetics model for high-temperature ethanol oxidation validated against experimental results of ignition delay time in shock tube from Dunphy and Simmie (1991) and Dunphy et al. (1991) for temperatures between 1300 – 1700 K, a pressure range of 1 – 3.4 bar and equivalence ratios between 0.5 – 2.0. Afterwards, Cancino et al. (2009) upgraded Marinov's ethanol kinetics and proposed a detailed kinetics model for ethanol oxidation in air, at pressures of 10, 30 and 50 bar, and intermediate temperatures of 690 – 1200 K in stoichiometric mixtures.

In this work we propose a detailed kinetics model for ternary mixtures of gasoline surrogates involving PRFs and ethanol. Simultaneously, we report experimental data of ignition delay time of the binary mixture ethanol/iso-octane (25%/75% by volume) at pressure of 30 bar and temperatures between 800 – 1217 K for stoichiometric composition. Figure 1 shows the molecular structure of the three fuels ethanol, iso-octane and n-heptane molecules considered in the detailed kinetics model proposed here.

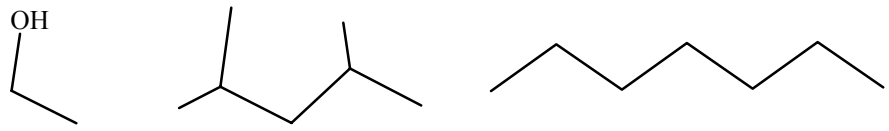

Ethanol 2,2,4-trimethyl-pentane (iso-octane) n-heptane

Figure 1. Molecular structure of fuels considered in this work

The proposed gasoline surrogate model is composed by ethanol (oxygenate hydrocarbon), iso-octane (saturated iso-paraffin), n-heptane (saturated n-paraffin).

2. EXPERIMENTS

The experiments were carried out in the high-pressure shock tube at the University of Duisburg-Essen, Germany. This facility, depicted in Figure 2, has an internal diameter of 90 mm, divided by an aluminum diaphragm into a driver section of 6.1 m and a driven section of 6.4 m in length. The driven section is pumped down to pressures below 10^{-2} mbar in between the experiments. Gas mixtures were prepared by injecting liquid ethanol - iso-octane (25%/75%) mixture into a stainless-steel mixing vessel and subsequent complete evaporation and mixing. The total amount of fuel mixture and air was controlled manometrically in order to ensure the desired equivalence ratio. The shock speed was measured over two intervals using three piezo-electric pressure gauges.

Pressure data were recorded with a time resolution of 0.1 μs. The temperature and pressure behind the reflected shock wave were computed from the measured incident shock speed and the speed attenuation using a one-dimensional shock-tube model (shock-tube code of the CHEMKIN package Kee et al. (2000)). The estimated uncertainty in reflected shock temperature is less than ±25 K. The experiments were carried out with synthetic air containing 79.5% N_2 and 20.5% O_2. The ignition was observed by measuring pressure profiles with a piezo-electric gauge (PCB HM 112 A03) located 15 mm upstream of the end flange. Also, the CH* emission at 431.5 nm was selected by a narrow band

pass filter (5 nm HWHM) and detected with a photomultiplier. All ignition delay times shown in this work were determined by extrapolating the steepest increase of the CH* chemiluminescence emission signal to its zero level on the time axis as shown in Figure 2.

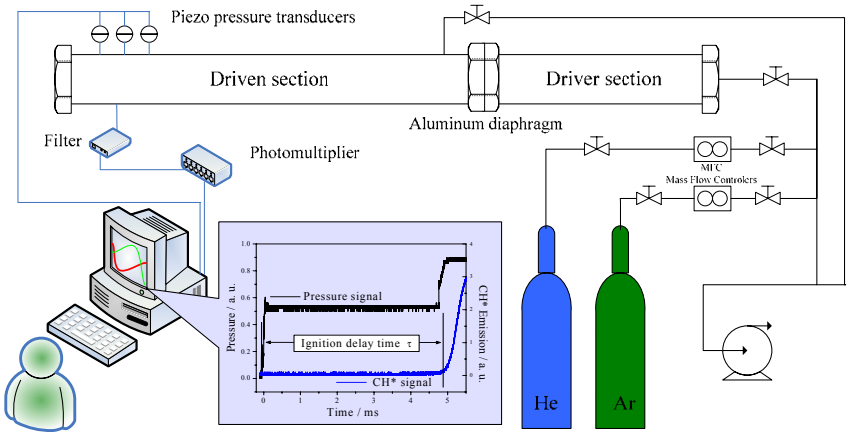

Figure 2. Experimental setup of the high-pressure shock tube facility

The driver gas was mixed in-situ by using two high-pressure mass-flow controllers (Bronkhorst Hi-Tec flow meter F-136AI-FZD-55-V and F-123MI-FZD-55-V). Helium was used as the main component and Argon was added to match the acoustic impedance of the test gas. The required driver gas composition was calculated by a spreadsheet analysis prior to the experiments using equations by Oertel (1966) and Palmer and Knox (1961). Concentrations of 5 to 20% Ar in He were required to generate tailored shock waves.

2.1. Measured ignition delay times

The ignition delay times evaluated from the CH* emission, are listed in Table 1 along with the respective temperatures T and pressures *p*, for stoichiometric ethanol - iso-octane (25%/75%) / air mixture. At temperatures lower than those shown in Table 1 no ignition was observed within the test time of our experiment (15 ms).

Table 1. Measured ignition delay time in shock tube, stoichiometric ethanol 25% - iso-octane 75% mixtures in air

Φ	T_5 [K]	p_5 [bar]	τ_{ing} [µs]
1.0	1217	30.9	35
1.0	1215	30.8	34
1.0	1169	29.2	58
1.0	1164	30.7	74
1.0	1132	31.9	78
1.0	1059	30.6	404
1.0	1004	30.3	791
1.0	967	31.2	683
1.0	909	30.7	2039
1.0	862	31.1	2097
1.0	809	30.7	N-I

N-I No Ignition

Figure 3 shows the measured ignition delay time for the mixture ethanol / iso-octane (25%/75%) / air mixtures. A regression analysis taking ln(τ) as dependent variable and $1000/T_5$ as independent variable was performed obtaining a apparent activation temperature of ~13,273 K

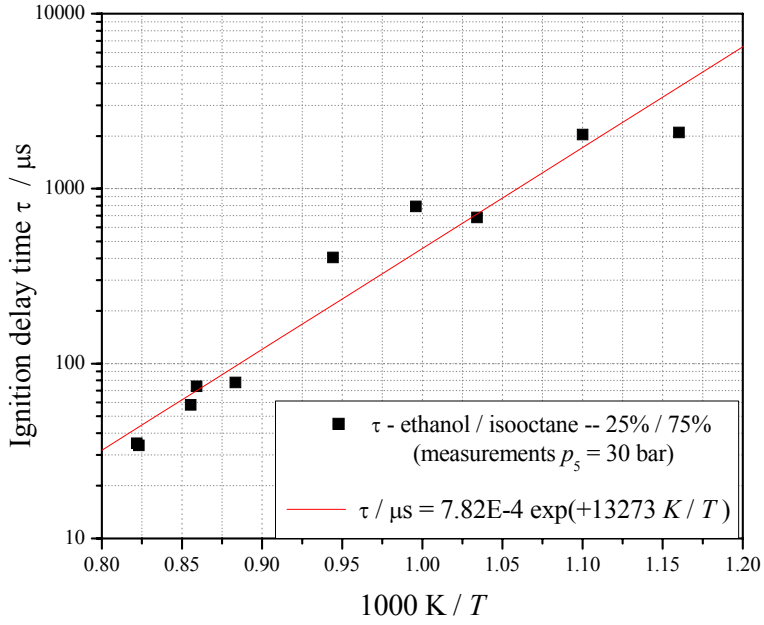

Figure 3. Ignition delay time for mixture ethanol/isooctane (25%/75% by liquid volume) / air.

3. DETAILED KINETICS MODELING

3.1. Blending process

The strategy to tailor the detailed kinetics model requires a sequence of steps that are outlined here:

1. Analyze and potentially adjust the kinetics information of both mechanisms for their use in CHEMKIN.
2. Check the species names in both mechanisms and remove duplicate reactions from the second (minor) mechanism.
3. Add the missing reactions into the main mechanism.
4. Check the thermodynamic data base of the major mechanism and upgrade it with data for the missing species.
5. Test the blended kinetics model with the CHEMKIN interpreter and validate it against measured ignition delay times to make sure that the added reactions for an additional fuel component does not change the behavior of the mechanism in case this component is not present.
6. Optimize the blended kinetics mechanism: Determine the rate-determining route for autoignition via a sensitivity analysis and figure out whether the major reactions have reliable (directly measured) kinetics data.

The blending procedure is time consuming. When two chemical species have the same empirical formula, it is necessary to check their thermodynamic databases by comparing the enthalpy h, heat capacity c_p, and entropy s at several temperatures. If their thermodynamic properties return the same (or similar) values, then both chemical species are identical despite different names or abbreviations used in the original kinetics models. Productivity increases with the use of computational tools. The programs of Rolland and Simmie (2004) were used to compare the kinetics mechanisms and thermodynamic databases.

3.2. Proposed detailed kinetics model for ethanol-PRF blends

A detailed kinetics model for ternary gasoline surrogates involving ethanol, iso-octane and n-heptane is proposed here. The chemical species were selected based on the availability of detailed chemistry in the literature. The starting point was the PRF model of Curran et al. (1998). The chemical kinetics of ethanol oxidation was taken from Cancino et al (2009), which is an upgraded chemistry of ethanol based on Marinov (1999) and Konnov (2000) kinetics mechanisms. Table 2 shows the origin of the sub-mechanisms.

Table 2. Fuels and base mechanisms considered in this work.

	Ethanol and small hydocarbons	n-heptane	iso-octane or 2,2,4-trimethyl-pentane
Chemical formula	$C_2H_5OH,\ C_1 - C_3$	nC_7H_{16}	iC_8H_{18}
Number of species	136	1034	
Number of elementary reactions	1136	1236	
Validated range	0.9 - 50 bar	40 bar	
	700 - 1200 K	690 - 1220 K	
	$\Phi = 1.0$	$\Phi = 1.0$	
References	Cancino et al. (2009)	Curran et al. (1998)	

4. NUMERICAL SIMULATIONS

The average computational time for each simulation was about ~ 25 minutes, by using a computer Intel Pentium Core Duo Processor, 1.66 GHz with 2.0 GB of RAM. A total of 80 simulations were performed in this work. A FORTRAN source code for the data post-processing of the CHEMKIN output files.

4.1. Results for pure ethanol

Figure 4 shows the numerical predictions of ignition delay time for ethanol-air mixtures at stoichiometric composition, at pressures of 10, 30 and 50 bar for both the Curran PRF model and the proposed detailed kinetics model of this work. These numerical results are compared to experimental conditions from Cancino et al. (2009).

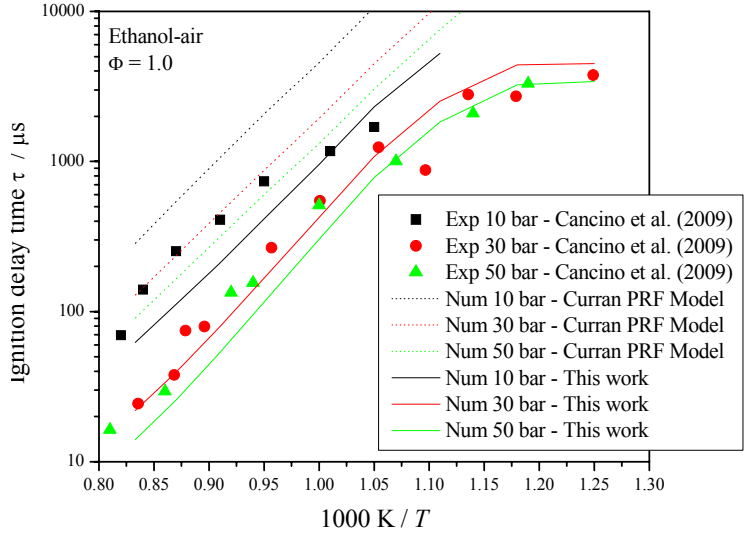

Figure 4. Experimental results from Cancino et al (2009) and numerical predictions of both, the Curran PRF model and of the blended proposed model in this work.

The Curran PRF model was developed specifically for iso-octane and n-heptane fuels and it was expected that the PRF model would fail in the predictions of ignition delay times for ethanol-air mixtures, especially at temperatures below 1000 K. However, the PRF model is sensitive to the pressure dependence of the ignition delay time, as observed in experiments. After adding the ethanol chemistry from recent studies from Cancino et al. (2009) the resulting kinetics model is able to reproduce ignition delay times for ethanol-air mixtures.

4.2. Results for pure iso-octane

Figure 5 shows the numerical predictions of both, the Curran PRF model and the proposed detailed kinetics model for iso-octane / air mixtures at pressures of 16.8 and 49.4 bar, temperatures between 950 – 1200 K and stoichiometric composition. The experimental data was obtained from Davidson et al. (2005).

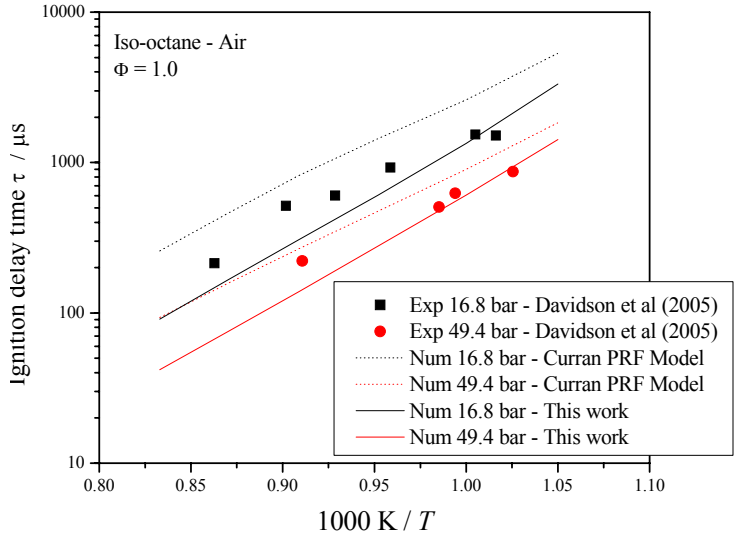

Figure 5. Experimental results from Davidson et al (2005) and numerical predictions of both, the Curran PRF model and of the blended proposed model in this work.

Figure 5 shows that the Curran PRF model overestimates the experimental results, and the discrepancy is more evident at pressures of 16.8 bar. The proposed model slightly underestimates the experimental results at higher temperatures. However, the proposed model captures the general trends of the experiments.

4.3. Results for the gasoline surrogate ethanol / iso-octane (25% / 75%)

Figure 6 shows the numerical and experimental results for the binary mixture investigated in this study.

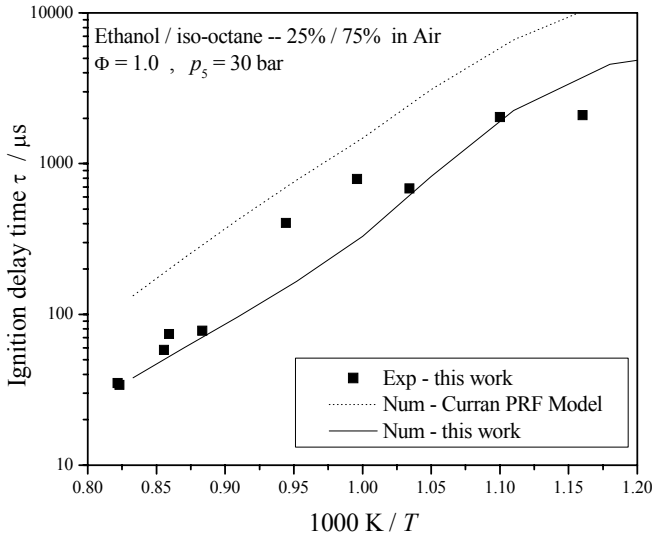

Figure 6. Numerical and experimental results of ignition delay time for ethanol - iso-octane (25%/75%) in air.

The PRF model overestimates the values of ignition delay time in the temperature range of this study. Adding the upgraded ethanol chemistry, the performance of the resulting detailed kinetics model improves. The proposed model underestimates the values of ignition delay time for temperatures about ~1050 K. However, the model captures the general trends of the experiments.

5. CONCLUSIONS

Ignition delay times were measured in a shock tube for a binary mixture comprised of ethanol and iso-octane at a composition of 25% / 75% by liquid volume, with calculated RON/MON numbers of 109/101. The experiments were carried out for stoichiometric mixtures in air behind reflected shock waves in a high-pressure shock tube. Initial reflected shock conditions were varied with the temperature range of 750 – 1200 K at a pressure of 30 bar. An activation temperature obtained by data post-processing of experimental results was found to be ~13,273 K for the investigated conditions at stoichiometric mixture composition. A detailed kinetics model is proposed and validated against our experimental results, and against experimental results of ignition delay times in shock tube for the pure fuels available at literature. The numerical results of ignition delay time of the proposed kinetics model shows good agreement to the experimental data of ethanol and iso-octane available in the literature.

For iso-octane/air mixtures, the Curran PRF model overestimates the experimental results, and the discrepancy is more evident at pressures of 16.8 bar. The proposed model underestimates the experimental results. However, the proposed model captures the general trend of the experiments.

For the binary mixture analyzed in this work, the PRF model overestimates the values of ignition delay time in the temperature range of this study. Adding the upgraded ethanol chemistry, the performance of the resulting detailed kinetics model improves. The proposed model underestimates the values of ignition delay time for temperatures about ~1050 K.

Acknowledgements

The authors gratefully acknowledge the Conselho Nacional de Desenvolvimento Científico e Tecnológico – CNPq – Brazil, Deutscher Akademischer Austausch Dienst – DAAD – Germany, and the German Research Foundation (DFG) for the support given in the development of this work. The help of Dr. Gautam Kalghatgi in the calculation of RON/MON numbers of the binary mixture is also greatly appreciates as well as the help of Ms. N Schlösser in conducting the experiments.

6. REFERENCES

Westbrook, C.K., Mizobuchi, Y., Poinsot, T.J., Smith, P.J., Warnatz, J., Computational combustion. Proc. Combust. Inst. 30, 125–157 (2005).

Griffiths J.F., Reduced kinetic models and their application to practical combustion systems, Progress in Energy and Combustion Science 21, 25-107 (1995).

Simmie J.M., Detailed chemical kinetic models for the combustion of hydrocarbon fuels, Progress in Energy and Combustion Science 29, 599-634 (2003).

Curran H.J., Gaffuri P, Pitz W.J., Westbrook C.K., A Comprehensive Modeling Study of iso-Octane Oxidation., Combust. Flame 129, 253-280 (2002).

Metcalfe W.K., Pitz W.J., Curran H.J., Simmie J.M., Westbrook C.K., The development of a detailed chemical kinetic mechanism for diisobutylene and comparison to shock tube ignition times. Proc. Combust. Inst. 31, 377-384 (2007).

Curran H.J., Gaffuri P, Pitz W.J., Westbrook C.K., A comprehensive study of n-heptane oxidation. Combust. Flame 114,149–77 (1998).

Curran H.J., Pitz W.J., Westbrook C.K., Callahan C.V., Dryer F.L., Oxidation of automotive primary reference fuels at elevated pressures., Proc. Combust. Inst. 27, 379–387 (1998).

Marinov N.M., A detailed chemical kinetic model for high temperature ethanol oxidation., Int. J. Chem. Kinet 31 (1999) 183-220.

Dunphy, M.P., Simmie, J.M., High temperature oxidation of ethanol. Part 1.-Ignition Delays in Shock Waves. J. Chem. Soc. Faraday Trans. 87, 1691-1696 (1991).

Dunphy, M.P., Patterson, P.M., Simmie, J.M., High-temperature oxidation of ethanol. Part 2.-Kinetic Modelling. J. Chem. Soc. Faraday Trans. 87, 2549-2559 (1991).

Cancino L.R., Fikri M., Oliveira A.M.M., Schulz C., Thermal Oxidation of Ethanol: Experimental and Numerical Analysis of Ignition Chemistry of Ethanol-Air Mixtures in Shock-Heated Gases, Paper 30074, 27th International Symposium on Shock Waves, St. Petersburg, Russia, 2009.

Natarajan K., Bhaskaram K.A., An experimental and analytical investigation of high temperature ignition of ethanol. Proc 13th Int. Shock Tube Symp., Niagara Falls, 1981. pp. 834.

Cancino L.R., Fikri M., Oliveira A.M.M., Schulz C., Autoignition of ethanol: Analysis and experiment of ethanol ignition in shock tube. 12th Brazilian Congress of Thermal Engineering and Sciences, Proceedings of ENCIT 2008, November 10-14, 2008, Belo Horizonte, MG, Brazil.

Davidson D.F., Oehlschlaeger M.A., Herbon J.T., Hanson R.K., shock tube measurements of iso-octane ignition times and oh concentration time histories., Proc. Combust. Inst. 29, 1295-1301 (2002).

Gauthier B.M., Davidson D.F., Hanson R.K., Shock tube determination of ignition delay times in full-blend and surrogate fuel mixtures, Combust. Flame 139 (2004) 300–311.
R.J. Kee, et al., (2000). CHEMKIN Collection, Release 3.7.1 Reaction Design, Inc., San Diego, CA
Oertel H., Stossrohre, Springer-Verlag,Wien/New York, 1966.
Palmer H.B., Knox B.E., ARS J. 31 (1961) 826–828
Konnov A., Development and validation of a detailed reaction mechanism for the combustion of small hydrocarbons., 28-th Symposium (Int.) on Combustion, Edinburgh, 2000. Abstr. Symp. Pap. p. 317.
Rolland S., Simmie J.M., The comparison of detailed kinetic mechanisms: Application to the combustion of methane. Int. J. Chem. Kinet. 36, 467-471 (2004).
Rolland S., Simmie J.M., The comparison of detailed kinetic mechanisms: Application to the combustion of methane. Int. J. Chem. Kinet. 36, 467-471 (2004).
Davidson D.F., Gauthier B.M., Hanson R.K., Shock tube ignition measurements of iso-octane/air and toluene/air at high pressures., Proc. Combust. Inst. 30, 1175-1182 (2005).

7. RESPONSIBILITY NOTICE

The authors are the only responsible for the printed material included in this paper.